Linear and non-linear modelling of thermoacoustic instabilities in a laboratory burner

Béla Kosztin

Submitted in partial fulfilment of the requirements of the degree of Doctor of Philosophy in Applied Mathematics

March 2014

Keele University

There is nothing more practical than a good theory.

- Theodore von Karman

Acknowledgements

I am very grateful to Dr. Maria Heckl and Prof. Viktor Shrira for their helpful comments, supervision and support in the research and in the preparation of the thesis. I am also indebted to Dr. Jakob Hermann and Roel Müller for their useful comments and measurements. I would like to take the opportunity to express my gratitude to my parents, Mária and Béla, and to my wife, Terézia, for their constant support. I wish to thank Dr. Michael Lutianov, Steven Metcalfe and Iohanna Pallura for the late night discussions.

The presented work is part of the Marie Curie Initial Training Network LIMOUSINE. The financial support from the European Commission is gratefully acknowledged.

Abstract

Thermoacoustic instabilities are a mayor problem in industrial combustors, where they can lead to catastrophic hardware damage. An industrial gas turbine combustion chamber is a very complex and expensive system. Thus, a laboratory burner has been built for research purposes, where a large number of parameters can be varied. This study is part of the Marie Curie research network LIMOUSINE, which was set up to model thermoacoustic instabilities in the combustor chamber of gas turbines. The objective of the present thesis is to theoretically model and analyze thermoacoustic instabilities in the LIMOUSINE laboratory burner.

A mathematical model of the laboratory burner has been developed. A more general form of the wave equation has been derived in the time-domain, in which the mean temperature gradient was taken into account. The governing differential equation has been solved by applying the Green's function approach, which allows separating the effects of the unexcited burner and the fluctuating heat-release. Using perturbation techniques general solutions are given for the cases when the temperature increase is either small or large. Conclusions have been drawn about the necessary complexity of thermoacoustic models by comparing increasingly complex configurations. The forcing term of the wave equation is studied by investigating the kinematics of ducted premixed flames theoretically, and a new heat-release law is derived. Instability criterion has been derived by applying the non-linear source term. The stability parameter map of the burner has been also investigated. Expressions for the limit-cycle amplitudes and frequencies were derived using weakly non-linear theory. The predictions of the mathematical model have been compared to measurements.

Contents

Nomenclature

Dimensionless Numbers

Le	Lewis number
Ma	Mach number
Mn	Markstein number
Pé	Péclet number
Pr	Prandtl number
Re	Reynold's number
St	Strouhal number
Ze	Zeldovich number

Abbreviations

BC	boundary condition
HHV	higher heating value
IC	initial condition
FDF	flame describing function
FT	Fourier transform
FTF	flame transfer function
LHV	lower heating value
LSM	level set method
LT	Laplace transform

Upper case variables

$\mathscr{A}$ ..... cross sectional area

G ..... Green's function

$\mathcal{G}$ ..... scalar in the $\mathcal{G}$-Equation

H ..... Heaviside function

L ..... tube length

P ..... thermal power

Q ..... local heat release rate

$\mathcal{R}$ ..... specific gas constant

R ..... reflection coefficient

S_l^0 ..... laminar flame speed

T ..... temperature

Lower case variables

c ..... speed of sound

c_p ..... specific heat capacity at constant pressure

c_v ..... specific heat capacity at constant volume

i ..... imaginary unit

q ..... global heat release rate

r ..... radial coordinate

r_0 ..... radius of the flame holder

r_1 ..... radius of the combustion chambers wall

s ..... Laplace domain variable

t ..... time

u ..... velocity

x ..... axial coordinate

Greek variables

γ ..... specific heat capacity ratio

δ ..... delta function

ν ..... viscosity

ξ ..... source position

ρ ..... density

τ ..... source time

φ ..... phase of reflection

Φ ..... stoichiometric ratio

χ ..... time-lag

ω_r ..... eigenfrequency of the non-excited burner

ω_i ..... damping rate of the non-excited burner

Superscripts

α' ..... fluctuating component of α

$\bar{\alpha}$ ..... mean component of α

α^* ..... complex conjugate of α

$\hat{\alpha}$ ..... Fourier transform of α

$\tilde{\alpha}$ ..... non-dimensional form of α

List of Figures

List of Tables

Chapter 1

Introduction

In this chapter we give a brief introduction and outline the problem which is going to be addressed in this thesis. We discuss the importance of thermoacoustic instabilities and review previous studies. Thus, we will identify the remaining open questions, and explain which ones of them and why are going to be considered in the thesis.

1.1 Setting the problem

In order to meet strict emission regulations, combustors are operating in premixed mode. This is beneficial for reducing emission, however premixed flames are particularly susceptible to self-excited oscillations. The prediction of these instabilities is technologically very important. Under certain circumstances perturbations in the flow affect the flame dynamics, hence the rate of heat released by the flame. This change in the rate of heat-release affects the acoustic waves, creating a feedback loop between the acoustic waves and the heat-release rate fluctuations (this is shown in Figure (1.1)). This feedback between acoustics and combustion may lead to instability with highly undesirable and often dangerous consequences. Prediction of combustion instabilities requires a suitable description of the feedback of the flame to the incoming perturbations, the geometry of the burner and the boundary conditions. This is a fundamental problem of combustion of huge practical significance in the gas turbine industry [Cor-

rea, 1998; Putnam, 1971].

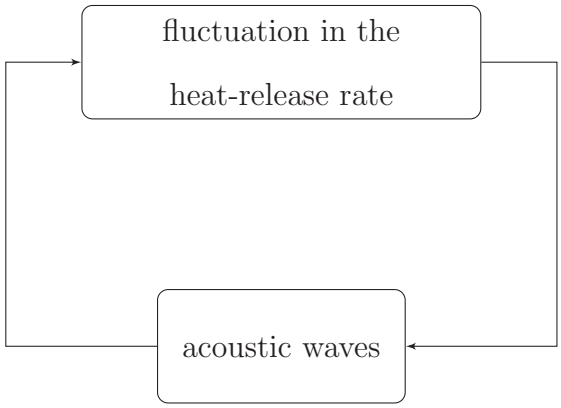

Figure 1.1: Schematic loop of thermoacoustic excitations

1.2 Bibliographical review

Most of the experimental investigations of thermoacoustic systems aim at determining the boundaries of instabilities as function of the system parameters and to study the unstable regions in the parameter space. Theoretical investigations are focusing on modelling the instability boundaries and the limit cycles in the parameter space. In this section we review the most relevant papers on this subject. In most of the applications the heat is provided by either a gauze or by a flame, therefore we review the studies which describes these setups. Comprehensive reviews of earlier thermoacoustic studies are given by [Candel, 1992; Culick, 1994; Harrje and Reardon, 1972; Raun et al., 1993]. These reviews are analyzed and extended with the results of the last decades. In the first half of the following sections (both in case of gauze and flame heating) we review the experimental investigations, in the second one we summarize the analytical studies.

1.2.1 Gauze heating

Rijke [1859] found that when he heated up wires inside a tube with open ends, a clear tone was produced. The sound was nearly the fundamental tone of the tube, and it stopped immediately when the top of the tube was closed or the tube was turned horizontally, which indicated that current of air is necessary for the phenomenon. The

sound stopped as the gauze cooled down, which showed that a gauze hot enough was also necessary. Maximum of the sound intensity was measured when the gauze was located in the middle of the lower half of the tube. Bosscha and Riess [1859] performed a similar experiment in the same year, when he produced sound by forcing hot air through a pipe with a refrigerated gauze and open ends. The location of maximum sound intensity was found when the gauze was located in the middle of the upper half of the tube, i.e. the opposite of Rijke's experiment. Lord Rayleigh [1878] noted that tones higher than the fundamental one could be excited for certain positions of the heated gauze. He suggested a criterion for the instabilities of heat-driven oscillations: pulsations can be triggered or sustained if the heat release is in phase with the pressure fluctuations. This criterion has been widely quoted and applied for many different setups. Richardson [1922] experimentally confirmed Rayleigh's criterion.

Saito [1965] was the first to measure the growth rates of the oscillations in a Rijke-tube, and developed a simple model, which was derived from linear conservation equations. He also explained the weak points of earlier models. Collyer and Ayres [1972] extended experimental observations by measuring higher modes. They placed heated wires into a Rijke-tube at certain locations. They found optimal triggering positions for the second and third modes, and confirmed Rayleigh's criterion for higher modes. Katto and Sajiki [1977] performed a series of measurements with Rijke-tubes as well. They investigated the dependence of the instability boundaries on the system parameters. They observed that the heat input has a minimum value for which instability can build up and found the optimal locations to excite the first and the second modes. This result (the heat input must have a minimum value) confirms the observation that sound attenuates as the gauze cools down.

The first study to describe the heat-release rate of a hot wire was performed by King [1914]. He introduced a non-linear relationship between the instantaneous velocity and the heat-release, however, it was not widely applied to study the Rijke-tube until Heckl [1990]. The first attempt to analyze the phenomenon analytically was carried

out by Lehmann [1937]. He assumed that energy was added to the vibration only during part of the cycle, when cold air layers crossed the gauze. Once the layers were heated they no longer extracted energy during flow reversal. Feldman [1968] showed the following error in Lehmann's theory: the temperature of the air downstream of the gauze is still lower than the one of the gauze, therefore during backflow the air can extract energy when it passes through the heater second time. Flow reversal is not a necessary condition but the consequence of thermoacoustic oscillations. Neuringer and Hudson [1951] investigated under which conditions the sound might be maintained or built up. Experiments showed that the velocity was critical for a given energy input and gauze position, there was only a small range of velocities which would produce the tone. They assumed that turbulence was the dominant source mechanism which leads to instability. Carrier [1955] assumed that flow downstream from the heater was not isentropic, and the viscous losses at the wall resulted in temperature fluctuations. He assumed that viscosity is the most important source of instability.

Merk [1957a,b] created the basis of analytical studies by developing a general equation for predicting the excitations of duct oscillations. A new direction of thermoacoustic research was set, when he introduced the concept of the transfer function method and calculated it for his setup. His analytical predictions showed good agreement with the measurements of Katto and Sajiki [1977]. The first study which applied the wave equation was carried out by Mailing [1963]. He assumed that the width of the heater was small enough to be represented as a point source, and that the released heat was proportional to the velocity fluctuation. The analysis using conservation equations led to very complicated equations. The results showed good agreement with measurements in the low frequencies, but high frequencies were overestimated.

Chu and Ying [1963] arrived theoretically at the conclusion that in their setup the oscillating heat-source can be modeled as an oscillating piston. Rott [1980] arrived theoretically at the same conclusion as Chu and Ying [1963] by using a different geometry. Kwon and Lee [1985] emphasized that the criteria to get instability had been first described by Rayleigh experimentally, and by Putnam and Dennis [1953] theoretically.

They solved the equations of continuity, momentum and energy conservations numerically, and verified Rayleigh's criterion. They showed that dissipation losses play a more important role than radiation or convection losses even for low Mach numbers. Nicoli and Pelce [1987] assumed that the heater was localized, therefore the heat transfer occurred in a small region around the heater. Outside this region the temperature was uniform and the flow disturbances were acoustic waves. They showed that for small Mach number the mean pressure jump across the heat-release region can be neglected, and therefore the tube can be considered isobaric. Their calculation of the heat transfer function is very laborous since it involves the calculation of unsteady heat transfer in a compressible flow of gas.

Culick [1987] provided a general mathematical derivation of Rayleigh's criterion. He extended the observations of [Chu and Ying, 1963; Rott, 1980] to a general geometry, i.e. the effect of an oscillating heat source is analogous to the effect of an oscillating piston. Heckl [1988] used active control to suppress oscillations in a Rijke tube. Pressure oscillations were measured, phase shifted, amplified and fed to a loudspeaker, which significantly reduced the noise level.

1.2.2 Flame heating

Higgins [1802] made the observation that flames might produce tones when a jet of gas was ignited in a tube. The frequency of the tone was near the natural frequency of the tube. Flame driven thermoacoustic oscillations gained attention first during the development of rocket motors and jet propulsion engines in the United States, and later during the development of gas turbines. An overview of the early era of the research in solid propellant rocket motors is given by [Berl, 1963; Culick, 2006]. Instabilities in liquid rockets are simpler than in solid rockets, largely because the geometry of the combustion system is simpler. By the end of the 1940s, there was agreement among researchers that combustion instabilities were present in rocket motors and they were related to the waves in the combustion products. Since the 1950s, instabilities have been observed in case of both small and large rockets. The basics of combustion insta-

bilities had been discovered. Many of the relationships with acoustical properties were identified. In the 1950s and 1960s, lot of theoretical works were published about the oscillations in solid rockets (e.g. [Bird et al., 1963; Cantrell and Hart, 1964; Cheng, 1954, 1962; Hart and McClure, 1959, 1965; Reardon, 1961; Sirignano, 1964; Sirignano and Crocco, 1964]). In this era the view of an instability as a perturbation of classical acoustics was extensively investigated. During the 1960s, the major efforts on combustion instabilities in liquid rockets were motivated by the Apollo vehicle. The research interest was significant in the Cold War as well: launching spacecrafts and missiles, furthermore changing their trajectories. Sub-scale and laboratory tests were the main interests of a lot of research, since large-scale tests were very expensive. Although the problem had been observed in ramjet engines after World War II, it became a mayor problem in the 1970s and 1980s. New programs about instabilities of liquid rockets appeared only in the 1980s ([Fang, 1984; Liang et al., 1986, 1987; Mitchell et al., 1987; Nguyen, 1988; Philippart, 1987; Philippart and Moser, 1988]). In the 1990s, works on instabilities of rocket motors were investigated in Europe mainly due to oscillations in the boosters of Ariane 5.

Acoustic-flame interactions in premixed laminar flames were studied by [Blackshear, 1953; Chu, 1956; Kaskan, 1957; Merk, 1958, 1959; Putnam and Dennis, 1953, 1954, 1956]. Putnam and Dennis [1953] analyzed experimentally combustion driven thermoacoustic oscillations for premixed hydrogen flames. They measured the natural frequencies of the system. The locations for maximum excitation showed good agreement with Rayleigh's criterion. Blackshear [1953] and Kaskan [1957] found that in case of open premixed flames the main source of acoustic driving is the flame surface area variation. This observation has been later widely applied in theoretical studies. Tsuji and Takeno [1965] experimentally investigated the instability boundaries of a laboratory burner with rectangular cross section. They plotted the instability map for the first three modes as a function of the mean pressure and the equivalence ratio. Their plot shows symmetry for the equivalence ratio of 1.1.

Merk [1958, 1959] studied premixed flames by applying the transfer function concept which he had developed for the Rijke-tube. He obtained first order transfer functions and calculated the stability regimes. He confirmed that fluctuation in the heat-release rate is the consequence of the variation of the flame surface area. Thermoacoustic instabilities were analytically investigated by Culick [1963]. He calculated the complex eigenfrequencies by applying linearized equations. Culick [1976] was the first to derive an analytical criterion to obtain instability and limit-cycle behavior.

The idea of a time-lag model was first suggested by von Karman for interpreting instabilities discovered in experiments with liquid propellant rockets at Caltech (Summerfield et al. [1951]). This representation, which became later well-known as the n-τ model in the combustion literature, was a major breakthrough, and it was developed most extensively by Crocco [1951, 1952, 1969]. It was found that the fluctuating heat-release rate can be coupled to the acoustic velocity. Schimmer and Vortmeyer [1977] performed measurements with premixed propane flames. The authors observed a minimum period of oscillations, below which oscillations did not occur. Poinsot et al. [1986] measured the reflection coefficients by microphones when the heat-source was a ducted premixed flame. It was found that the maximum of the reflection coefficient coincides with the resonant frequency of the flame.

The first attempt to describe the flame surface by using the level-set method (LSM) was carried out by Williams [1985]. He derived an equation, which describes the position of the flame, known as the $\mathcal{G}$-Equation in the combustion literature. Since then, the level-set method has become a widely accepted and applied analytical tool to study premixed flame dynamics. Fleifil et al. [1996] studied the radial dependence of the acoustic velocity on the flame kinematics theoretically by using the $\mathcal{G}$-Equation. It was found that the radial dependence of the acoustic velocity is negligible. Dowling [1999] considered a premixed, ducted and bluff-body stabilized flame theoretically. She applied the $\mathcal{G}$-Equation to calculate the flame position and derived a linear transfer function for small amplitude fluctuations analytically. The results of the model showed

good agreement with experiments across a wide range of frequencies.

The linear interaction of the acoustic perturbations with flames was studied by many authors, e.g. [Ducruix et al., 2000; Schuller et al., 2002, 2003]. They found that when the phase-lag is around π, the gain of the transfer function decreases strongly, and it is almost vanishing for phase-lags larger than 10π. The reduced cutoff frequency was close to a frequency corresponding to a wavelength equal to the flame cone length. It has been concluded that the linear model predicts the flame behavior correctly if the phase-lag is less than approximately 2π, however for intermediate and large frequency values the experimental phase-lag is significantly larger than that predicted by their theory.

1.2.3 Non-linearity

1.2.3.1 Non-linearity of the heat release

Combustion instabilities are the dynamics of a self-excited nonlinear system (Culick [2006]). When a combustion chamber is non-linearly unstable, the amplitude tends to a finite value. Understanding the properties of the limit cycles will yield some understanding of those variables which determine its behavior. It is common to model the system as a non-linear oscillator, thereby simply adding a nonlinear term to the acoustic wave equation, and assume that the instability involves only a single mode. [Jensen, 1971; Jensen and Beckstead, 1972] applied this theory to the data taken in laboratory devices. It was found that the data could not be matched with theory well, and no particular kind of nonlinearity seemed to dominate the motions. As a result, the single mode assumption was not successful, i.e. it seemed to be necessary to include at least two modes in the mathematical model, with coupling due to nonlinear processes. The work by [Jensen, 1971; Jensen and Beckstead, 1972] motivated the extension of Galerkin's method to treat nonlinear behavior in liquid rockets ([Powell and Zinn, 1971; Zinn, 1968; Zinn and Lores, 1972; Zinn and Powell, 1970a,b]).

If the power transformed from the heat released to the acoustical motions exceeds the losses, then instabilities grow until either non-linear factors limit this process or

the device is destroyed. Dowling [1997] assumed that the main nonlinear mechanism is the result of the 'saturation' of the heat release rate. Dowling [1999] found that the resulting amplitudes obtained by the numerical solutions of the level-set method are in satisfactory agreement with experiments. She predicted flow reversal during part of the limit-cycle oscillation, which means that the resulting acoustic velocity was larger than the mean flow velocity. In this case the flame was not attached to the flame holder. This property of the flame clearly exhibits the importance of the boundary conditions when one is modeling the flame behavior.

Yoon et al. [2001] found that the non-linear convection becomes important in unstable situations. The heat transfer magnitude should approach zero at low mean flow velocities, the phase shift, which is necessary for thermoacoustic energy conversion, tends to zero at high mean flow velocities, therefore is it possible to have instability only in the intermediate range, which was verified by experiments.

In their theoretical study Wu et al. [2001] used matched-asymptotic-expansion techniques, assumed large activation energy and low Mach number. They gave a general asymptotic formulation for the lower-frequency regime, for which the acoustic source is found to be directly linked to the shape of the flame. This might be the reason why the $\mathcal{G}$-Equation yields results that are in a very good agreement with the measurements. Schuller et al. [2002] showed that the flame motion observed in the experiments may be calculated more accurately if one uses a suitable description of the velocity field in the fresh mixture and a nonlinear flame model. It was found that the flame motion can be accurately described if the acoustic velocity has a convective character. A radial component turned out to be less important.

Matveev and Culick [2003b] argued that since the magnitude of the acoustic velocity tends to be stabilized near the mean flow, and it grows slowly with increase of supplied power, this suggests that flow reversal at the heater location is critical for non-linear modeling. This is related to the convection from the gauze, hence temperature difference must have an important role, and the assumption that the direction of the flow is unimportant is not appropriate. Linear laws, which were obtained by

correlation techniques, can be valid if there is no backflow, since when a particle is crossing the heater more than once, correlation laws are not valid.

1.2.3.2 Other non-linear effects

Disselhorst and van Wijngaarden [1979] investigated the effect of the exit geometry on the flow behavior. It was found that if the end of the tube was round, separation did not occur at high frequencies. In case of a sharp edge, vortices were formed during inflow and shed from the pipe during outflow. They emphasized that taking non-linear viscous and thermal losses into account resulted in obtaining limit-cycles. Nonlinearity in waves became effective only when velocity disturbances were taken into account up to third order of the amplitude of the resulting standing wave. The showed that nonlinearity can be linked to the Strouhal number. It has been confirmed by experiments that at very large Strouhal numbers no vortex formation or separation takes place, the end radiation tends to zero. In case of sharp edges viscosity and end radiation do not contribute to end losses, it is only function of the Strouhal number.

Heckl [1990] described two nonlinear properties that had an important role in the Rijke phenomenon. The first was the sound radiation from the open ends. At high amplitudes the displacement of the particles becomes so large that the air particles leave the tube in form of a jet, but sucked back from all directions and return with a smaller velocity. Therefore the reflection coefficient should include the effect of two different mechanisms, the one of end radiation and the one of non-linear losses.

Matveev and Culick [2002] showed that neither non-linear gas dynamics nor non-linear boundary conditions at the tube ends are of importance for determining the limit cycle properties.

1.2.4 Non-normality

A new direction of thermoacoustic research is non-normality, since recent studies showed the existence of non-normal modes in thermoacoustic systems. In a non-normal system linearly stable modes can trigger instability. An overview of the recent research

in this area is given by Mariappan [2012]. Nicoud and Poinsot [2007] found that the eigenmodes of thermoacoustic systems are non-normal if heat-source is present in the flow and the boundary conditions are described by complex impedance. Kedia et al. [2008] showed that the non-orthogonal property of the system changes the stability significantly. Balasubramanian and Sujith [2008] analyzed the stability of a Rijke-tube using King's law given in [Heckl, 1990; King, 1914]. They found transient growth even in the linearly stable regime. Subramanian and Sujith [2011] performed similar study for premixed flames using the $\mathcal{G}$-Equation. Wieczorek et al. [2011] studied one-dimensional flames and found that the eigenmodes of the system are not orthogonal. They concluded that entropy fluctuation should be accounted in a stability analysis. Juniper [2011a,b] studied the effect of initial conditions on the stability of a Rijke-tube. It was observed that higher noise amplitudes at low frequencies can trigger instability and limit-cycles. Recently, Magri et al. [2013] demonstrated that non-normality in combustion systems is weak, however, Juniper [2011a] also showed that weak non-normality can make a system more unstable. The exact role of non-normality in instabilities therefore remains an interesting question.

1.3 Overview

The review of the literature allows us to summarize us the current understanding of the potential sources for thermoacoustic instabilities:

1. **Pulsating feed supply**

   Pressure oscillations in a combustion chamber can result in pulsation of the fuel supply. If the heat release and pressure oscillations are in phase, then the oscillations will be amplified. It is more important in case of diffusion flames, but it may be also important in some cases of premixed flames. It can be eliminated by creating a choked feed and therefore a large pressure drop.

2. **Turbulence**

   Turbulence may occur when velocity is high or bluff body flame holders are

used. Mugridge [1980] reported experimental and theoretical work on stability of turbulent flames in a burner. Valk [1981] measured acoustic power and frequency change in propane combustion.

3. **Pressure coupling**

   Pressure coupling is common in high-pressure combustion systems operated with undiluted oxidizer, such as in case of solid propellant rocket motors. It's the coupling between acoustic pressure oscillations at the surface of a burning solid propellant and the combustion processes of the propellant, which can lead to the amplification of the combustion process.

4. **Pulsating laminar flame speed and variation of the flame surface area**

   Many of the studies confirmed that the variation in the heat-release rate is the result of the oscillation of the flame surface area. For premixed flames the heat release rate is usually coupled with the acoustic velocity.

In the theoretical investigations the following assumptions have been widely used (as reviewed in e.g. Raun et al. [1993]):

1. **Constant properties in the cold and hot sections**

   In most of the studies uniform properties were assumed in the cold and hot regions, with a jump in the region of the energy release.

2. **One-dimensional flow without boundary layer effects**

   Usually the properties are assumed to be one-dimensional and uniform in the cross section. The exception is the study by Carrier [1955], in which he included the effects of the walls.

3. **Small amplitude oscillations**

   This assumptions allows linearization of the governing equations.

4. **Compact heat-source**

   Since usually the width of the heat-release region is much smaller than the acoustic wavelength, it is often treated as a discontinuity.

5. **Negligible body forces**

   In most of the experimental setups current of air or mixture is forced to flow through a duct, hence gravity is assumed to have negligible effects.

6. **Small Mach number**

   Since the Mach number is usually of order $O(10^{-2})$, interaction of the mean flow and the acoustic field is neglected. The exception is Neuringer and Hudson [1951], who did not neglect this effect.

In the thesis the assumptions (2-6) are applied. Assumption (1) is found restrictive and it is not used, the effect of the non-uniform axial mean temperature is studied.

1.4 Scope of the thesis

The scope of the present thesis is to extend the earlier models and draw conclusions by comparing the analytical predictions to measurements.

It has been shown that the most important mechanism of thermoacoustic oscillations is the non-linear feedback of the flame, however, a general model has not been derived yet, which separates the effects of the unexcited system and the non-linear feedback of the heat-source. We focus on this problem by introducing the concept of the Green's function method. Using the Green's function approach we aim at deriving the governing equation of an active single mode of the acoustic velocity assuming a general flame model.

Once the non-excited resonator is described accurately, we focus on the description of the non-linear heat-release. It has been found by many authors experimentally that the flame surface area variation is the primary reason of the fluctuations in the heat-release rate. A general non-linear heat-release rate law has not been derived yet, therefore we aim at analyzing the kinematics of flames theoretically, and deriving a new non-linear heat-release law.

This non-linear heat-release law is applied to derive an analytical instability criterion. At the last stage we aim at identifying a weakly non-linear regime in the parameter space, and describing the effect of the parameters on the resulting limit-cycle amplitudes and frequencies.

1.5 Structure of the thesis

Earlier studies concluded that accurate modelling of thermoacoustic instabilities requires the suitable description of the unexcited system and the non-linear feedback of the flame. By applying this conclusion we focus on five main objectives in the thesis. Each of them are addressed in separate chapters. The structure of the thesis is shown in Figure (1.2).

In §2 an industrial gas turbine is presented and compared to the LIMOUSINE lab-

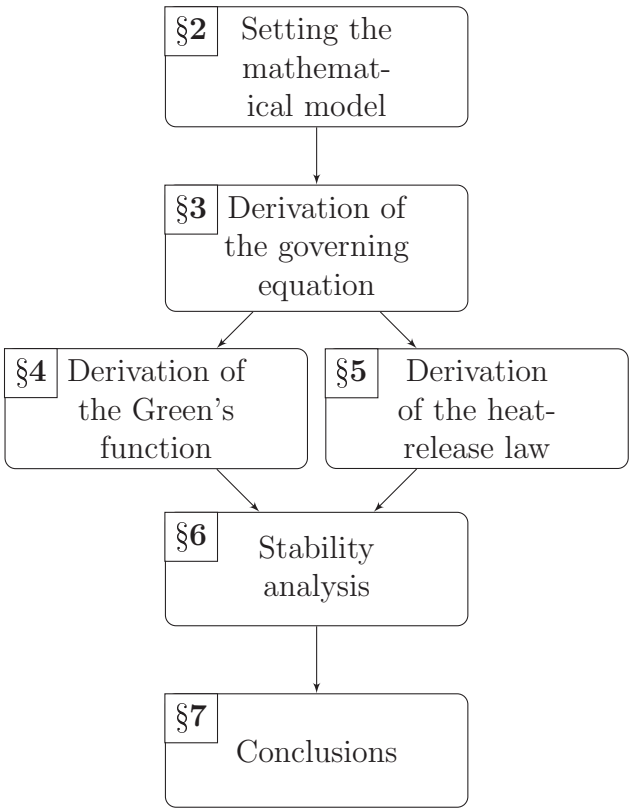

Figure 1.2: Structure of the thesis

oratory burner. The first objective is to set the mathematical model of the laboratory burner, furthermore analyze the assumptions. In the mathematical model the effect of the mean temperature gradient is included.

In §3 the governing differential equation of the acoustic pressure is derived in the time-domain from the most general form of the conservation equations. Thus, a more general form of the wave equation with heat-source and non-uniform mean temperature is obtained. The simplifying assumptions and their consequences are discussed.

In §4 the Green's function concept is introduced following the description of Heckl and Howe [2007]. General solutions are derived and applied to solve the wave equation with a heat source and non-uniform mean temperature. Five, increasingly complex versions of the mathematical model are developed. Conclusions about the required complexity of a mathematical model are drawn by comparing the results to measurements.

In §5 the kinematics of the ducted premixed flames are analyzed by applying an

analytical tool, the $\mathcal{G}$-Equation. Non-linearities of different origins and the importance of the boundary conditions are studied. The solutions are compared, and a new non-linear heat-release rate law is derived.

In §6 the governing differential equation of an active single mode for an arbitrary heat-release rate law is presented. By applying our non-linear model of §5, the criterion of thermoacoustic instability in our laboratory burner is obtained. The stability parameter map of the LIMOUSINE burner is derived as function of the system parameters. By applying weakly non-linear theory solutions are derived for the limit-cycle amplitudes and frequencies. The effect of the parameters on these quantities are discussed.

In §7 the thesis is concluded by a short summary of the results, discussion of the new questions that arise, and directions of further research.

Chapter 2

Real and model burners

The objective of the present chapter is to introduce a real gas turbine combustor, a laboratory burner, and the mathematical model of the laboratory burner. A real burner is a very complex hence expensive system, therefore a laboratory burner is more suitable for research purposes. We describe a particular laboratory burner, the LIMOUSINE burner, and the details of the measurements. We develop a mathematical model of the laboratory burner, and justify every simplification, which was applied during the model building. We also show that our laboratory burner exhibits the properties of a real burner, which are important from a thermoacoustic point of view.

2.1 Real burners

First J. Barber proposed in 1791 that gas turbines may be used to produce energy, however, the first industrial gas turbine was installed only around 1930 [Bohl and Elmendorf, 2004, p.195]. At the beginning it was mostly applied for energy production in mountains, because the energy producing capability of the internal combustion engines drops significantly with increasing altitude. A real gas turbine and its components are shown in Figure (2.1).

The thermodynamic process of the complete gas turbine is described in theory

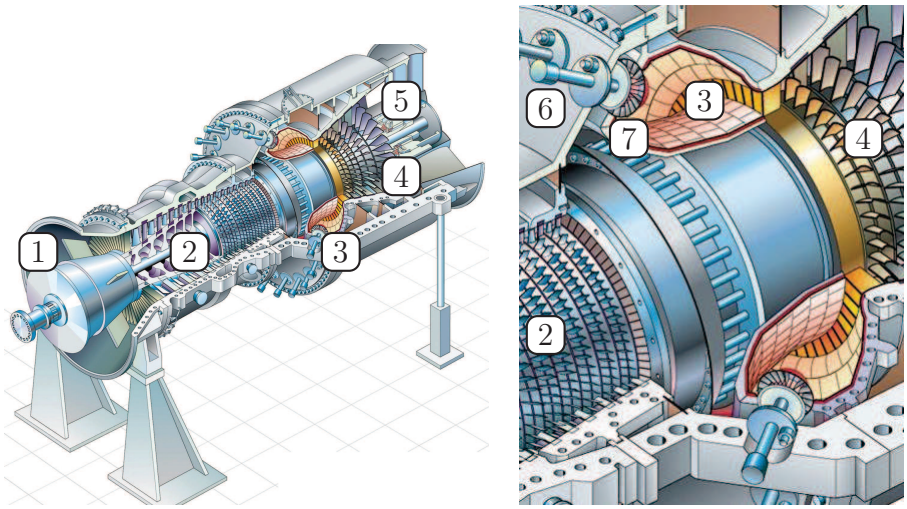

(a) Sectional view of a turbine (b) Details of the combustor zone

Figure 2.1: Siemens SGT5-4000F gas turbine 1 - Inlet, 2 - Compressor, 3 - Combustion chamber, 4 - Turbine, 5 - Exhaust, 6 - Fuel inlet, 7 - Swirler (image source: www.siemens.com)

by the Brayton cycle (Figure (2.2)). A small pocket of working gas goes through an adiabatic compression and expansion, and of an isobaric combustion and heat rejection.

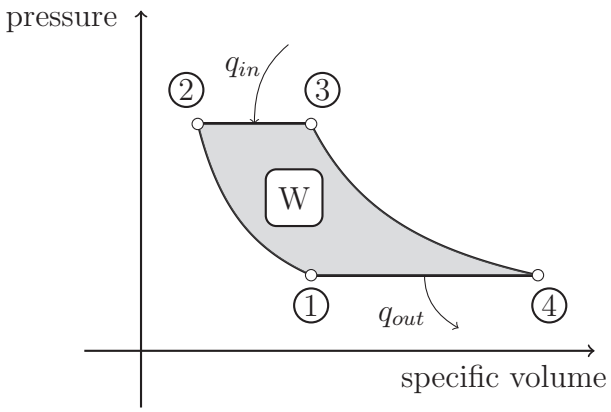

Figure 2.2: Brayton cycle, 1→2: compression, 2→3: combustion, 3→4: expansion, 4→1: rejection, W: mechanical energy

The efficiency increases with higher temperature and pressure of the combustion chamber, therefore the effect of increasing these two quantities has been the subject of a lot of research. In modern gas turbines the temperature in the combustion chamber is around 1600K. The temperature in the core of the flame is close to the adiabatic flame temperature. The adiabatic flame temperature is a thermodynamic property of fuels, for a wide range of practically applied gases it is approximately 2200K. The

temperature changes at every stage of the Brayton cycle. It is increased during the compression and combustion, and it is decreased during the expansion and rejection. The pressure is increased in the compressor, decreased in the turbine, and it is approximately constant while combustion occurs. This property allows building a model turbine operating under non-pressurized conditions and studying the underlying phenomena in a laboratory.

As shown in Figure (2.1), an industrial gas turbine is a very complex, hence expensive system. To investigate such a system analytically and experimentally, simplifications need to be made. These simplifications must be such, that they preserve the important physical effects, but eliminate those, which are unimportant from a thermoacoustic point of view.

This study is part of the Marie Curie research network LIMOUSINE, which was set up to model thermoacoustic instabilities in gas turbines. LIMOUSINE is a multidisciplinary network of individual research projects that focus on the combustion chamber of a gas turbine and model it with experimental, numerical and analytical approaches. The core of the LIMOUSINE network is a laboratory burner, which has been specifically designed to simulate thermoacoustic instabilities in the combustion chamber of an industrial gas turbine. The role of this PhD study was to model the laboratory burner using largely analytical tools. A corresponding experimental study was performed by Müller and Hermann, who built the model burner and provided experimental data Kosztin et al. [2013].

2.2 The LIMOUSINE model burner

The model burner is shown in Figures (2.3) and (2.4). It consists of a rectangular tube with a large aspect ratio. The flame is partially premixed and stabilized by a bluff body. Air enters at the bottom of the combustor (1). The prismatic flame holder (7), triangular in cross section, is placed at about one quarter of the height of the combustor. The cross-sectional area is piecewise constant with a step at the flame-holder, where it jumps to double the value of the upstream section. The combustor burns methane

at atmospheric pressure, which is injected at the flame holder through 2×33 holes of 1.2 mm diameter (2). The air required for combustion flows into the pre-combustion chamber (1) through a 3mm thick injector plate with a grid of 3×22 holes of 0.8 mm diameter (6). The rectangular walls are made from 1.5 mm stainless steel. There are holes along the length of the combustor wall for sensors (4). These holes are closed while performing the measurement. The burner is divided into two parts by the flame: a cold upstream and a hot downstream region. The length of the cold and hot sections are 0.324 m and 1.1 m respectively. The total length of the burner is 1.424 m.

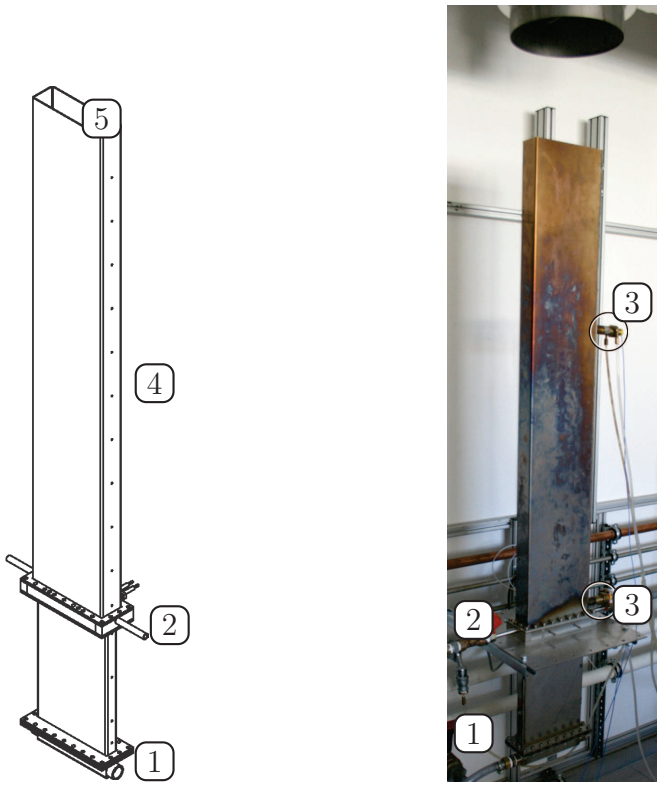

(a) Ifta model burner (b) Installation in the lab

Figure 2.3: Model gas turbine of IfTA GmbH 1 - Air inlet, 2 - Fuel inlet, 3 - Pressure transducers, 4 - Measurement holes, 5 - Outlet

Thermoacoustic instability was observed and measured in the model combustor at an operating point of P = 21 kW thermal power and an air ratio of 1.4, implying an air flow of $\dot{m}$ = 10 g/s. This operating point was chosen to guarantee combustion instability at a relatively low power, while avoiding blow-out of the flame. Figure (2.6) shows the time-history (a) and the corresponding spectrum (b) of the pressure oscillation,

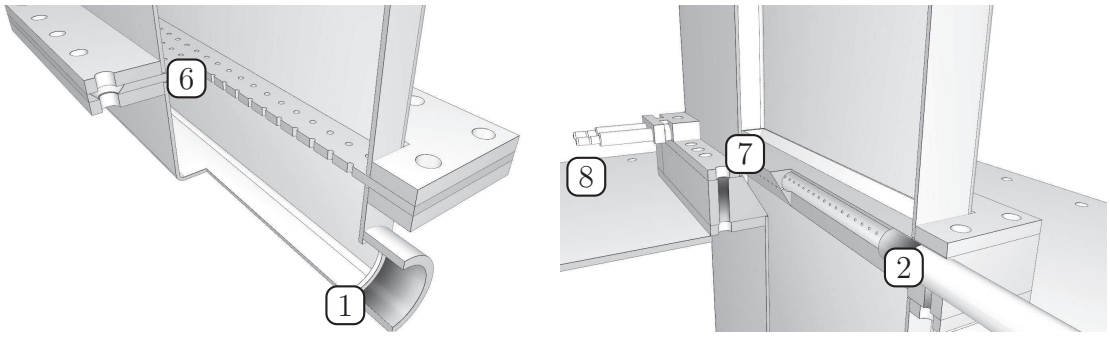

(a) Air inlet (b) Flame holder

Figure 2.4: Model gas turbine of IfTA GmbH 1 - Air inlet, 2 - Fuel inlet, 6 - Grid, 7 - Flame holder, 8 - Igniter

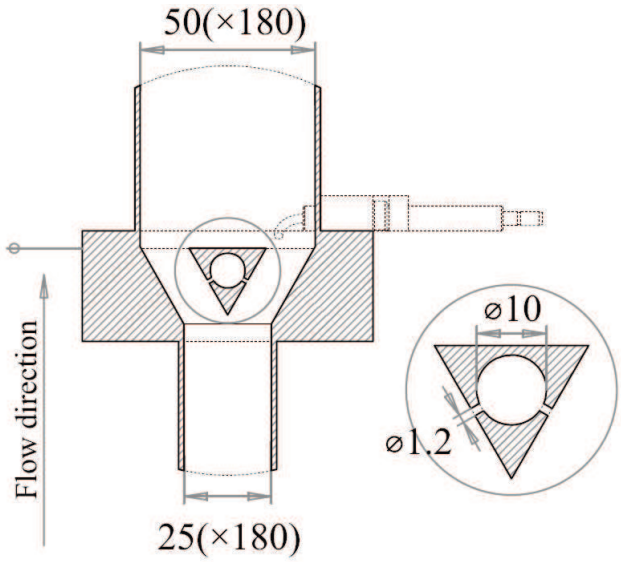

Figure 2.5: Cross-section of the burner at the height of the flame holder

measured 21.4 mm above the flame holder. The dominant frequency is 115 Hz, and the pressure amplitude at that frequency is about 1800 Pa; this about 2% of the mean pressure. The axial distribution of the mean temperature and the acoustic pressure amplitude were measured. The data are plotted in Figure (2.7). The temperature values have not been corrected to take account of the heat radiation by the wall and by the flame on the thermocouple that was used for the measurements. Therefore, there is a potential error in the plotted temperature values. The temperature profile is approximately piecewise linear with positive gradient in the inlet section and a negative gradient in the outlet section, due to the preheating and cooling effects of the wall. The temperature inside the flame could not be measured.

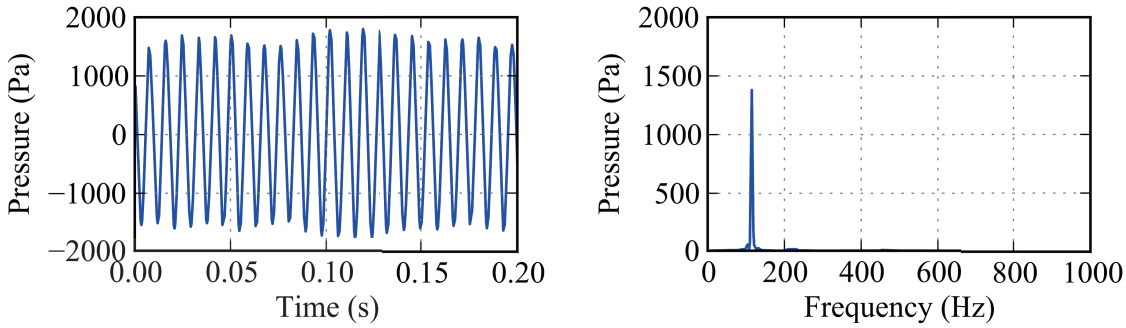

(a) Time history of the oscillation

(b) Frequency response of the burner

Figure 2.6: Measurement results: (a) time history and (b) critical frequency of the burner

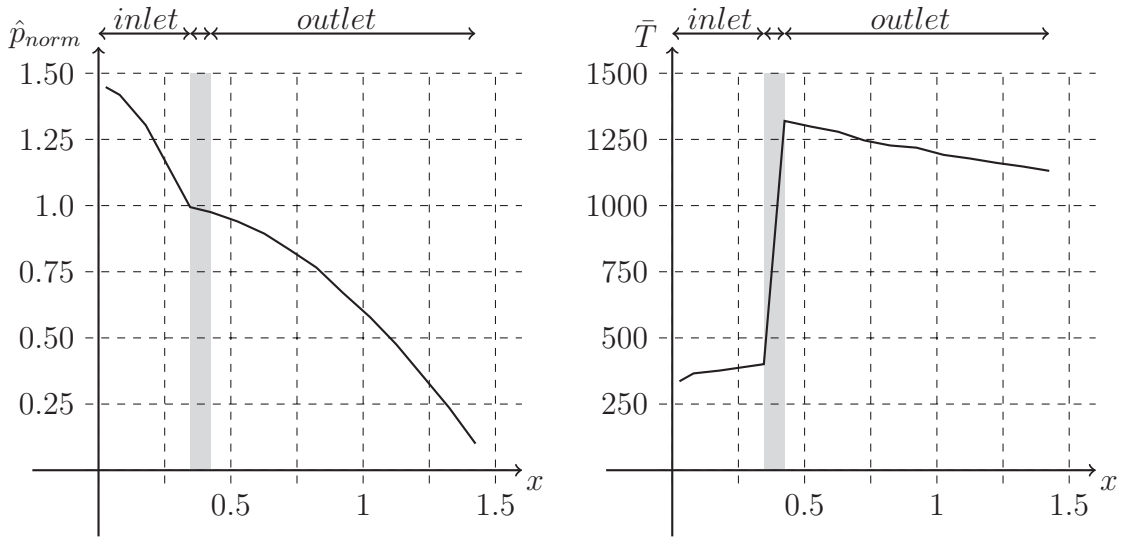

(a) Pressure

(b) Temperature

Figure 2.7: (a) Normalized pressure and (b) axial temperature [K] in function of the axial position [m] of the model burner (measurement by IfTA GmbH, Gröbenzell near Munich, Germany)

Pressure reflection coefficients were measured directly in the unstable burner by applying the two-microphone method (Seybert [1988]) at the instability frequency of 115 Hz. The two-microphone method involves measuring the sound pressure simultaneously at two locations near the end of interest. The forward and backward traveling waves can then be identified individually, and the ratio of their complex pressure amplitudes at the end gives the reflection coefficient. At the lower end, the pressure was measured with microphones at $x = 180$ mm and 80 mm; these positions were chosen because they

have a relatively large difference in pressure amplitude, giving more accurate results for the argument of the reflection coefficient. This was found to be $R_0 = 0.8 - i0.22$. It is quite similar to that of a rigidly closed end, where $R = 1$, but in this case there are also losses, as indicated by $|R_0| = 0.83 < 1$. At the upper end, the pressure was measured at the positions of x=1426 mm and 1326 mm (to minimize the influence of the temperature gradient), and the reflection coefficient turned out to be $R_1 = -0.95 + i0.14$. The magnitude is 0.964, indicating that only minor losses occur at this duct end. Also, there is a pressure node just outside the tube at a distance of 66.5 mm. The wavelength of the fundamental mode is approximately one quarter of the tube length. The mean velocity in the burner is 2-4 m/s. Further details about the model burner can be found in Kosztin et al. [2013].

2.3 The mathematical model for the LIMOUSINE burner

In order to develop a mathematical model, several simplifying assumptions need to be made. In this section we will describe the modelling assumptions and justify them. We treat the fuel-air mixture as a perfect gas carrying linear acoustic waves. Non-linear acoustic effects are neglected. The geometry of our model is shown in Figure (2.8). The tube is divided into three regions: inlet region, flame region and outlet region, and we assume one dimensional conditions in each of these regions. The combustor extends from $x = 0$ (upstream end) to $x = L$ (downstream end). The interfaces between these three regions are at $x = l_1$ and $x = l_2$ (see Figure (2.8)). The locations of the interfaces are fixed. We neglect the mean flow velocity. The axial mean temperature is not uniform. We will apply 5 different mean temperature profiles. The ends of the burner are modelled by complex pressure reflection coefficients.

We list and justify our modeling assumptions:

- perfect gas. In thermoacoustics it is usually applied that the working fluid is

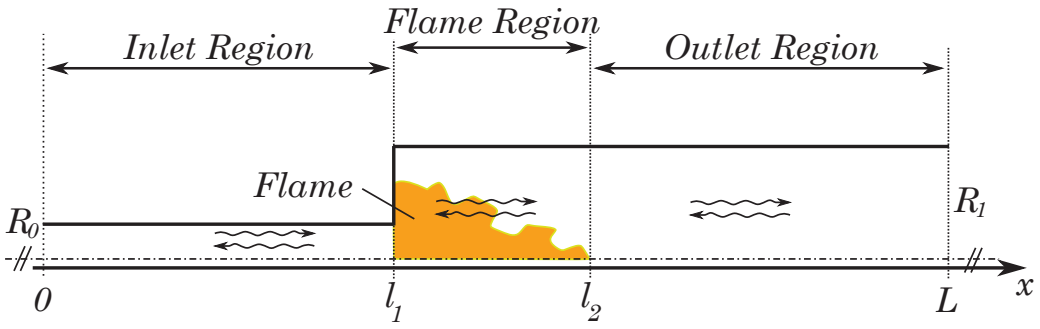

Figure 2.8: Analytical model of the burner

perfect, which implicitly assumes that the molecules do not interact. It is more valid at low pressure and high temperature. The compressibility factor based on the state equation is defined as $p/\rho RT$. For ideal gases it is unity, for real gases it is non-unity and depends on the pressure and on the temperature. At temperatures present in gas turbines the compressibility factor of air can be taken as unity with less than 5 percent error even at extremely high pressure [Green, 1999, p.188].

- low Mach number. The mean flow velocity in the model turbine is 2-4 m/s and the speed of sound varies between 350 and 650 m/s, therefore the Mach number is of the order of 10^{-2}.

- one dimensional wave propagation. The frequency of the fundamental mode is approximately determined by the geometry. At frequencies where the acoustic wavelength is of the order of the cross-section peripheral length, or less, interference between wall reflections produces non-plane propagating forms of sound field that are characteristic of the shape of the duct cross section, which are termed as acoustic duct modes. In rectangular waveguides the condition for axially propagating waves is that $\omega H/c > \pi$, where H is the height of the waveguide [Fahy, 2001, p.220]. In the LIMOUSINE burner the maximal width is $H = 0.18$ m and the minimal speed of sound is $c = 350$ m/s, therefore the cut-off frequency for transverse mode propagation is approximately 1000 Hz, which is much larger than the unstable frequency, therefore the one-dimensional assumption is reasonable.

- constant axial mean pressure. Because the mean flow Mach number is small and

waves are one-dimensional, we assume that the axial mean pressure is constant. The mathematical justification is provided in the following chapter.

- perfectly rigid walls. We assume that the walls of the model turbine are perfectly rigid, i.e. the boundary condition is that the normal velocity component vanishes. In real burners the walls might vibrate, the coupling of these vibrations with the oscillations is however beyond the scope of this thesis.

- locations of the interfaces are fixed. In the mathematical model we distinguish regions with different mean temperatures and connect them by conservation laws. We assume that the location of these interfaces are fixed and they are not influenced by the oscillations.

- linear acoustic waves. Measurement showed that the amplitude of the pressure oscillation is two orders of magnitude smaller than its mean value. It is therefore reasonable to neglect any non-linear effects in the purely acoustic realm.

- turbulence. The flow and therefore the flame in the burner is turbulent, however we neglect it because we focus on analytic description of the phenomena, furthermore we have no reliable measurement data for turbulence.

- simplification of the geometry. Around the flame holder the real geometry has been simplified, i.e. we focus on the change of the cross section only (see Figure (2.5)). We also neglect the drag force acting on the flow from the flame holder.

- axial mean temperature profile. The temperature and therefore the speed of sound varies significantly as the working gas flows through the burner. To model this we use 5 different versions of the mathematical model. The only difference between these versions is the approximation of the measured axial mean temperature profile in the inlet, flame and outlet regions.

    1. In the first configuration we aim to give explicit analytical formulas for the critical acoustic properties, such as the eigenfrequency and damping rate. To this end we assume that the flame region is infinitely thin and located at

the point where the cross section changes ($x = l_1 = l_2$). The temperature is constant in the inlet and outlet regions. In the next chapter we show that if there is no heat-source in the domain and neglect thermal conduction then the axial mean temperature is constant for low mean flow Mach number.The flame region of this version is modelled as a point in which the axial mean temperature has a jump.

2. In the second configuration we take the width of the flame into account, therefore the location of the jump in the cross-section ($x = l_1$) and the location of the jump in the mean temperature ($x = l_2 \neq l_1$) differs. We assume constant mean temperature in the inlet, flame and outlet regions. We solve the governing equation for the eigenfrequency and damping rate numerically.

3. In the third configuration we develop the second version by assuming that the axial mean temperature in the flame region is linear. In the inlet and outlet regions it remains constant.

4. In the fourth configuration we assume linear axial mean temperature in the inlet, flame and outlet regions, i.e. we consider the pre-heating and cooling effect of the walls. It can be shown that both in case of laminar and turbulent flows that axial temperature profile is linear if there is constant heat flux through the walls [Bird et al., 2002, pp.310-414.]. The non-uniformity is the consequence of taking transverse heat conduction into account.

5. In the fifth configuration we use quadratic axial mean temperature profile in the flame region, and linear profiles in the inlet and outlet regions.

We will compare the predictions of each configurations of the mathematical model with the measurement data. Conclusions will be drawn about the applied temperature profiles.

- thermal conduction and viscosity. In order to neglect viscosity and thermal conduction the following conditions need to be satisfied [Blackstock, 2000, pp.304-

310]:

$$\frac{\mu\omega}{\rho_0 c_0^2} = \frac{\mathrm{St}}{\mathrm{Re}}\mathrm{Ma}^2 \ll 1 \tag{2.3.1a}$$

$$\frac{\kappa\omega}{\rho_0 c_0^2 c_p} = \frac{\mathrm{St}}{\mathrm{Re}\cdot\mathrm{Pr}}\mathrm{Ma}^2 = \frac{\mathrm{St}}{\mathrm{Pé}}\mathrm{Ma}^2 \ll 1 \tag{2.3.1b}$$

where St denotes the Strouhal number ($\omega l_0/v_0$), Re is the Reynolds number ($l_0 v_0 \rho_0/\mu$), Pr is the Prandtl number ($c_p\mu/\kappa$), Ma is the Mach number (v_0/c_0), and Pé is the Péclet number ($\mathrm{Re}\cdot\mathrm{Pr}$). Measurements showed that these conditions are satisfied.

2.4 Conclusions

In this chapter an industrial turbine, an unstable laboratory burner and its mathematical model were presented. A real gas turbine is a very complex, hence expensive system, therefore a model combustor is more suitable for research purposes, in which we can study the effect of varying a large number of parameters. Figure (2.9) shows the modelling steps. The emphasis in this thesis is on the second step.

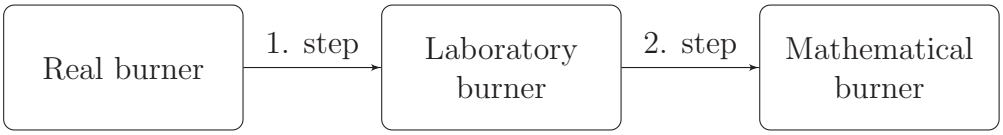

Figure 2.9: Illustration of the modelling steps

We have also justified the simplifications of the second step. Figure (2.10) summarizes the assumptions that have been applied through the analysis.

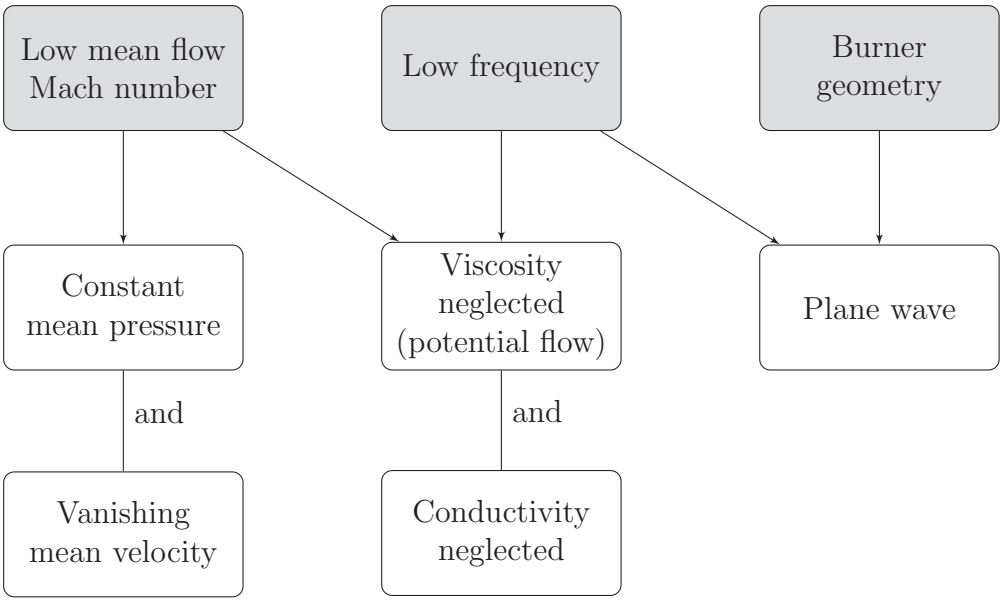

Figure 2.10: Summary of assumptions and their consequences

Chapter 3

Governing equation for one-dimensional waves in a medium with non-uniform temperature

In this chapter we derive the governing equation of the acoustic pressure in a medium with non-uniform temperature. We show the consequences of the simplifications which were discussed in the previous chapter. Exact solutions of some special cases of the axial mean temperature profile will be analyzed.

3.1 Derivation of the governing equation

In this chapter we derive the governing differential equation of the acoustic pressure, in which the axial mean temperature gradient is taken into account. The starting point is the most general form of the conservation of the extensive properties: mass,

momentum and energy.

$$\frac{\partial \rho}{\partial t} + \nabla \cdot (\rho \boldsymbol{u}) = 0 \ , \tag{3.1.1a}$$

$$\rho \frac{\partial \boldsymbol{u}}{\partial t} + \rho \boldsymbol{u} \cdot \nabla \boldsymbol{u} = -\nabla p + \rho \boldsymbol{g} - \nabla \cdot \boldsymbol{\tau} \ , \tag{3.1.1b}$$

$$\rho c_p \frac{\partial T}{\partial t} + \rho c_p \boldsymbol{u} \cdot \nabla T = \kappa \nabla^2 T + Q - \left(\frac{\partial \ln \rho}{\partial \ln T} \right) \left(\frac{\partial p}{\partial t} + \boldsymbol{u} \cdot \nabla p \right) - \boldsymbol{\tau} : \nabla \boldsymbol{u} \ , \tag{3.1.1c}$$

where ρ is the density, $\boldsymbol{u}$ is the velocity vector, p is the pressure, c_p is the specific heat capacity at constant pressure, T is the temperature, κ is the thermal conductivity, Q is the local heat-release rate per unit volume, $\boldsymbol{g}$ is the body-force, $\boldsymbol{\tau}$ is the viscous momentum flux tensor, $\nabla \cdot \boldsymbol{\tau}$ is the divergence of tensor $\boldsymbol{\tau}$, and $-\boldsymbol{\tau} : \nabla \boldsymbol{u}$ is the scalar product of tensors $\boldsymbol{\tau}$ and $\nabla \boldsymbol{u}$, which describes the degradation of mechanical energy into thermal energy, sometimes called viscous dissipation heating. Applying the assumptions of Chapter 2 the conservation equations are simplified to

$$\frac{\partial \rho}{\partial t} + \frac{\partial}{\partial x}(\rho u) = 0 \ , \tag{3.1.2a}$$

$$\rho \frac{\partial u}{\partial t} + \rho u \frac{\partial u}{\partial x} = -\frac{\partial p}{\partial x} \ , \tag{3.1.2b}$$

$$\rho c_p \frac{\partial T}{\partial t} + \rho c_p u \frac{\partial T}{\partial x} = Q + \frac{\partial p}{\partial t} + u \frac{\partial p}{\partial x} \ . \tag{3.1.2c}$$

There are 5 unknowns in the system of conservation equations (Eq. 3.1.2a - 3.1.2c), therefore we need another 2 equations to calculate ρ, u, p, T and Q. We apply the state equation of a perfect gas,

$$p = \rho \mathcal{R} T \ , \tag{3.1.3}$$

where $\mathcal{R}$ is the specific gas constant. The fifth equation will be introduced later, which

relates the heat-release rate per unit volume Q to the remaining quantities. We decompose all quantities into steady and time-dependent parts, for instance $u(x,t) = \bar{u}(x) + u'(x,t)$. Carrying out this procedure yields equations for the mean and fluctuating quantities. For the mean quantities we get

$$\bar{\rho}\frac{\partial \bar{u}}{\partial x} + \bar{u}\frac{\partial \bar{\rho}}{\partial x} = 0 \ , \tag{3.1.4a}$$

$$\bar{\rho}\bar{u}\frac{\partial \bar{u}}{\partial x} = -\frac{\partial \bar{p}}{\partial x} \ , \tag{3.1.4b}$$

$$c_p\bar{\rho}\bar{u}\frac{\partial \bar{T}}{\partial x} = \bar{Q} + \bar{u}\frac{\partial \bar{p}}{\partial x} \ . \tag{3.1.4c}$$

Combining the first two equations gives

$$\frac{\partial}{\partial x}\left(\bar{\rho}\bar{u}^2 + \bar{p}\right) = 0 \ . \tag{3.1.5}$$

The definition of the speed of sound is $c = dp/d\rho$. The sound propagation in the burner is an isentropic process (p/ρ^γ=constant, where γ is the specific heat ratio), therefore we can express the speed of sound squared as $\bar{c}^2 = \gamma\bar{p}/\bar{\rho} = \gamma\mathcal{R}\bar{T}$. We insert $\bar{\rho} = \gamma\bar{p}/\bar{c}^2$ into Eq. (3.1.5) to get

$$\frac{\partial}{\partial x}\left[\bar{p}\left(1 + \gamma \mathrm{Ma}^2\right)\right] = 0 \ . \tag{3.1.6}$$

Eq. (3.1.6) shows that if the mean flow Mach number is small enough, the axial mean pressure is constant. Combining the mean momentum equation with the mean energy equation yields

$$\frac{\partial}{\partial x}\left[\bar{T}\left(1 + \frac{\gamma - 1}{2}Ma^2\right)\right] = \frac{\gamma - 1}{\gamma\mathcal{R}}\frac{\bar{Q}}{\bar{\rho}\bar{u}} \ . \tag{3.1.7}$$

We can see that for low mean flow Mach number the axial mean temperature (just like the axial mean pressure) is constant if there is no heat-source present in the flow, i.e. $\bar{Q} = 0$. In the equations which describe the fluctuating quantities we apply the vanishing mean flow velocity and linear wave assumptions to get

$$\bar{\rho}\frac{\partial u'}{\partial t} + \frac{\partial p'}{\partial x} = 0 \ , \tag{3.1.8a}$$

$$\frac{\partial p'}{\partial t} + \gamma\bar{p}\frac{\partial u'}{\partial x} = (\gamma - 1)Q' \ . \tag{3.1.8b}$$

We take the spatial derivative of the first equation, the time-derivative of the second, and subtract the first one from the second one:

$$\frac{1}{\bar{c}^2}\frac{\partial^2 p'}{\partial t^2} - \frac{\partial \bar{\rho}}{\partial x}\frac{\partial u'}{\partial x} - \frac{\partial^2 p'}{\partial x^2} = \frac{\gamma - 1}{\bar{c}^2}\frac{\partial Q'}{\partial t} \ . \tag{3.1.9}$$

We then substitute for $\partial u'/\partial x$ by using the momentum equation

$$\frac{1}{\bar{c}^2}\frac{\partial^2 p'}{\partial t^2} + \frac{1}{\bar{\rho}}\frac{\partial \bar{\rho}}{\partial x}\frac{\partial p'}{\partial x} - \frac{\partial^2 p'}{\partial x^2} = \frac{\gamma - 1}{\bar{c}^2}\frac{\partial Q'}{\partial t} \ . \tag{3.1.10}$$

Because the axial mean pressure gradient vanishes, taking the spatial derivative of the mean component of Eq. (3.1.3) yields

$$\frac{1}{\bar{\rho}}\frac{\partial \bar{\rho}}{\partial x} = -\frac{1}{\bar{T}}\frac{\partial \bar{T}}{\partial x} \ , \tag{3.1.11}$$

and therefore the governing differential equation of the acoustic pressure at low Mach number is

$$\frac{1}{\bar{c}^2}\frac{\partial^2 p'}{\partial t^2} - \frac{1}{\bar{T}}\frac{\partial \bar{T}}{\partial x}\frac{\partial p'}{\partial x} - \frac{\partial^2 p'}{\partial x^2} = \frac{\gamma - 1}{\bar{c}^2}\frac{\partial Q'}{\partial t} \ . \tag{3.1.12}$$

This is the wave equation of the acoustic pressure in a fluid with non-uniform axial mean temperature. The fluctuating heat-release rate appears as forcing term on the R.H.S. . Sujith et al. [1995] focused on the exact analytical description of the effect of the temperature gradient on the acoustic wave propagation. They assumed that there is no heat-source in the flow ($Q = 0$), and derived the homogeneous form of Eq. (3.1.12). This study was followed by Sujith [2001], in whose analysis the heat-source term Q was included. He derived Eq. (3.1.12) in the frequency domain in a similar way. He showed that the axial mean pressure is constant for a one-dimensional system, if the mean flow Mach number is small. This is in line with our Eq. (3.1.6). We also derived an equation for the axial mean temperature (Eq. (3.1.7)), and found that the axial mean temperature is constant if there is no heat-source in the domain of interest, and the mean flow Mach number is small.

3.2 Solutions of the governing equation without forcing

There is no general solution of Eq. (3.1.12) for an arbitrary axial mean temperature profile $\bar{T}(x)$, therefore we consider three special cases. The homogeneous form of Eq. (3.1.12) in the frequency domain is

$$\bar{T}\frac{d^2\hat{p}}{dx^2} + \frac{d\bar{T}}{dx}\frac{d\hat{p}}{dx} + \frac{\omega^2}{\gamma\mathcal{R}}\hat{p} = 0. \tag{3.2.1}$$

3.2.1 Uniform mean temperature profile

In case of vanishing temperature gradient Eq. (3.2.1) becomes the ordinary wave equation:

$$\frac{\partial^2 \hat{p}}{\partial x^2} + \frac{\omega^2}{\bar{c}^2}\hat{p} = 0 \ . \tag{3.2.2}$$

The solutions are complex exponentials.

$$\hat{p} = C_0 \exp\left(i\frac{\omega}{\bar{c}}x\right) + C_1 \exp\left(-i\frac{\omega}{\bar{c}}x\right) \ , \tag{3.2.3}$$

where C_0 and C_1 are constants to be determined from the boundary conditions. Figure (3.1) shows the real and imaginary parts of $\exp(i\omega x/\bar{c})$ in function of the axial position x for typical values of laboratory burners, $\omega = 1000\ 1/s$ and $\bar{c} = 500\ m/s$.

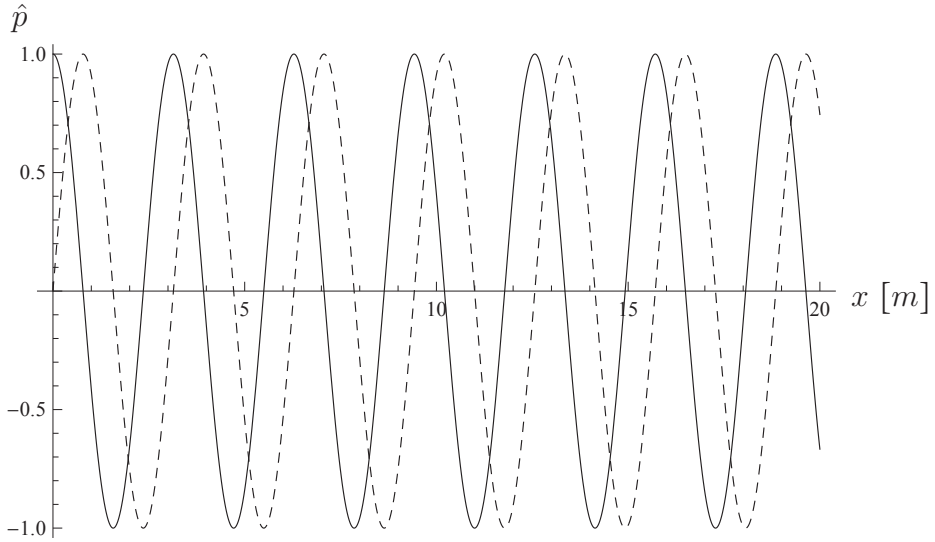

Figure 3.1: Real and imaginary parts of $\exp(i\omega x/\bar{c})$ for typical values of laboratory burners, $\omega = 1000\ 1/s$ and $\bar{c} = 500\ m/s$ (——: cosine, − − −: sine)

3.2.2 Linear mean temperature profile

If the mean temperature profile is linear ($\bar{T} = T_0 + mx$, where T_0 is the temperature at $x = 0$, m is the temperature gradient, which is constant in this case), Eq. (3.2.1) becomes

$$(T_0 + mx)\frac{d^2\hat{p}}{dx^2} + m\frac{d\hat{p}}{dx} + \frac{\omega^2}{\gamma\mathcal{R}}\hat{p} = 0 \ . \tag{3.2.4}$$

This is a zeroth order Bessel-equation. Applying complex notations the traveling wave solutions are the zeroth order Hankel functions of the first and second kind

$$\hat{p} = C_0 H_0^{(1)}\left(\frac{2\omega}{|m|}\sqrt{\frac{T_0 + mx}{\gamma\mathcal{R}}}\right) + C_1 H_0^{(2)}\left(\frac{2\omega}{|m|}\sqrt{\frac{T_0 + mx}{\gamma\mathcal{R}}}\right), \tag{3.2.5}$$

where C_0 and C_1 are constants to be determined from the boundary conditions, $H_0^{(1)}$ and $H_0^{(2)}$ are the zeroth order Hankel functions of the first and second kind. The Hankel functions are related to the Bessel functions as $H_0^{1,2}(z) = J_0(z) \pm iY_0(z)$, where $J_0(z)$ and $Y_0(z)$ are the zeroth order Bessel functions of first and second kind respectively. Figure (3.2) shows the real and imaginary parts of the Hankel function with argument given in Eq. (3.2.5) in function of the axial position x. It was normalized by its maximum absolute value in the region of $0 \leq x \leq 20$. To demonstrate the effect of the linear temperature increase we applied typical values of laboratory burners, i.e. $\omega = 1000\ 1/s$, $T_0 = 400\ K$ and $m = 500\ K/m$.

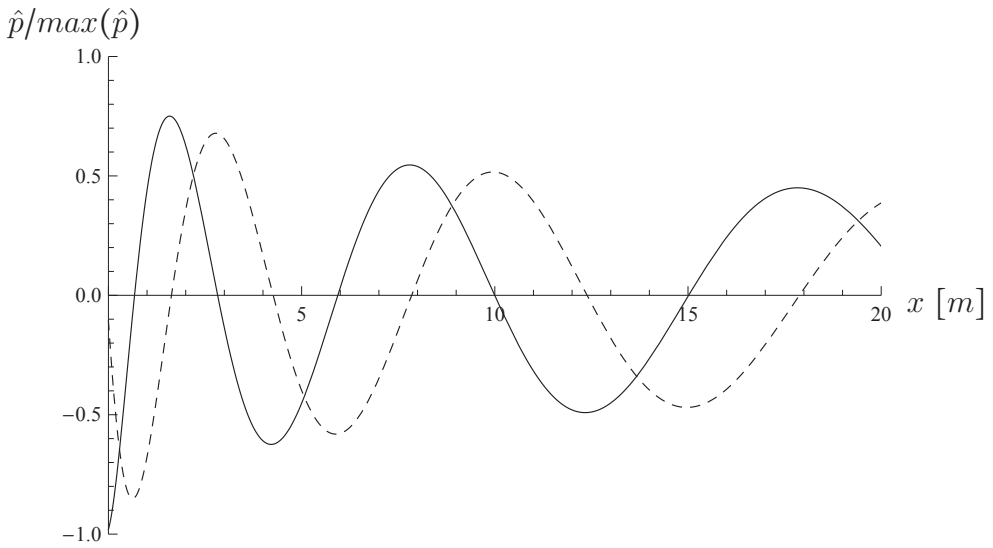

Figure 3.2: Normalized Bessel function of the first and second kind for typical values of laboratory burners, $\omega = 1000\ 1/s$, $T_0 = 400\ K$ and $m = 500\ K/m$ (———: Bessel function of the first kind, − − −: Bessel function of the second kind)

3.2.3 Quadratic mean temperature profile

For a quadratic axial mean temperature profile ($\bar{T} = ax^2 + bx + T_0$) Eq. (3.2.1) is a Legendre differential equation

$$\left(ax^2 + bx + T_0\right)\frac{d^2\hat{p}}{dx^2} + \left(b + 2ax\right)\frac{d\hat{p}}{dx} + \frac{\omega^2}{\gamma\mathcal{R}}\hat{p} = 0 \ . \tag{3.2.6}$$

The solutions are the Legendre functions of the first and second kind:

$$\hat{p} = C_0 P_\Phi\left(i\left[\frac{b}{a} + 2x\right]\sqrt{\frac{b^2 + 4aT_0}{16T_0^2 - \frac{b^4}{a^2}}}\right) + C_1 Q_\Phi\left(i\left[\frac{b}{a} + 2x\right]\sqrt{\frac{b^2 + 4aT_0}{16T_0^2 - \frac{b^4}{a^2}}}\right) \ , \tag{3.2.7}$$

where the order of the functions is given by

$$\Phi = -\frac{1}{2} + i \cdot \sqrt{\frac{\omega^2}{aR\gamma} - \frac{1}{4}} \ . \tag{3.2.8}$$

Figure (3.3) shows the normalized real and imaginary parts of Legendre function of the first kind P for typical values of laboratory burners: $T_0 = 400\ K$, $a = 36\ K/m^2$, $b = 140\ K/m$, and $\omega = 1000\ 1/s$. Legendre functions having the order of the form $-1/2 + i \cdot \alpha$ are called conical ($\alpha \in \mathbb{R}$). $\alpha \in \mathbb{R}$ is a necessary condition to have an oscillatory solution of Eq. (3.2.7).

Comparing Figure (3.3) and Figure (3.2) with Figure (3.1) shows that the wavelength increases with increasing temperature.

3.3 Conclusions

In this chapter we derived the governing differential equation for the acoustic pressure assuming low mean flow Mach number. We showed that the axial mean pressure and

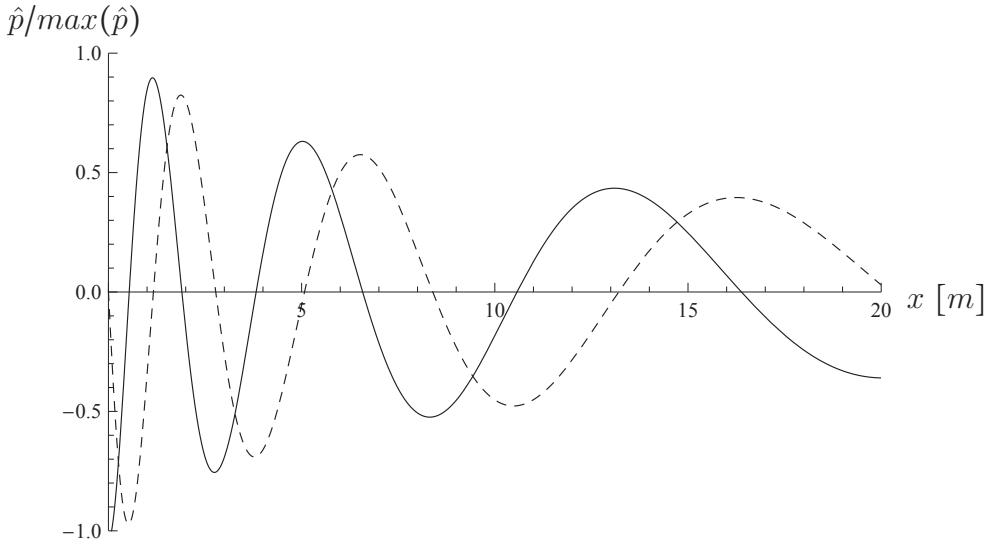

Figure 3.3: Normalized Legendre function of the first kind for a typical laboratory burner, $T_0 = 400\ K$, $a = 36\ K/m^2$, $b = 140\ K/m$, $\omega = 1000\ 1/s$. (———: real part, − − −: imaginary part)

temperature is constant if there is no heat-source in the flow. The solutions of the unforced wave equation for constant, linear and quadratic axial mean temperature profiles were provided.

Chapter 4

Green's function method

In this chapter we treat the burner as a passive resonator and study various configurations with different mean temperature profiles. To this end we introduce the concept of the Green's function method. First we derive the solution of a linear problem in terms of the Green's function, later we present the solution of the acoustic pressure in integral form. We calculate the Green's functions for the LIMOUSINE burner both in the frequency and time-domain. Conclusions will be drawn by comparing the analytical results with measurements.

4.1 General description

Green's function is a tool for solving problems involving linear partial and ordinary differential equations subject to initial and boundary conditions. It is very similar to the Transfer Function concept applied in control theory, i.e. the output of a linear system can be investigated by the input and the system separately. The Green's function method consists of calculating an auxiliary function, which describes the system itself only, independently of the forcing. The solution is written in terms of an integral equation, in which the auxiliary function becomes the kernel. The main advantage of this method is that the Green's function is independent of the forcing, therefore it is very powerful when one would like to compare systems which differ only in the forcing

term. Another major advantage of providing the problem in integral form rather than in differential form is that integral equations are easier to handle numerically.

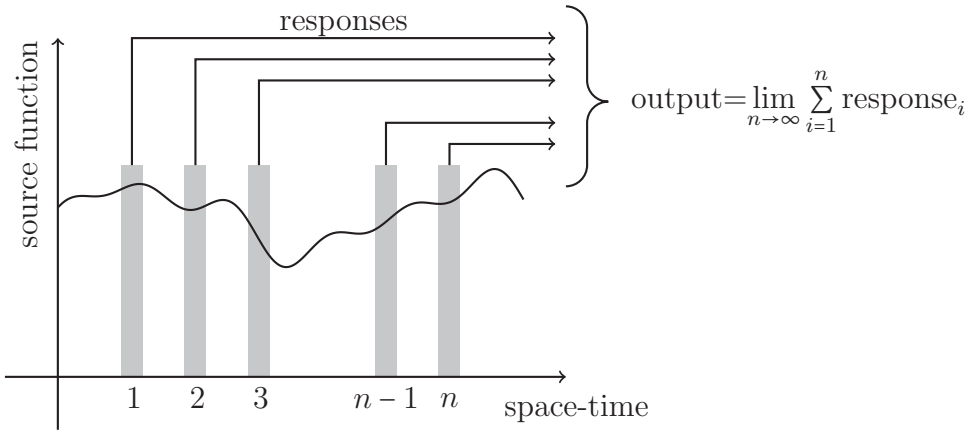

Figure 4.1: Concept of the Green's function method

Figure (4.1) shows the concept of the Green's function method. It calculates the system response from one point of the space-time domain of the forcing function, and sums the individual responses to get the response of the complete forcing.

4.1.1 The Dirac-delta function

One point of a domain can be picked by a special function, by the use of Dirac-delta (δ) function, which has a value of infinity at zero, but vanishes everywhere else

$$\delta(t) = \begin{cases} \infty & \text{if} \quad t = 0 \ , \\ 0 & \text{if} \quad t \neq 0 \ . \end{cases} \tag{4.1.1}$$

In physical studies, the δ function is used to represent a unit point force or a sudden impulse. The point in which is does not vanish is called the singularity of the delta function (t_0). By definition

$$\int_{-\infty}^{\infty} \delta(t - t_0) dt = 1 \ . \tag{4.1.2}$$

This function is not analytic, but can be obtained as a limit of analytical functions, and it is useful only as part of an integrand, but not as an end result. It follows from Eq. (4.1.2), that the dimension of the delta function depends on its argument as $[\delta(t)] = 1/[\mathrm{t}]$, where $[\ldots]$ denotes the dimension of a quantity. The sifting property of the delta function for a function $\varphi(t)$ can be derived from Eq. (4.1.2), using that for an infinitesimal small interval $\varphi(t)$ can be considered constant, therefore

$$\int_{-\infty}^{\infty} \varphi(t)\delta(t-t_0)dt = \varphi(t_0)\int_{-\infty}^{\infty} \delta(t-t_0)dt = \varphi(t_0), \tag{4.1.3}$$

i.e. the delta function picks a given point from the domain of φ, as it was shown in Figure (4.1). Integration of the delta function yields the Heaviside function

$$\int \delta(t)dt = H(t) = \begin{cases} 1 & \text{if} \quad t > 0 \ , \\ \frac{1}{2} & \text{if} \quad t = 0 \ , \\ 0 & \text{if} \quad t < 0 \ , \end{cases} \tag{4.1.4}$$

where the value of the Heaviside function is specified at $t = 0$ in such a way that its Fourier Transform, Laplace Transform and their inverse are unique. One approach is to view the delta function as the limit of a strongly peaked ordinary function. Figure (4.2) shows how the function $n/\sqrt{\pi}\exp(-n^2t^2)$ approaches the delta-function as n goes to infinity.

The limiting function satisfies Eq. (4.1.2)

$$\int_{-\infty}^{\infty} \frac{n}{\sqrt{\pi}} e^{-n^2t^2} dt = 1 \quad \forall \quad n \in \mathbb{N} \ . \tag{4.1.5}$$

Detailed mathematical analysis of the delta function can be found in [Duffy, 2001; Kythe, 2011; Meyberg and Vachenauer, 2001; Roach, 1982].

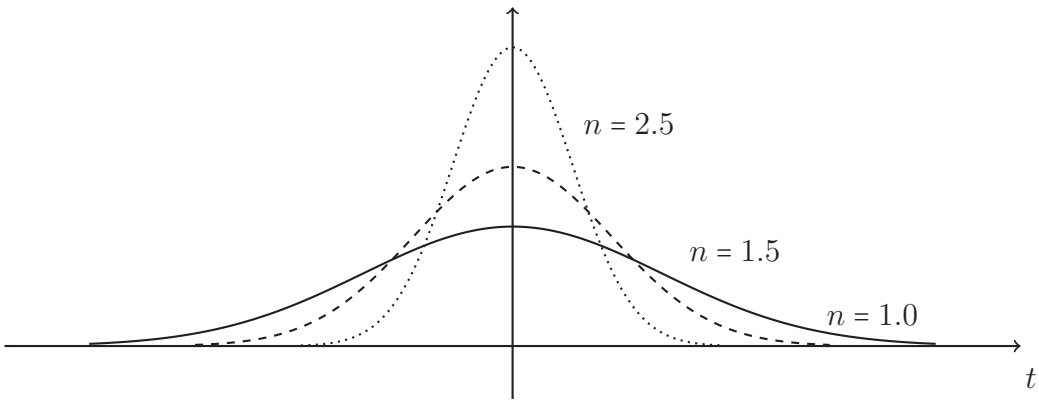

Figure 4.2: Approximation of the Dirac-delta function by $n/\sqrt{\pi}\exp(-n^2t^2)$ (———: $n = 1$, – – –: $n = 1.5$, ·····: $n = 2.5$)

4.1.2 The Green's function as a mathematical tool

4.1.2.1 What is the Green's function

As already mentioned, the Green's function gives the systems response when it is excited in a certain point of the domain at a given time. Mathematically a linear differential problem generally can be written as

$$L[p'] = f \ , \tag{4.1.6}$$

where f is the forcing function, p' is the unknown quantity to be calculated, L is a linear operator acting on p'. In this case the corresponding Green's function can be calculated by solving

$$L[G] = \delta(\boldsymbol{x} - \boldsymbol{\xi})\delta(t - \tau) \ , \tag{4.1.7}$$

where $\boldsymbol{x}$ and t are the observer position vector and time, $\boldsymbol{\xi}$ and τ are the source position vector and time respectively. Generally solving a problem by using the Green's function method consists of finding the corresponding adjoint operator, however in this thesis the applied operators are self-adjoint. One can find problems involving not self-adjoint operators in [Duffy, 2001; Kythe, 2011; Meyberg and Vachenauer, 2001; Roach, 1982].

To find the solution we multiply Eq. (4.1.6) by G, Eq. (4.1.7) by p' and subtract them

$$G \cdot L[p'] - p' \cdot L[G] = G \cdot f - p' \cdot \delta(\boldsymbol{x} - \boldsymbol{\xi})\delta(t - \tau) \ . \tag{4.1.8}$$

We integrate Eq. (4.1.8) over the space-time domain of the problem Ω and apply the sifting property of the delta function

$$\int_{\Omega} G \cdot L[p'] - p' \cdot L[G] d\Omega = \int_{\Omega} G \cdot f d\Omega - p'(t, \boldsymbol{x}) \ . \tag{4.1.9}$$

The key step of the Green's function method is to rewrite the integrand on the L.H.S. of Eq. (4.1.9) as the divergence of a function of p' and G

$$G \cdot L[p'] - p' \cdot L[G] = \nabla\theta(p', G) \ . \tag{4.1.10}$$

θ depends on the operator L. Eq. (4.1.10) is called Lagrange's identity. We substitute with Eq. (4.1.10) for the integrand on the L.H.S. of Eq. (4.1.9) and apply Gauss' theorem

$$p'(t, \boldsymbol{x}) = \int_{\Omega} G \cdot f d\Omega - \int_{\partial\Omega} (\theta \cdot \boldsymbol{n}) dS \ , \tag{4.1.11}$$

where $\partial\Omega$ is the boundary of domain Ω. Eq. (4.1.11) is called the superposition integral or Duhamel's integral. We present the output, the unknown function p' as the superposition of the systems response due to the forcing f, which is the first term in Eq. (4.1.11), and the response due to the initial and boundary conditions (second term on the R.H.S.). Using this method we split the differential problem of Eq. (4.1.6) into an integral problem of Eq. (4.1.11) and to a differential problem of finding the solution of Eq. (4.1.7).

4.1.2.2 What is the tailored Green's function

It is common to calculate the general Green's function, in which case boundary conditions are not specified for Eq. (4.1.7). In the thesis we require that the Green's function satisfies the same boundary condition as the unknown quantity p'. The Green's function formulated in this way is called tailored.

4.2 Solution of the forced wave equation in terms of the Green's function

4.2.1 Time domain

Now we formulate the solution of the forced wave equation for a non-uniform axial mean temperature profile Eq. (3.1.12), using the steps described in the previous section. The governing equations for the acoustic pressure is

$$\frac{1}{\gamma\mathcal{R}}\frac{\partial^2 p'}{\partial t^2} - \frac{\partial \bar{T}}{\partial x}\frac{\partial p'}{\partial x} - \bar{T}\frac{\partial^2 p'}{\partial x^2} = \frac{\gamma-1}{\gamma\mathcal{R}}\frac{\partial Q'}{\partial t} \ , \tag{4.2.1}$$

and that for the corresponding Green's function $G(x,\xi,t,\tau)$ is

$$\frac{1}{\gamma\mathcal{R}}\frac{\partial^2 G}{\partial t^2} - \frac{\partial \bar{T}}{\partial x}\frac{\partial G}{\partial x} - \bar{T}\frac{\partial^2 G}{\partial x^2} = \delta(x-\xi)\delta(t-\tau) \ , \tag{4.2.2}$$

where x and t are the observer location and time respectively, ξ and τ are the source location and time respectively. From Eq. (4.2.1) it follows that

$$L_{\tau,\xi} = \frac{1}{\gamma\mathcal{R}}\frac{\partial^2}{\partial \tau^2} - \frac{\partial \bar{T}}{\partial \xi}\frac{\partial}{\partial \xi} - \bar{T}\frac{\partial^2}{\partial \xi^2} \ . \tag{4.2.3}$$

We apply the operator L with respect to the variables τ and ξ because we are going to sum the infinitesimally small responses at time τ and space ξ. We can write $GL[p'] -$

$p'L[G]$ as

$$G\left[\frac{1}{\gamma\mathcal{R}}\frac{\partial^2 p'}{\partial\tau^2}-\frac{\partial\bar{T}}{\partial\xi}\frac{\partial p'}{\partial\xi}-\bar{T}\frac{\partial^2 p'}{\partial\xi^2}\right]-p'\left[\frac{1}{\gamma\mathcal{R}}\frac{\partial^2 G}{\partial\tau^2}-\frac{\partial\bar{T}}{\partial\xi}\frac{\partial G}{\partial\xi}-\bar{T}\frac{\partial^2 G}{\partial\xi^2}\right]=$$
$$=\frac{1}{\gamma\mathcal{R}}\frac{\partial}{\partial\tau}\left[G\frac{\partial p'}{\partial\tau}-p'\frac{\partial G}{\partial\tau}\right]-\frac{\partial}{\partial\xi}\left(G\bar{T}\frac{\partial p'}{\partial\xi}-p'\bar{T}\frac{\partial G}{\partial\xi}\right)\ . \quad (4.2.4)$$

Comparing Eq. (4.2.4) with Eq. (4.1.10) yields that θ is the R.H.S. of Eq. (4.2.4), i.e.

$$\nabla\theta(p',G)=\frac{1}{\gamma\mathcal{R}}\frac{\partial}{\partial\tau}\left[G\frac{\partial p'}{\partial\tau}-p'\frac{\partial G}{\partial\tau}\right]-\frac{\partial}{\partial\xi}\left(G\bar{T}\frac{\partial p'}{\partial\xi}-p'\bar{T}\frac{\partial G}{\partial\xi}\right)\ . \quad (4.2.5)$$

As we discussed in the general introduction, now we sum the responses, i.e. we integrate the equation over the space-time domain $[0,t]\times[0,L]$ with respect to τ and ξ to get

$$\int_0^t\int_0^L\left[G\left(\frac{1}{\gamma\mathcal{R}}\frac{\partial^2 p'}{\partial\tau^2}-\frac{\partial\bar{T}}{\partial\xi}\frac{\partial p'}{\partial\xi}-\bar{T}\frac{\partial^2 p'}{\partial\xi^2}\right)-p'\left(\frac{1}{\gamma\mathcal{R}}\frac{\partial^2 G}{\partial\tau^2}-\frac{\partial\bar{T}}{\partial\xi}\frac{\partial G}{\partial\xi}-\bar{T}\frac{\partial^2 G}{\partial\xi^2}\right)\right]d\tau\ d\xi=$$
$$=\int_0^t\int_0^L\left[\frac{1}{\gamma\mathcal{R}}\frac{\partial}{\partial\tau}\left(G\frac{\partial p'}{\partial\tau}-p'\frac{\partial G}{\partial\tau}\right)-\frac{\partial}{\partial\xi}\left(G\bar{T}\frac{\partial p'}{\partial\xi}-p'\bar{T}\frac{\partial G}{\partial\xi}\right)\right]d\tau\ d\xi\ . \quad (4.2.6)$$

Substituting for the bracketed terms in the integral on the L.H.S. with Eq. (4.2.1) and Eq. (4.2.2) gives

$$\int_0^t\int_0^L G\frac{\gamma-1}{\gamma\mathcal{R}}\frac{\partial Q'}{\partial\tau}\ d\tau\ d\xi-\int_0^t\int_0^L p'(\xi,\tau)\delta(t-\tau)\delta(x-\xi)\ d\tau\ d\xi=$$
$$=\frac{1}{\gamma\mathcal{R}}\int_0^L\left(G\frac{\partial p'}{\partial\tau}-p'\frac{\partial G}{\partial\tau}\right)\Bigg|_{\tau=0}^{\tau=t}d\xi-\int_0^t\left(G\bar{T}\frac{\partial p'}{\partial\xi}-p'\bar{T}\frac{\partial G}{\partial\xi}\right)\Bigg|_0^L d\tau\ . \quad (4.2.7)$$

Before the impulse ($t<\tau$) the system must be dormant, which is often referred to as

the causality condition: the principle stating that an event cannot precede its cause. Therefore we now require that the Green's function possess the property of $G(x,\xi,t,\tau = t) = 0$ and $\partial G(x,\xi,t,\tau = t)/\partial\tau = 0$. We assume that the boundary conditions at the ends of the domain are linear, homogeneous and unmixed, i.e. that we can write them as

$$\left(\alpha p' + \beta\frac{\partial p'}{\partial x}\right)\Bigg|_{x=0,L} = 0 \ , \tag{4.2.8}$$

where α and β are constants of the boundary conditions. In the thesis we use complex pressure reflection coefficient boundary conditions. Are such boundary conditions of homogeneous type? In order to answer this question we investigate a duct with uniform mean temperature, therefore we can apply the solutions of Eq. (3.2.3). It can be shown that the complex pressure reflection coefficient boundary conditions are indeed of homogeneous type, therefore fulfill Eq. (4.2.8), if

$$\alpha(R+1) + \beta i\frac{\omega}{c}(R-1) = 0 \ , \quad \text{where} \quad R = \frac{C_0}{C_1}\Bigg|_{x=0} \ . \tag{4.2.9}$$

C_0 and C_1 are the amplitudes of the reflected and the incident pressure waves respectively. A boundary condition is said to be unmixed if it involves the function and its derivative at only one boundary, i.e. at $x = 0$ or at $x = L$. The tailored Green's function satisfies the same boundary conditions. Then the last term on the R.H.S. of Eq. (4.2.7) vanishes, therefore the solution is

$$p'(x,t) = \int_0^t \int_0^L G\frac{\gamma-1}{\gamma R}\frac{\partial Q'(\xi,\tau)}{\partial\tau}d\tau \ d\xi + \frac{1}{\gamma R}\int_0^L \left(G\frac{\partial p'}{\partial\tau} - p'\frac{\partial G}{\partial\tau}\right)\Bigg|_{\tau=0} d\xi \ . \tag{4.2.10}$$

The first term on the R.H.S. is the systems response, the second one is due to the initial conditions.

4.2.2 Frequency domain

We would like to investigate the system independently of the initial conditions, therefore we apply Fourier Transform with respect to time and work in the frequency domain. The frequency-domain equivalent of the governing Eq. (3.1.12) is

$$\bar{T}\frac{d^2\hat{p}}{dx^2} + \frac{d\bar{T}}{dx}\frac{d\hat{p}}{dx} + \frac{\omega^2}{\gamma\mathcal{R}}\hat{p} = -\frac{\gamma-1}{\gamma\mathcal{R}}i\omega\hat{Q} \ , \tag{4.2.11}$$

and that of Eq. (4.2.2) for the Green's function is

$$\bar{T}\frac{d^2\hat{G}}{dx^2} + \frac{d\bar{T}}{dx}\frac{d\hat{G}}{dx} + \frac{\omega^2}{\gamma\mathcal{R}}\hat{G} = \delta(x-\xi) \ . \tag{4.2.12}$$

We require that the Green's function satisfies the given boundary conditions. From Eq. (4.2.11) it follows that the operator $\hat{L}_\xi$ acting on $\hat{p}$ is

$$\hat{L}_\xi = \frac{\omega^2}{\gamma\mathcal{R}} + \frac{\partial\bar{T}}{\partial\xi}\frac{\partial}{\partial\xi} + \bar{T}\frac{\partial^2}{\partial\xi^2} \ . \tag{4.2.13}$$

We apply Lagrange's identity, i.e. we rewrite $\hat{G}\hat{L}_\xi[\hat{p}] - \hat{p}\hat{L}_\xi[\hat{G}]$ as

$$\hat{G}\left[\frac{\omega^2}{\gamma\mathcal{R}}\hat{p} + \frac{\partial\bar{T}}{\partial\xi}\frac{\partial\hat{p}}{\partial\xi} + \bar{T}\frac{\partial^2\hat{p}}{\partial\xi^2}\right] - \hat{p}\left[\frac{\omega^2}{\gamma\mathcal{R}}\hat{G} + \frac{\partial\bar{T}}{\partial\xi}\frac{\partial\hat{G}}{\partial\xi} + \bar{T}\frac{\partial^2\hat{G}}{\partial\xi^2}\right] = \frac{\partial}{\partial\xi}\left(\hat{G}\bar{T}\frac{\partial\hat{p}}{\partial\xi} - \hat{p}\bar{T}\frac{\partial\hat{G}}{\partial\xi}\right) \ . \tag{4.2.14}$$

We integrate the equation over the space domain $[0, L]$ with respect to ξ and substitute for the bracketed terms on the L.H.S. with Eq. (4.2.11) and Eq. (4.2.12) to get

$$-\int_0^L \hat{G}i\omega\frac{\gamma-1}{\gamma\mathcal{R}}\hat{Q}'(\xi,\omega)\ d\xi - \int_0^L \hat{p}(\xi,\omega)\delta(x-\xi)\ d\xi = \left(\hat{G}\bar{T}\frac{\partial\hat{p}}{\partial\xi} - \hat{p}\bar{T}\frac{\partial\hat{G}}{\partial\xi}\right)\Bigg|_0^L . \tag{4.2.15}$$

For linear, homogeneous and unmixed boundary conditions the second term on the R.H.S. vanishes, and the solution is

$$\hat{p}(x,\omega) = \int_0^L \hat{G}(x,\xi,\omega)\left[-\frac{\gamma-1}{\gamma\mathcal{R}} i\omega\hat{Q}(\xi,\omega)\right] d\xi \ . \tag{4.2.16}$$

4.3 Calculation of the tailored Green's function

4.3.1 Eigenfrequencies and eigenfunctions

We consider a system described by a homogeneous differential equation and given boundary conditions, for instance by Eq. (3.2.1) and Eq. (4.2.8). The non-trivial solutions of the system are called the eigenfunctions. They represent the shape of the vibrational modes. Parameter ω of an eigenfunction is its eigenfrequency. Physically, at the eigenfrequencies ($\omega = \omega_n$) the system can be perturbed out of its stable state if forcing is absent.

4.3.2 The operator method applied to the wave equation

There are two techniques to find the Green's function of an ordinary differential equation with given boundary conditions. The first is the operator method, when the solution is constructed from the homogeneous solutions of the right and left regions of the point of excitation, and pieced together to give the complete solution. The second is the modal expansion, which represents the Green's function as the superposition of orthonormal eigenfunctions that are valid over the entire domain and satisfy the given boundary conditions.

We are going to apply the operator method, as presented in Kosztin et al. [2011]. We assume that the solutions of the homogeneous, i.e. source-free, equation are known as $\hat{p}_1$ and $\hat{p}_2$ in the regions upstream and downstream respectively of the source. Because $\hat{p}_1$ and $\hat{p}_2$ satisfy the boundary conditions, the resulting Green's function is called tailored. Hence the Green's function over the entire domain can be written in terms of

the Heaviside function as

$$\hat{G}(x,\xi,\omega) = H(\xi - x)A(\xi,\omega)\hat{p}_1(x,\omega) + H(x-\xi)C(\xi,\omega)\hat{p}_2(x,\omega) \ , \tag{4.3.1}$$

where $A(\xi,\omega)$ and $C(\xi,\omega)$ are complex amplitudes which are going to be determined. The derivatives of Eq. (4.3.1) are

$$\begin{aligned}\frac{d\hat{G}}{dx}(x,\xi,\omega) =& H(\xi - x)A(\xi,\omega)\frac{d\hat{p}_1}{dx}(x,\omega) + H(x-\xi)C(\xi,\omega)\frac{d\hat{p}_2}{dx}(x,\omega) \\ &- \delta(x-\xi)A(\xi,\omega)\hat{p}_1(x,\omega) + \delta(x-\xi)C(\xi,\omega)\hat{p}_2(x,\omega) \ ,\end{aligned} \tag{4.3.2}$$

and

$$\begin{aligned}\frac{d^2\hat{G}}{dx^2}(x,\xi,\omega) =& H(\xi - x)A(\xi,\omega)\frac{d^2\hat{p}_1}{dx^2}(x,\omega) + H(x-\xi)C(\xi,\omega)\frac{d^2\hat{p}_2}{dx^2}(x,\omega) \\ &- \delta(x-\xi)A(\xi,\omega)\frac{d\hat{p}_1}{dx}(x,\omega) + \delta(x-\xi)C(\xi,\omega)\frac{d\hat{p}_2}{dx}(x,\omega) \\ &- \frac{d\delta(x-\xi)}{dx}A(\xi,\omega)\hat{p}_1(x,\omega) + \frac{d\delta(x-\xi)}{dx}C(\xi,\omega)\hat{p}_2(x,\omega) \ .\end{aligned} \tag{4.3.3}$$

We substitute Eqs. (4.3.1), (4.3.2) and (4.3.3) into Eq. (4.2.12) using the fact that the terms with the Heaviside function vanish since they are the solutions of the homogeneous equation. Equating the coefficients for $d\delta(x-\xi)/dx$ and $\delta(x-\xi)$ yields two linear equations

$$\bar{T}(x)\left[-\frac{d\delta(x-\xi)}{dx}A(\xi,\omega)\hat{p}_1(x,\omega) + \frac{d\delta(x-\xi)}{dx}C(\xi,\omega)\hat{p}_2(x,\omega)\right] = 0 \ , \tag{4.3.4a}$$

$$\bar{T}(x)\left[-\delta(x-\xi)A(\xi,\omega)\frac{d\hat{p}_1}{dx}(x,\omega) + \delta(x-\xi)C(\xi,\omega)\frac{d\hat{p}_2}{dx}(x,\omega)\right] = \delta(x-\xi) \ , \tag{4.3.4b}$$

from which we can express the solutions A and C by using Cramer's rule. It follows that

$$C(\xi,\omega) = \frac{1}{\bar{T}(\xi)} \frac{\hat{p}_1(\xi,\omega)}{\hat{p}_1(\xi,\omega)\frac{d\hat{p}_2(\xi,\omega)}{d\xi} - \hat{p}_2(\xi,\omega)\frac{d\hat{p}_1(\xi,\omega)}{d\xi}} \ , \tag{4.3.5a}$$

$$A(\xi,\omega) = \frac{1}{\bar{T}(\xi)} \frac{\hat{p}_2(\xi,\omega)}{\hat{p}_1(\xi,\omega)\frac{d\hat{p}_2(\xi,\omega)}{d\xi} - \hat{p}_2(\xi,\omega)\frac{d\hat{p}_1(\xi,\omega)}{d\xi}} \ , \tag{4.3.5b}$$

and the Green's function in the frequency domain can then be written in compact form as $\hat{G}(x,\xi,\omega) = \hat{G}_T(x,\xi,\omega)/\bar{T}(\xi)$, where

$$\hat{G}_T(x,\xi,\omega) = \begin{cases} \dfrac{\hat{p}_1(x,\omega)\hat{p}_2(\xi,\omega)}{\hat{p}_1(\xi,\omega)\frac{d\hat{p}_2(\xi,\omega)}{d\xi} - \hat{p}_2(\xi,\omega)\frac{d\hat{p}_1(\xi,\omega)}{d\xi}}, & x < \xi \\ \dfrac{\hat{p}_2(x,\omega)\hat{p}_1(\xi,\omega)}{\hat{p}_1(\xi,\omega)\frac{d\hat{p}_2(\xi,\omega)}{d\xi} - \hat{p}_2(\xi,\omega)\frac{d\hat{p}_1(\xi,\omega)}{d\xi}}, & x > \xi \ . \end{cases} \tag{4.3.6}$$

The symmetry of the Green's function can be noticed, $\hat{G}(x,\xi,\omega) = \hat{G}(\xi,x,\omega)$. This is referred to as the reciprocity, which is the property of the Green's functions of self-adjoint operators. At $x = \xi$ the Green's function is continuous, and its derivative has a jump of $-1/\bar{T}(\xi)$. The denominator of the Green's function is the Wronskian of the homogeneous system. The frequency domain Green's function does not exist at $\omega = \omega_n$, these poles are called the point spectrum of the Green's function.

4.3.3 Tailored Green's function in the frequency-domain for the LIMOUSINE burner

4.3.3.1 Configuration 1: constant mean temperature in the inlet and outlet regions, jump in the cross-section and mean temperature at the same point.

In the first configuration we would like to present explicit formulas for the key acoustic properties, such as the eigenfrequency and damping rate. To this end we assume that the flame region is infinitely thin and located at the point where the cross section changes. The temperature is uniform in the inlet and outlet regions, and has a jump at the point where the cross-section changes ($x = x'$). Reflection coefficients R_0 and R_1 are used to describe the boundary conditions at $x = 0$ and $x = L$, respectively. $\mathscr{A}_0$ and $\mathscr{A}_1$ are the cross sectional area upstream and downstream of the flame respectively. In our notation subscript 0 refers to the cold region, subscript 1 refers to the hot region.

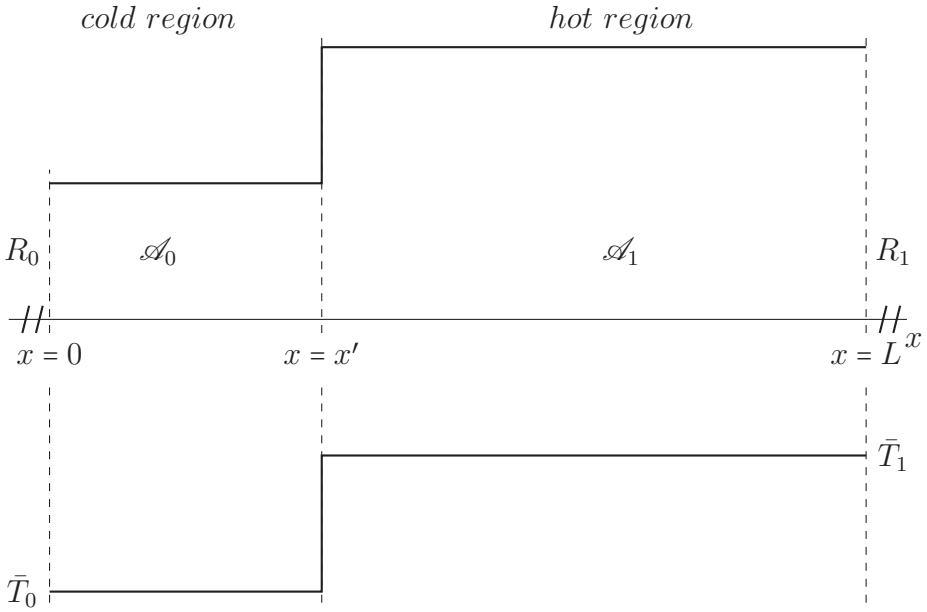

Figure 4.3: Schematic representation of the burner and temperature profile in Configuration 1

We use harmonic wave solutions with uniform mean temperature (Eq. (3.2.3)),

$$\hat{p} = \begin{cases} \hat{p}_0 = Ae^{ik_0 x} + Be^{-ik_0 x} & x < x' \ , \\ \hat{p}_1 = Ce^{ik_1(x-L)} + De^{-ik_1(x-L)} & x > x' \ , \end{cases} \tag{4.3.7}$$

where $k_i = \omega/c_i$ and the capitals A, B, C, D are complex amplitudes to be determined. $\exp(ik_i x)$ represents a wave travelling in the positive x direction, $\exp(-ik_i x)$ represents a wave travelling in the negative x direction. We describe the boundary conditions by complex pressure reflection coefficients, therefore $A = BR_0$ and $D = CR_1$. Furthermore we use continuous pressure ($\hat{p}_0 = \hat{p}_1$) and volume velocity ($\mathscr{A}_0\hat{u}_0 = \mathscr{A}_1\hat{u}_1$) at the interface $x = x'$, which yields the following equation for the eigenfrequency

$$\frac{\mathscr{A}_1}{\bar{\rho}_1\bar{c}_1}\Big[R_0e^{ik_0x'} + e^{-ik_0x'}\Big]\Big[e^{ik_1(x'-L)} - R_1e^{-ik_1(x'-L)}\Big] - \\ - \frac{\mathscr{A}_0}{\bar{\rho}_0\bar{c}_0}\Big[R_0e^{ik_0x'} - e^{-ik_0x'}\Big]\Big[e^{ik_1(x'-L)} + R_1e^{-ik_1(x'-L)}\Big] = 0 \ . \tag{4.3.8}$$

Eq. (4.3.8) gives the eigenfrequencies of configuration 1. In order to obtain the solutions we divide the complex frequency into a real and imaginary part, i.e. $\omega = \omega_r + i\omega_i$, furthermore we introduce the polar representation of the reflection coefficients, $R_i = |R_i|\exp(-i\varphi_i)$. Performing the multiplications yields

$$|R_1|\left[\frac{\mathscr{A}_0}{\bar{\rho}_0\bar{c}_0} - \frac{\mathscr{A}_1}{\bar{\rho}_1\bar{c}_1}\right]\theta(x',\omega_r)\phi_0(x',\omega_r)\mu^-(x',\omega_i) - |R_0|\left[\frac{\mathscr{A}_0}{\bar{\rho}_0\bar{c}_0} - \frac{\mathscr{A}_1}{\bar{\rho}_1\bar{c}_1}\right]\theta(x',\omega_r)\frac{\phi_1(L-x',\omega_r)}{\mu^-(x',\omega_i)} \\ + \left[\frac{\mathscr{A}_0}{\bar{\rho}_0\bar{c}_0} + \frac{\mathscr{A}_1}{\rho_1c_1}\right]\mu^+(x',i\omega_r)\mu^+(x',\omega_i) - |R_0||R_1|\left[\frac{\mathscr{A}_0}{\bar{\rho}_0\bar{c}_0} + \frac{\mathscr{A}_1}{\rho_1c_1}\right]\theta(x',\omega)\frac{1}{\mu^+(x',\omega_i)} = 0 \ , \tag{4.3.9}$$

where $\theta(x',\omega)$, $\phi(x',\omega)$ and $\mu(x',\omega)$ are given by

$$\theta(x',\omega) = \exp\left[-i\left(\varphi_0 + \varphi_1 - \omega\frac{x'}{c_0} - \omega\frac{L-x'}{c_1}\right)\right] \tag{4.3.10a}$$

$$\phi_k(x',\omega) = \exp\left[i\left(\varphi_k - 2\omega\frac{x'}{c_k}\right)\right] \tag{4.3.10b}$$

$$\mu^{\pm}(x',\omega) = \exp\left[\omega\left(\frac{x'}{c_0} \pm \frac{L-x'}{c_1}\right)\right] \ . \tag{4.3.10c}$$

Asymptotic solutions for the eigenfrequency and damping rate can be calculated, if the change in $\mathscr{A}/\bar{\rho}\bar{c}$ is either small or large. This quantity is called characteristic impedance. In case of the LIMOUSINE burner the value of this quantity in the hot region is approximately four times its value in the cold region. To assume that this jump is small, it should be smaller than 1.5, and to apply large jump asymptotic solution it should be at least 100. Because the jump in the characteristic impedance is closer to the criteria of being small, we treat it as small, but expect some discrepancy from the measured results. We neglect terms with $\mathscr{A}_0/\bar{\rho}_0\bar{c}_0 - \mathscr{A}_1/\bar{\rho}_1\bar{c}_1$ compared to terms with $\mathscr{A}_0/\bar{\rho}_0\bar{c}_0 + \mathscr{A}_1/\bar{\rho}_1\bar{c}_1$ and Eq. (4.3.9) is simplified to

$$\mu^{+}(x', 2\omega_i) = |R_0||R_1|\theta(x', 2\omega_r) \ . \tag{4.3.11}$$

Eq. (4.3.11) is a complex equation, therefore in order to obtain a solution we divide it into real and imaginary parts. Since the L.H.S. of Eq. (4.3.11) is purely real and positive, the imaginary part of the R.H.S. vanishes

$$\sin\left(\varphi_0 + \varphi_1 - 2\omega_r\frac{x'}{c_0} - 2\omega_r\frac{L-x'}{c_1}\right) = 0 \ . \tag{4.3.12}$$

The imaginary part of the R.H.S. of Eq. (4.3.11) vanishes, therefore its real part is ± 1. Without solving the real part of Eq. (4.3.11) we can see that μ^{+} represents a real

exponential, therefore it is always positive. Hence the real part of the R.H.S. of Eq. (4.3.11) must be positive as well, therefore the solution of Eq. (4.3.12) can be written as

$$\omega_r \frac{L}{\tilde{c}} = \frac{\varphi_0 + \varphi_1}{2} + n\pi \quad n \in \mathbb{N} \ , \quad \text{where} \quad \frac{1}{\tilde{c}} = \frac{1}{c_0}\frac{x'}{L} + \frac{1}{c_1}\frac{L - x'}{L} \ . \tag{4.3.13}$$

$\tilde{c}$ is the weighted average of the speed of sound in the cold and hot regions. The weights are the length of the regions. Figure (4.4) shows the distribution of the eigenfrequencies depending on the length of the burner, the weighted speed of sound and the average phase of the reflections.

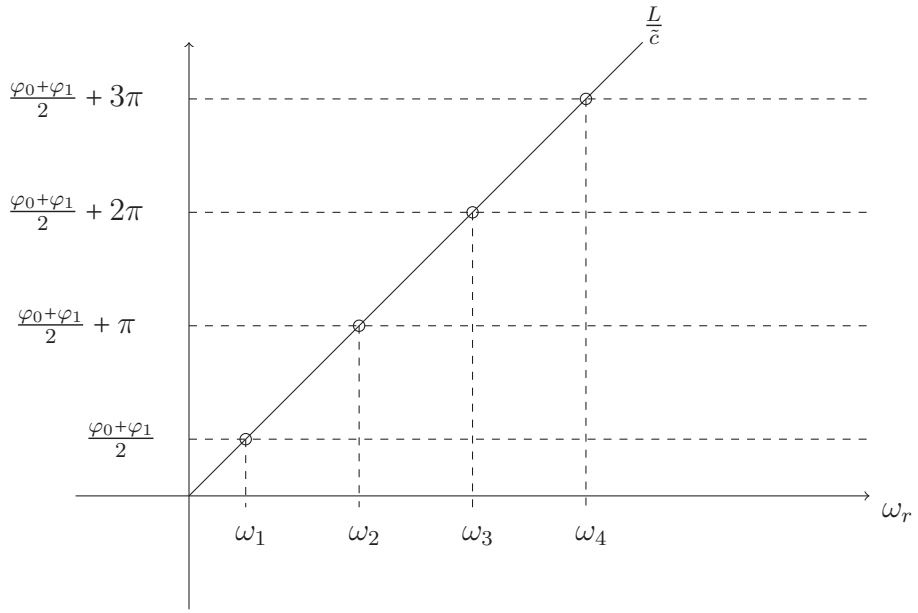

Figure 4.4: Schematic representation of the eigenfrequencies

Inserting Eq. (4.3.13) into Eq. (4.3.11) yields the damping rate

$$\omega_i \frac{L}{\tilde{c}} = \ln\left[\sqrt{|R_0||R_1|}\right] , \tag{4.3.14}$$

where ln denotes the natural logarithm. The damping rate is negative, if $|R_0||R_1| < 1$,

which is the case if energy is lost at the boundaries. We introduce $|R_i| = 1 - \eta_i$ and linearize the R.H.S. of Eq. (4.3.14) for small losses as

$$\omega_i \frac{L}{\tilde{c}} = \ln\left[\sqrt{|R_0||R_1|}\right] = -\frac{1}{2}(\eta_0 + \eta_1) \ . \tag{4.3.15}$$

The relative damping rate yields the damping over one period

$$\frac{\omega_i}{\omega_{r,n}} = -\frac{\eta_0 + \eta_1}{\varphi_0 + \varphi_1 + n\pi} \ . \tag{4.3.16}$$

It is shown in Figure (4.5) that when $\eta_0 + \eta_1$ is less than approximately 25%, Eq. (4.3.14) can be approximated by its linear form, Eq. (4.3.15).

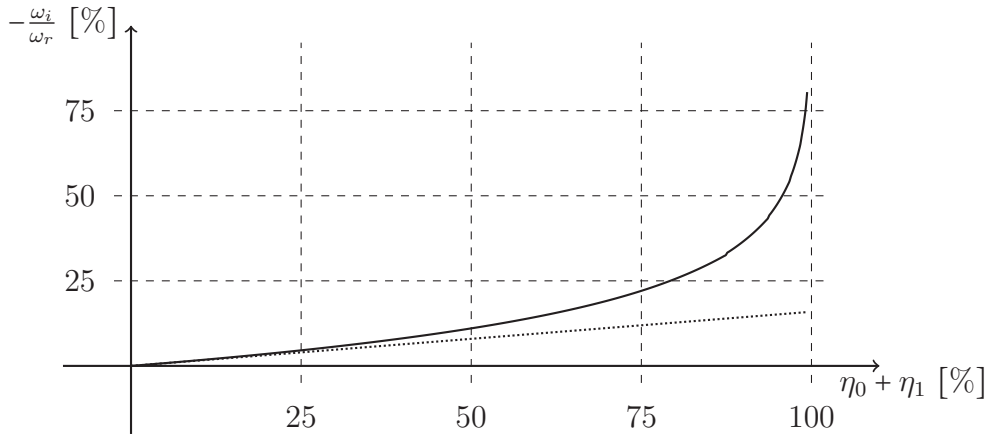

Figure 4.5: Effect of acoustic losses ($\eta_0 + \eta_1$) on the relative damping (———:exact, ·····:linearized)

We derived explicit expressions to calculate the eigenfrequency and damping rate of a burner by assuming that the jump in the characteristic impedance is small and approximating Eq. (4.3.9) accordingly. In order to get more accurate predictions,

we consider configurations with a more realistic mean temperature profile, because mode shapes and eigenfrequencies are very dependent on the temperature distribution (Matveev and Culick [2003a]). The new configurations are explained in detail in the next section.

4.3.3.2 More realistic configurations

In each of the following configurations the tube was divided into three regions: inlet, flame, and outlet.

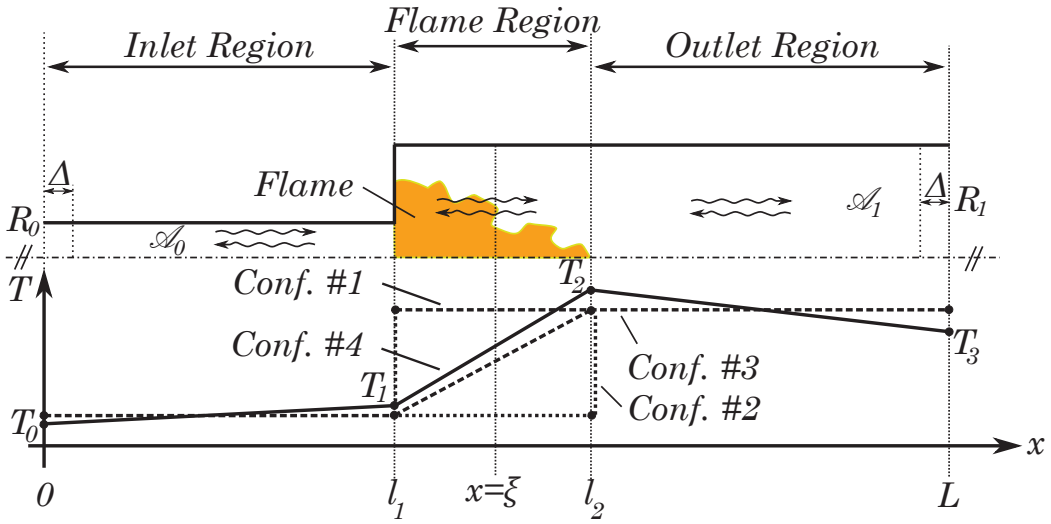

Figure 4.6: Analytical versions

In configuration 2 the location of the jump in the cross-section ($x = l_1$) and the location of the jump in the mean temperature ($x = l_2 \neq l_1$) differs. The mean temperature in the inlet, flame and outlet regions is uniform.

Configuration 3 takes the effect of the flame length into account and assumes that the temperature distribution along the flame is linear. However, outside the flame the temperature takes the constant upstream and downstream values as in configuration 1 and 2.

Configuration 4 considers the preheating effect of the wall, therefore a piecewise linear temperature profile is used. Outside the flame we assume linear profiles that fit the measured temperature curve shown in Figure (2.7). The profile within the flame area

is the same as that in configuration 3.

Configuration 5 considers the preheating effect of the walls as well. Outside the flame we assume linear profiles that fit the measured temperature curve shown in Figure (2.7), however the profile within the flame region is assumed to be quadratic.

For configurations 2-5 we solve the governing equation for the eigenfrequency and damping rate numerically.

4.3.3.3 Boundary conditions in the presence of mean-temperature gradient

At the ends of the burner measured pressure reflection coefficients R_0 and R_1 were used. In cases when the temperature-profile is constant, the reflection coefficient is simply the ratio of the pressure amplitudes of the reflected and incident waves. However, when the temperature is not constant, care must be taken and a more general form of the reflection coefficient must be applied. The method we used was to introduce an infinitesimally thin layer at each end ($0 \leq x \leq \Delta$ and $L - \Delta \leq x \leq L$), assuming constant temperature inside the layers, and connecting them to the neighboring regions by pressure and velocity continuity. The amplitude of the reflected wave was expressed as a function of the incident wave amplitude. At the left boundary the pressure is given by

$$\hat{p} = \begin{cases} B\left[R_0 e^{ikx} + e^{-ikx}\right] & 0 < x < \Delta \ , \\ C\hat{p}_1 + D\hat{p}_2 & x > \Delta \ , \end{cases} \tag{4.3.17}$$

where B is the amplitude of the incident wave approaching the boundary at $x = 0$. C and D are the amplitudes outside the thin layer ($x > \Delta$), where $\hat{p}_2$ is the travelling wave towards the interface at $x = \Delta$, $\hat{p}_1$ is the reflected one. In this region the mean temperature is non-uniform. Since there is no change in the temperature and in the cross-section across the interface at $x = \Delta$, we require that the pressure and its axial

derivative is continuous. This yields two equations

$$B\left[R_0 e^{ik\Delta} + e^{-ik\Delta}\right] = C\hat{p}_1\Big|_{x=\Delta} + D\hat{p}_2\Big|_{x=\Delta} , \tag{4.3.18a}$$

$$i\frac{\omega}{\bar{c}_0} B\left[R_0 e^{ik\Delta} - e^{-ik\Delta}\right] = C\frac{\hat{p}_1}{dx}\Big|_{x=\Delta} + D\frac{\hat{p}_2}{dx}\Big|_{x=\Delta} . \tag{4.3.18b}$$

The generalized reflection coefficient is $R_0^T = C/D$. Taking the limit of $\Delta \to 0$ gives

$$R_0^T = -\frac{(R_0+1)\frac{1}{i\frac{\omega}{\bar{c}_0}}\frac{d\hat{p}_2}{dx}\Big|_{x=0} - (R_0-1)\hat{p}_2\Big|_{x=0}}{(R_0+1)\frac{1}{i\frac{\omega}{\bar{c}_0}}\frac{d\hat{p}_1}{dx}\Big|_{x=0} - (R_0-1)\hat{p}_1\Big|_{x=0}} . \tag{4.3.19}$$

If the mean temperature profile is linear, we can apply the solutions given by (3.2.5), and using the Hankel functions R_0^T can be written simply as

$$R_0^T = -\frac{i\frac{m_0}{|m_0|}(R_0+1)H_1^{(2)}\left(\frac{2\omega}{|m_0|}\frac{T_0}{c_0}\right) - (R_0-1)H_0^{(2)}\left(\frac{2\omega}{|m_0|}\frac{T_0}{c_0}\right)}{i\frac{m_0}{|m_0|}(R_0+1)H_1^{(1)}\left(\frac{2\omega}{|m_0|}\frac{T_0}{c_0}\right) - (R_0-1)H_0^{(1)}\left(\frac{2\omega}{|m_0|}\frac{T_0}{c_0}\right)} . \tag{4.3.20}$$

T_0 is the inlet temperature, c_0 is the speed of sound at T_0, m_0 is the temperature gradient in the inlet region. To obtain the solution of (4.3.20) we have written the derivative of the Hankel functions as

$$\frac{d}{dx}H_0^{(1,2)}\left(2q\sqrt{\alpha+\beta x}\right) = -\frac{q\beta}{\sqrt{\alpha+\beta x}}H_1^{(1,2)}\left(2q\sqrt{\alpha+\beta x}\right) , \tag{4.3.21}$$

where q, α, β are constants. We are going to apply these results in configuration 3. Using the LIMOUSINE setup of Table (4.1) at the left boundary ($x = 0$) the ratio of the amplitudes of the outgoing to the incoming wave is $R_0^T = 0.79 + i \cdot 0.246$. At the right boundary we have $R_1^T = -0.94 - i \cdot 0.333$. We can see that the temperature gradient changes the pressure reflection coefficients significantly.

QUANTITY	NOTATION	VALUE
duct inlet temperature	T_0	340 K
duct outlet temperature	T_3	1120 K
reflection at inlet	R_0	0.80 + i 0.22
reflection at outlet	R_1	-0.954 - i 0.137
temperature gradient at inlet	m_0	185.2 K/m
temperature gradient at outlet	m_1	-181.82 K/m
frequency of the fundamental mode	ω_1	723 $1/s$

Table 4.1: Measured properties of the LIMOUSINE setup

4.3.3.4 Green's function of configuration 3

We present the calculation of the Green's function of configuration 3, the calculation of the Green's functions of the other configurations can be carried out in the same way. We assume that the source lies in the flame region: $l_1 < \xi < l_2$. Therefore we assume that the Green's function of the pressure has the form

$$\hat{G}(x,\xi,\omega) = \begin{cases} A_2(\xi,\omega)\Big\{R_1 \exp[ik_0 x] + \exp[-ik_0 x]\Big\} & 0 \le x \le l_1 \\ B_1(\xi,\omega) H_0^{(1)}\left(\frac{2\omega}{|m|}\sqrt{\frac{T_0+mx}{\gamma\mathcal{R}}}\right) + B_2(\xi,\omega) H_0^{(2)}\left(\frac{2\omega}{|m|}\sqrt{\frac{T_0+mx}{\gamma\mathcal{R}}}\right) & l_1 \le x \le \xi \\ \tilde{B}_1(\xi,\omega) H_0^{(1)}\left(\frac{2\omega}{|m|}\sqrt{\frac{T_0+mx}{\gamma\mathcal{R}}}\right) + \tilde{B}_2(\xi,\omega) H_0^{(2)}\left(\frac{2\omega}{|m|}\sqrt{\frac{T_0+mx}{\gamma\mathcal{R}}}\right) & \xi \le x \le l_2 \\ C_1(\xi,\omega)\Big\{\exp[ik_1(x-L)] + R_2 \exp[-ik_1(x-L)]\Big\} & l_2 \le x \le L \end{cases} \tag{4.3.22}$$

where k_0 and k_1 are the wavenumbers of the inlet and outlet regions respectively. $A_j, B_j, \tilde{B}_j, C_j$ are complex amplitudes, $H_0^{(1)}$ and $H_0^{(2)}$ are the zeroth order Hankel functions of the first and second kind, and m is the temperature gradient in the flame. First we start with the interface at $x = l_1$. At this position the pressure and the volume velocity are continuous. Continuity of pressure yields

$$A_2\Big\{R_0 \exp[ik_0 l_1] + \exp[-ik_0 l_1]\Big\} = B_1 H_0^{(1)}\left(\frac{2\omega}{|m|}\frac{T_0}{c_0}\right) + B_2 H_0^{(2)}\left(\frac{2\omega}{|m|}\frac{T_0}{c_0}\right), \tag{4.3.23}$$

continuity of the volumetric flow rate gives

$$\frac{\mathscr{A}_0}{\mathscr{A}_1} A_2 \Big\{ R_0 \exp[ik_0 l_1] - \exp[-ik_0 l_1] \Big\} = B_1 i H_1^{(1)} \left(\frac{2\omega}{|m|} \frac{T_0}{c_0} \right) + B_2 i H_1^{(2)} \left(\frac{2\omega}{|m|} \frac{T_0}{c_0} \right) \ , \quad (4.3.24)$$

where $\bar{T}_0$ and c_0 are the mean temperature and speed of sound in the cold inlet region respectively. The unknown amplitudes B_1 and B_2 can now be expressed as functions of A_2, say, $B_1 = \beta_1(\omega) A_2$ and $B_2 = \beta_2(\omega) A_2$. Next we consider the interface at $x = l_2$. At this position the pressure and the velocity is also continuous. Continuity of pressure yields

$$\tilde{B}_1 H_0^{(1)} \left(\frac{2\omega}{|m|} \frac{T_2}{c_2} \right) + \tilde{B}_2 H_0^{(2)} \left(\frac{2\omega}{|m|} \frac{T_2}{c_2} \right) = C_1 \Big\{ \exp[ik_1(l_2 - L)] + R_1 \exp[-ik_1(l_2 - L)] \Big\} \ , \quad (4.3.25)$$

where $\bar{T}_2$ and c_2 are the mean temperature and the speed of sound at $x = l_2$. The continuity of the velocity gives

$$\tilde{B}_1 i H_1^{(1)} \left(\frac{2\omega}{|m|} \frac{T_2}{c_2} \right) + \tilde{B}_2 i H_1^{(2)} \left(\frac{2\omega}{|m|} \frac{T_2}{c_2} \right) = C_1 \Big\{ \exp[ik_1(l_2 - L)] - R_1 \exp[-ik_1(l_2 - L)] \Big\} \ . \quad (4.3.26)$$

Now we can express $\tilde{B}_1$ and $\tilde{B}_2$ as functions of C_1, i.e. $\tilde{B}_1 = \gamma_1(\omega) C_1$ and $\tilde{B}_2 = \gamma_2(\omega) C_1$. Using the Heaviside function we can write the Green's function in the flame region as:

$$G(x,\xi,\omega) = H(\xi - x)A_2(\xi,\omega)\left[\beta_1(\omega)H_0^{(1)}\left(\frac{2\omega}{|m|}\sqrt{\frac{T_0+mx}{\gamma\mathcal{R}}}\right) + \beta_2(\omega)H_0^{(2)}\left(\frac{2\omega}{|m|}\sqrt{\frac{T_0+mx}{\gamma\mathcal{R}}}\right)\right] +$$
$$+ H(x-\xi)C_1(\xi,\omega)\left[\gamma_1(\omega)H_0^{(1)}\left(\frac{2\omega}{|m|}\sqrt{\frac{T_0+mx}{\gamma\mathcal{R}}}\right) + \gamma_2(\omega)H_0^{(2)}\left(\frac{2\omega}{|m|}\sqrt{\frac{T_0+mx}{\gamma\mathcal{R}}}\right)\right] . \quad (4.3.27)$$

Applying the method described in Subsection (4.3.2), the solution of the unknown amplitudes A_2 and C_1 can be calculated from the following nonhomogeneous system of linear equations:

$$A_2(\xi,\omega)\left[\beta_1(\omega)H_0^{(1)}\left(\frac{2\omega}{|m|}\sqrt{\frac{T_0+m\xi}{\gamma\mathcal{R}}}\right) + \beta_2(\omega)H_0^{(2)}\left(\frac{2\omega}{|m|}\sqrt{\frac{T_0+m\xi}{\gamma\mathcal{R}}}\right)\right] +$$
$$- C_1(\xi,\omega)\left[\gamma_1(\omega)H_0^{(1)}\left(\frac{2\omega}{|m|}\sqrt{\frac{T_0+m\xi}{\gamma\mathcal{R}}}\right) + \gamma_2(\omega)H_0^{(2)}\left(\frac{2\omega}{|m|}\sqrt{\frac{T_0+m\xi}{\gamma\mathcal{R}}}\right)\right] = 0 , \quad (4.3.28a)$$

$$A_2(\xi,\omega)\frac{\omega}{\sqrt{\gamma\mathcal{R}(T_0+m\xi)}}\left[\beta_1(\omega)H_1^{(1)}\left(\frac{2\omega}{|m|}\sqrt{\frac{T_0+m\xi}{\gamma\mathcal{R}}}\right) + \beta_2(\omega)H_1^{(2)}\left(\frac{2\omega}{|m|}\sqrt{\frac{T_0+m\xi}{\gamma\mathcal{R}}}\right)\right] -$$
$$C_1(\xi,\omega)\frac{\omega}{\sqrt{\gamma\mathcal{R}(T_0+m\xi)}}\left[\gamma_1(\omega)H_1^{(1)}\left(\frac{2\omega}{|m|}\sqrt{\frac{T_0+m\xi}{\gamma\mathcal{R}}}\right) + \gamma_2(\omega)H_1^{(2)}\left(\frac{2\omega}{|m|}\sqrt{\frac{T_0+m\xi}{\gamma\mathcal{R}}}\right)\right] = 1 . \quad (4.3.28b)$$

We introduce the following abbreviations

$$\begin{aligned}
A(x,\omega) =& R_0\exp[ik_0x] + \exp[-ik_0x] ,\\
B(x,\omega) =& \gamma_1(\omega)H_0^{(1)}\left(\frac{2\omega}{|m|}\sqrt{\frac{T_0+mx}{\gamma\mathcal{R}}}\right) + \gamma_2(\omega)H_0^{(2)}\left(\frac{2\omega}{|m|}\sqrt{\frac{T_0+mx}{\gamma\mathcal{R}}}\right) ,\\
C(x,\omega) =& \beta_1(\omega)H_0^{(1)}\left(\frac{2\omega}{|m|}\sqrt{\frac{T_0+mx}{\gamma\mathcal{R}}}\right) + \beta_2(\omega)H_0^{(2)}\left(\frac{2\omega}{|m|}\sqrt{\frac{T_0+mx}{\gamma\mathcal{R}}}\right) ,\\
D(x,\omega) =& \exp[ik_1(x-L)] + R_1\exp[-ik_1(x-L)] ,\\
F(x,\omega) =& \frac{2i|m|}{\pi(T_0+mx)}\Big[\beta_2(\omega)\gamma_1(\omega) - \beta_1(\omega)\gamma_2(\omega)\Big] ,
\end{aligned} \quad (4.3.29)$$

to write the Green's function in a compact form

$$\hat{G}(x,\xi,\omega) = \begin{cases} \dfrac{A(x,\omega)B(\xi,\omega)}{F(\xi,\omega)} & 0 \le x < l_1 \ , \\ \dfrac{C(x,\omega)B(\xi,\omega)}{F(\xi,\omega)} & l_1 \le x \le \xi \ , \\ \dfrac{B(x,\omega)C(\xi,\omega)}{F(\xi,\omega)} & \xi \le x \le l_2 \ , \\ \dfrac{D(x,\omega)C(\xi,\omega)}{F(\xi,\omega)} & l_2 < x \le L \ . \end{cases} \tag{4.3.30}$$

Physically it is reasonable to assume that the point-source lies in the flame region. The method described in this section also applies if it lies in the inlet or outlet regions. The property of reciprocity is clearly satisfied within the region that contains the source.

4.3.3.5 Measurements

Each configuration was analyzed for a setup with properties listed in Table (4.2). In configurations 2 and 3 the mean-temperature of the inlet and outlet regions were simply the arithmetic means of T_0, T_1 and T_2, T_3 respectively. (See Figure (4.6))

QUANTITY	NOTATION	VALUE
mean pressure	$\bar{p}$	1 atm
duct inlet temperature	T_0	340 K
flame inlet temperature	T_1	400 K
flame outlet temperature	T_2	1320 K
duct outlet temperature	T_3	1120 K
specific heat ratio	γ	1.35
gas constant of air	$\mathcal{R}$	286.9 $J/(kgK)$
length of the burner	L	1.424 m
length of inlet	l_1	0.324 m
downstream end of the flame region	l_2	0.394 m
cross-sectional area of inlet	$\mathscr{A}_0$	0.0045 m^2
cross-sectional area of outlet	$\mathscr{A}_1$	0.009 m^2
reflection coefficient at inlet	R_1	0.80 + i 0.22
reflection coefficient at outlet	R_2	-0.954 - i 0.137

Table 4.2: LIMOUSINE setup

4.3.3.6 Eigenfrequencies

The eigenfrequencies predicted for the five configurations were calculated. The results ω_n (n=1,2) are listed in Table (4.3). The real parts correspond to the frequencies of the first and second mode; the (negative) imaginary parts are due to energy losses at the tube ends.

mode no.	Conf. 1	Conf. 2	Conf. 3	Conf. 4	Conf. 5
1	530.35 - i 33.38	764.76 - i 32.50	760.34 - i 32.30	759.61 - i 30.66	758.07 - i 30.87
2	1468.3 - i 33.38	1720.8 - i 70.18	1738.6 - i 72.94	1755.7 - i 73.06	1741.3 - i 70.44

Table 4.3: Comparison of the eigenfrequencies in [rad/sec] (measurement: 723 s^{-1})

The first eigenfrequency of configurations 2,3,4,5 compares very well with the measured frequency of 723 s^{-1}. Configuration 1, which assumes a small jump in the characteristic impedance, gives results with 25 % error, therefore the change in this quantity is large enough to require numerical solutions. The reason why the linear and quadratic model does not improve the result is that the flame width is approximately two orders of magnitude smaller than the wavelength of the fundamental mode.

4.3.3.7 Pressure mode shape

The frequency domain tailored Green's function of configurations 2,3 and 4 are shown in Figure (4.7) at their eigenfrequencies respectively. We assumed that the point-source is located at $\xi = l_2$, where the axial mean temperature has its absolute maximum.

The agreement between the measured and predicted pressure mode shapes is remarkable for configurations 2,3 and 4. This is despite the fact that we neglected mean flow and preheating effects. Comparison of the configurations suggests that an abrupt jump in mean-temperature results in no loss of accuracy when predicting the eigenfrequency of the fundamental mode. The mode shapes are approximated very well by all configurations, there is no need to include temperature gradient even in the flame zone. In the next subsection we study the dependence of the relative damping rate (ω_i/ω_r) on

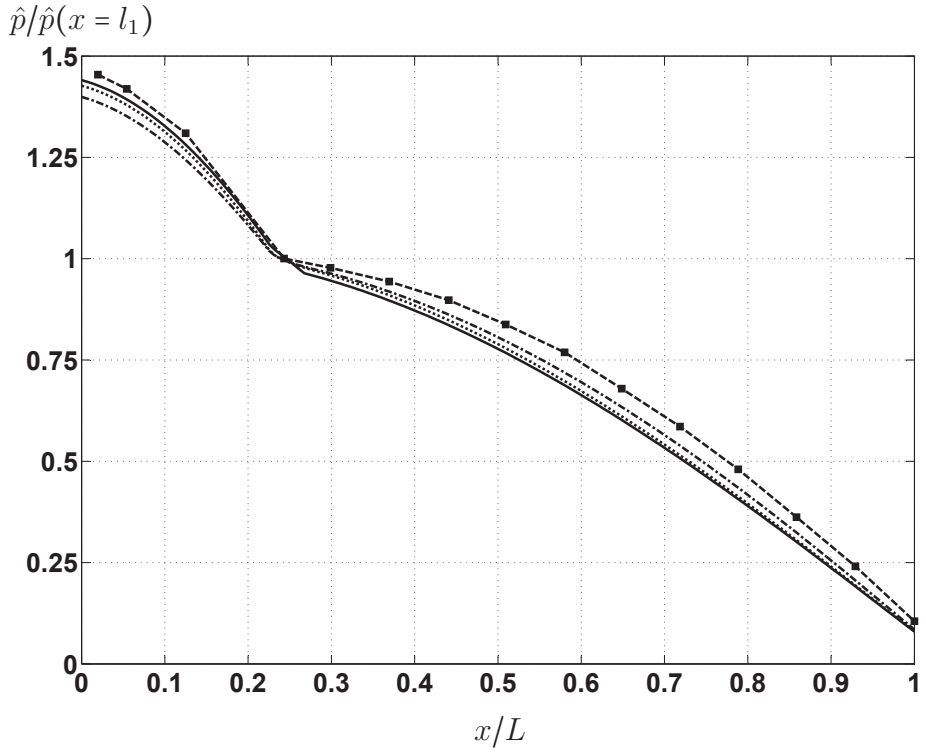

Figure 4.7: Comparison of the normalized pressure mode shapes (– ■ –: measurement, ———: configuration 2, – – –: configuration 3, – · –: configuration 4)

certain parameters, and if they give similar results in the total parameter space, we can conclude that the configuration 2 is sufficient to capture the phenomena quantitatively.

4.3.3.8 Dependence of the eigenfrequency and growth rate on the parameters

The predicted eigenfrequencies and mode shapes agree very well for configurations 2,3,4. Now we investigate how certain parameters affect the relative damping rate ($|\omega_i/\omega_r|$). We vary the following parameters:

- the jump in the cross sectional area ($\mathscr{A}_1/\mathscr{A}_0$),
- the total length of the burner (L), and
- the total phase of the reflections ($\varphi_0 + \varphi_1$).

Figure (4.8) shows the effect of the jump in the cross-sectional area on the relative

damping.

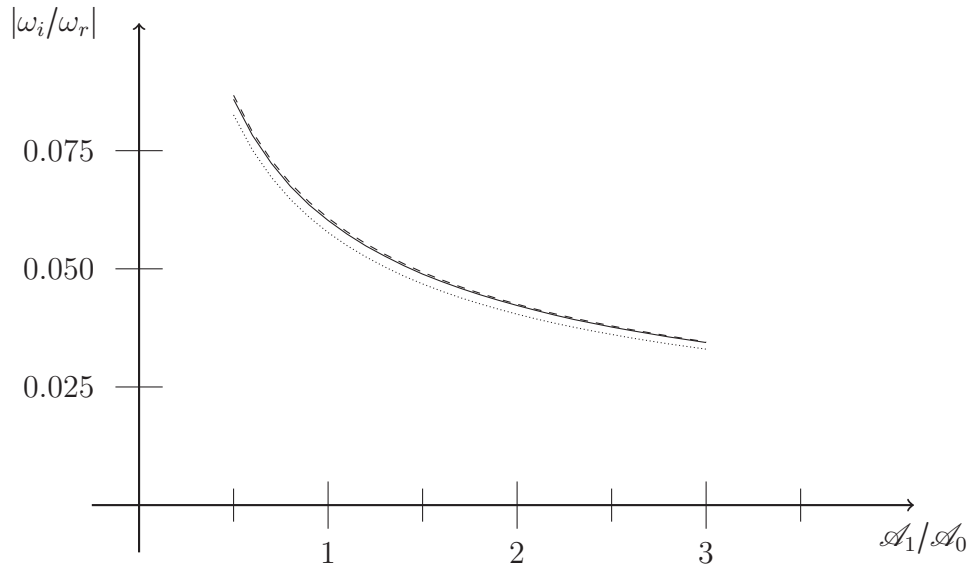

Figure 4.8: Relative damping as function of the area jump (———: configuration 2, – – –: configuration 3, ·····: configuration 4)

Figure (4.9) shows the effect of changing the length of the hot upstream section ($L-l_2$). The relative damping rate is plotted as function of the total length of the burner (L).

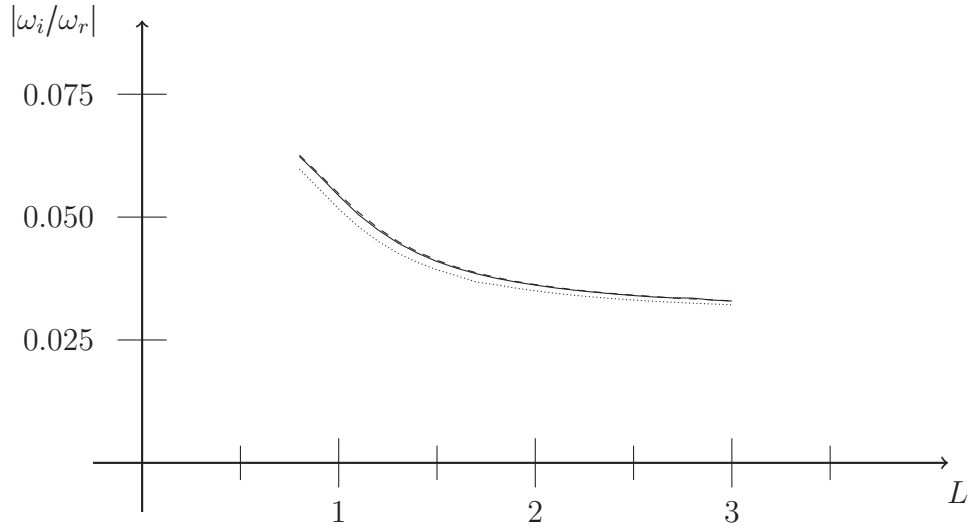

Figure 4.9: Relative damping as function of the burner length (———: configuration 2, – – –: configuration 3, ·····: configuration 4, l_1 kept constant)

Figure (4.10) shows the effect of changing the phase of the reflection coefficient at the

outlet (φ_1). The relative damping rate is plotted as function of the total phase of the reflections ($\varphi_0 + \varphi_1$).

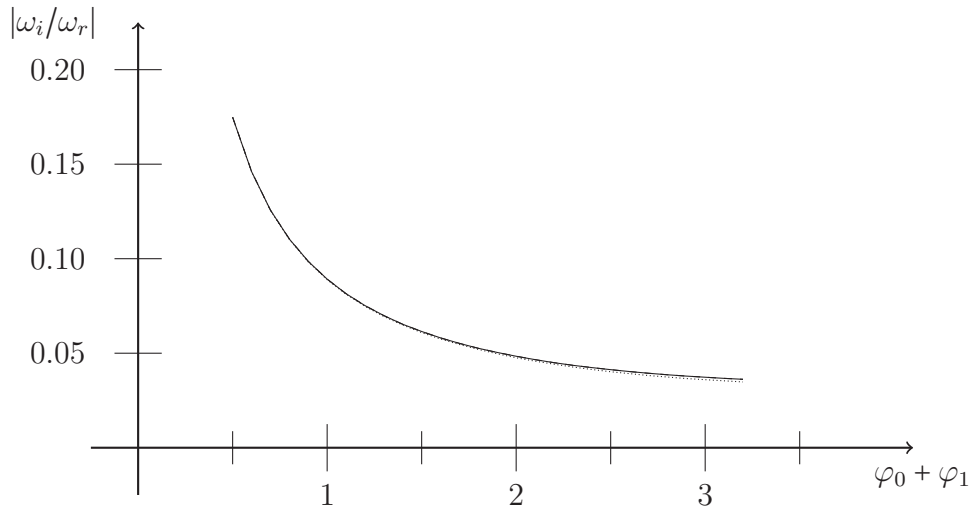

Figure 4.10: Relative damping as function of the total phase of reflections (———: configuration 2, – – –: configuration 3, ·····: configuration 4, φ_0 kept constant)

Comparing the figures shows that in Figures (4.8) and (4.9) the relative damping rate covers only a small range, in Figure (4.10) however the relative damping covers a large range. This property is reflected in Eq. (4.3.16). It shows that in a burner with (a small) jump in the characteristic impedance the relative damping rate is not affected to the leading order by changing the length of the burner or by changing the jump in the cross-sections, but it is strongly affected by changing the phase of the reflections at the boundaries. We can therefore conclude that the most efficient way to control the relative damping rate is to control the phase of the reflections at the boundaries.

4.3.3.9 Small temperature gradient

We found that including the temperature gradient in the inlet and outlet regions did not improve the results in case of the fundamental mode. To investigate under which conditions it can be neglected we apply a perturbation technique: the method of multiple scales. The method is described in [Mickens, 1981; Nayfeh and Mook, 1995; Zwillinger, 1998]. The technique consists of separating the time scale of the oscillation

from the time scale of the change in the amplitude. We introduce a small parameter, which is related to the temperature gradient: $\epsilon = (T_1 - T_0)/T_0 \ll 1$, where T_0 is the temperature at the beginning of a region, T_1 is the temperature at the end of a region. We introduce the following non-dimensional quantities

$$\begin{aligned} \tilde{x} =& x\frac{\omega}{c_0} \ , \\ \tilde{T} =& \frac{\bar{T} - T_0}{T_1 - T_0} \ . \end{aligned} \tag{4.3.31}$$

Since $0 \leq \tilde{T} \leq 1$, we can write $1/(1 + \epsilon\tilde{T})$ as $1 - \epsilon\tilde{T}$. We separate the scales, i.e.

$$\begin{aligned} \tilde{x} =& \tilde{x}_0 + \epsilon\tilde{x}_1 \ , \\ \tilde{p} =& \tilde{p}_0 + \epsilon\tilde{p}_1 \ , \\ \frac{d}{d\tilde{x}} =& \frac{\partial}{\partial\tilde{x}_0} + \epsilon\frac{\partial}{\partial\tilde{x}_1} \ . \end{aligned} \tag{4.3.32}$$

Applying (4.3.32) for Eq. (3.2.1) yields

$$\frac{d^2\tilde{p}}{d\tilde{x}^2} + \tilde{p} = \epsilon\tilde{p}\tilde{T} - \epsilon\frac{d\tilde{T}}{d\tilde{x}}\frac{d\tilde{p}}{d\tilde{x}} \ . \tag{4.3.33}$$

To the leading order we have a harmonic oscillation, i.e. $\tilde{p}_0 = A(\tilde{x}_1)\exp(i\tilde{x}_0) + C.C.$. At the order of ϵ^1 we have

$$\frac{\partial^2\tilde{p}_1}{\partial\tilde{x}_0^2} + \tilde{p}_1 = -2\frac{\partial^2\tilde{p}_0}{\partial\tilde{x}_0\partial\tilde{x}_1} + \tilde{p}_0\tilde{T}_0 - \frac{\partial\tilde{T}_0}{\partial\tilde{x}_0}\frac{\partial\tilde{p}_0}{\partial\tilde{x}_0} \ . \tag{4.3.34}$$

All terms on the R.H.S. are secular, therefore equating them to zero yields

$$\frac{\partial A}{\partial\tilde{x}_1} = -\frac{1}{2}A\left(i\tilde{T}_0 + \frac{\partial\tilde{T}_0}{\partial\tilde{x}_0}\right) \ . \tag{4.3.35}$$

The solution for $A(\tilde{x}_1)$ is

$$A(\tilde{x}_1) = a_0 \exp\left[-\frac{1}{2}\int\left(i\tilde{T}_0 + \frac{\partial\tilde{T}_0}{\partial\tilde{x}_0}\right)d\tilde{x}_1\right] = a_0 \exp\left[-i\frac{1}{2}\tilde{T}_0\epsilon\tilde{x}_0\right]\exp\left[-\frac{1}{2}\frac{\partial\tilde{T}_0}{\partial\tilde{x}_0}\epsilon\tilde{x}_0\right] , \tag{4.3.36}$$

where a_0 is constant. So far we derived an asymptotic solution of Eq. (3.2.1) for small temperature gradients. The investigation leading to Eq. (4.3.36) shows that the effect of the temperature gradient can be neglected, if $|\epsilon\tilde{x}_0|$ is small

$$|\epsilon\tilde{x}_0| = \left|\frac{T_1 - T_0}{T_0}\frac{\omega L}{c_0}\frac{x}{L}\right| = \left|\frac{T_1 - T_0}{T_0}\frac{L}{\lambda_0}\frac{x}{L}\right| \ll 1 , \tag{4.3.37}$$

where L is the length of the region. Eq. (4.3.37) shows that the temperature gradient is negligible if the total change in the temperature relative to the initial temperature is small enough, and if the wavelength at the initial temperature is larger than the length of the region. In the LIMOUSINE setup ϵ in the cold inlet region is 0.3, and in the hot outlet region it is 0.15, therefore the asymptotic solution of (4.3.36) is valid. Furthermore the value of $(T_1 - T_0)L/T_0\lambda_0$ in (4.3.37) is 0.18 and 0.17 in the cold and hot regions respectively, which shows that the temperature gradient can be neglected. In the flame region ϵ is approximately 4, therefore we cannot assume negligible temperature gradient there.

4.3.3.10 Large temperature gradient

Comparison of configuration 2 and 3 suggests that in case of the fundamental mode we can model the abrupt change in the temperature as a jump. The scale separation and the WKB methods are not applicable in this case, therefore we draw conclusions by investigating, under which conditions configuration 3 reduces to configuration 2. The pressure in the flame region of configuration 3 is described by the Hankel functions,

in configuration 2 by $\pm \exp ik_0(x - l_1)$. Eq. (4.3.23) shows that the jump condition is applicable if the argument of the Hankel function in Eq. (4.3.23) is small enough to approximate it by 1

$$H_0^{1,2}\left(\frac{2\omega}{|m|}\frac{T_0}{c_0}\right) \approx 1 \ . \tag{4.3.38}$$

Eq. (4.3.38) holds, if

$$\frac{\omega}{|m|}\frac{T_0}{c_0} \ll 1 \ . \tag{4.3.39}$$

Because the temperature gradient is $m = (T_1 - T_0)/L$, we can rewrite Eq. (4.3.39) as

$$\left|\frac{\omega L}{c_0}\frac{T_0}{T_1 - T_0}\right| = \left|\frac{L}{\lambda_0}\frac{T_0}{T_1 - T_0}\right| \ll 1 \ . \tag{4.3.40}$$

The value of the expression given by (4.3.40) in the flame region is 0.08, which shows the validity of modeling the temperature change as a jump. The same manipulation can be carried out for a quadratic temperature profile. Expression (4.3.40) gives correct results also for examples showed in Sujith [2001].

4.3.4 Tailored Green's function in the time-domain for the LIMOUSINE burner

We use Eq. (4.3.30) for the frequency-domain tailored Green's function. In order to obtain the Green's function in the time-domain, we apply Inverse Fourier Transform in the following form

$$G(x, \xi, t, \tau) = -\frac{1}{2\pi}\int_{-\infty}^{\infty} \hat{G}(x, \xi, \omega)e^{-i\omega t}d\omega \ . \tag{4.3.41}$$

The integral with respect to ω, which yields the inverse transform, is calculated with the residue theorem

$$-\frac{1}{2\pi}\int_{-\infty}^{\infty}\hat{G}(x,\xi,\omega)e^{-i\omega t}d\omega = -i\sum_{k} Res\left(\hat{G}(x,\xi,\omega)e^{-i\omega t}\right)\Big|_{\omega=\omega_n} . \tag{4.3.42}$$

For $t < 0$ we integrate along the closed path involving the semicircle in the upper half plane (see Figure 4.11). No poles are enclosed by this path, hence

$$-\frac{1}{2\pi}\int_{-\infty}^{\infty}\hat{G}(x,\xi,\omega)e^{-i\omega t}d\omega = 0 \quad \text{if} \quad t < 0 . \tag{4.3.43}$$

For $t > 0$ we integrate along the path involving the semicircle in the lower half plane. All poles are enclosed by this curve. Using Eq. (4.3.30) we can see that the frequency domain Green's function can be written generally as $p(\omega)/q(\omega)$. The residue of a quotient $p(\omega)/q(\omega)$ with simple poles can be obtained by [Osborne, 1999, p.158]

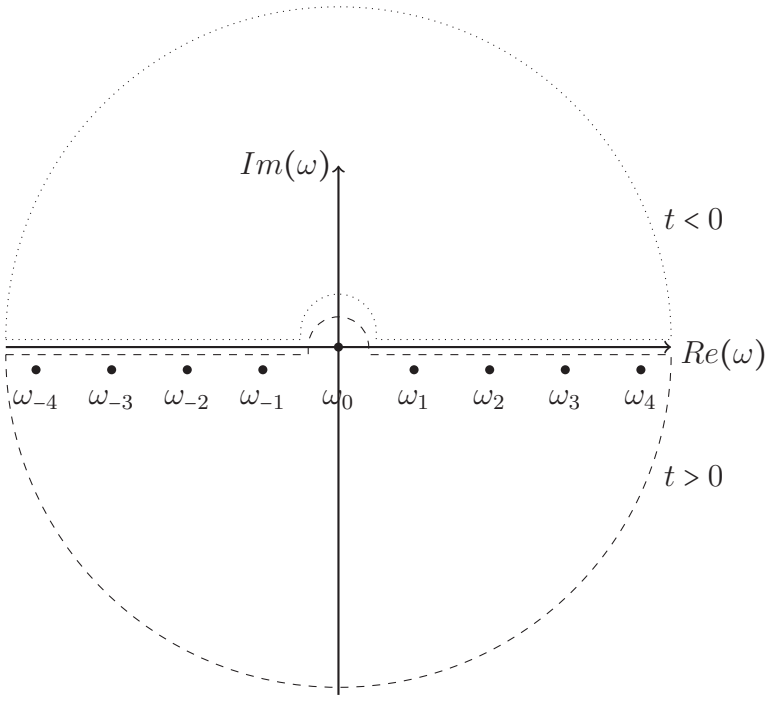

Figure 4.11: Distribution of the complex eigenfrequencies and integration paths (– – –: $t > 0$, ·····: $t < 0$)

$$Res\left(\frac{p(\omega_n)}{q(\omega_n)}\right) = \left.\frac{p(\omega)}{\frac{\partial q(\omega)}{\partial \omega}}\right|_{\omega=\omega_n} . \tag{4.3.44}$$

We can then combine the results for $t < 0$ and $t > 0$ by using the Heaviside function,

$$-\frac{1}{2\pi}\int_{-\infty}^{\infty} e^{-i\omega t}\frac{p(\omega)}{q(\omega)}d\omega = iH(t)\sum_{k=-\infty}^{\infty} e^{-i\omega t}\left.\frac{p(\omega)}{\frac{\partial q(\omega)}{\partial \omega}}\right|_{\omega=\omega_n} . \tag{4.3.45}$$

Sturm's oscillation theorem states that the poles are simple, and the Green's function has infinite number of them. It can be shown that the pole of the trivial solution $\omega = 0$ yields vanishing residue. The time-domain Green's function can be therefore calculated as

$$G(x,\xi,t,\tau) = \sum_{\substack{k=-\infty \\ k\neq 0}}^{\infty} iH(t-\tau)e^{-i\omega_k(t-\tau)}\hat{g}(x,\xi,\omega_k) \quad \text{where} \quad \hat{g}(x,\xi,\omega_k) = \left.\frac{p(\omega)}{\frac{\partial q(\omega)}{\partial \omega}}\right|_{\omega=\omega_k} . \tag{4.3.46}$$

The sum in Eq. (4.3.46) involves modes and their complex conjugate as well, because the eigenfrequencies are symmetric to the imaginary axis. To show this we multiply Eq. (3.2.1) by the complex conjugate of $\hat{p}$

$$\bar{T}\hat{p}^*\frac{d^2\hat{p}}{dx^2} + \frac{d\bar{T}}{dx}\hat{p}^*\frac{d\hat{p}}{dx} + \frac{\omega^2}{\gamma\mathcal{R}}\hat{p}^*\hat{p} = 0 . \tag{4.3.47}$$

We multiply the complex conjugate of Eq. (3.2.1) by $\hat{p}$

$$\bar{T}\hat{p}\frac{d^2\hat{p}^*}{dx^2} + \frac{d\bar{T}}{dx}\hat{p}\frac{d\hat{p}^*}{dx} + \frac{\omega^{*2}}{\gamma\mathcal{R}}\hat{p}\hat{p}^* = 0 . \tag{4.3.48}$$

We subtract Eq. (4.3.47) from Eq. (4.3.48) to get

$$\frac{d}{dx}\left[\bar{c}\left(\hat{p}^*\frac{d\hat{p}}{dx}-\hat{p}\frac{d\hat{p}^*}{dx}\right)\right]=(\omega^2-\omega^{*2})\hat{p}\hat{p}^*\ , \tag{4.3.49}$$

then we integrate Eq. (4.3.49) over $[0,L]$ with respect to x. Because the boundary conditions are linear, homogeneous and unmixed, the L.H.S. vanishes, and therefore we get

$$(\omega^2-\omega^{*2})\int_0^L|\hat{p}|^2\,dx=0\ , \tag{4.3.50}$$

which is satisfied if $\omega=\pm\omega^*$, i.e. the eigenfrequencies are symmetric to the imaginary axis. Applying this property we can write the time-domain Green's function in Eq. (4.3.46) as

$$G(x,\xi,t,\tau)=\sum_{n=1}^{\infty}iH(t-\tau)e^{-i\omega_n(t-\tau)}\hat{g}(x,\xi,\omega_n)+C.C.\ , \tag{4.3.51}$$

where $C.C.$ denotes the complex conjugate. One can pick a certain mode in Eq. (4.3.51) by taking a certain mode number n.

4.4 Conclusions

We considered 5 configurations (to model the laboratory burner) with increasingly complex mean temperature profiles and calculated the eigenfrequencies and pressure distribution with a Green's function approach. Comparing the results we found that the simplest configuration (burner with uniform temperature in the cold inlet and hot outlet regions, *small* jump in the mean temperature in the flame region) gave predictions with a substantial error, while the other configurations all predicted very similar results which agreed very well with the measurements. We can therefore conclude that

configuration 2 (piecewise uniform temperature profile with a jump at the flame) captures all important properties of the fundamental mode and that there is no need for more complex modelling.

We derived asymptotic solutions for the wave equation with non-uniform temperature when the temperature increase across a region is either small or large. The time-domain Green's function was also presented by applying inverse Fourier Transform. Summary of the chapter in keywords:

- we reduced the problem to finding the corresponding Green's function of the governing equation,
- we modelled realistic configurations,
- in case of the fundamental mode a simple configuration with a mean temperature jump gives accurate results in the total parameter space,
- we identified quantities, which show when the temperature jump can be neglected or modeled as a jump, and
- we presented the Green's function in the time-domain as superposition of the modes.

Chapter 5

Heat-release

In this chapter we extend our consideration from the passive resonator to the active resonator by relating the fluctuating heat-release to the acoustic quantities. We assume that the released heat is proportional to the flame surface area, which is going to be therefore calculated. To this end we apply an analytical approach: the level set method, which is capable to track the evolution of geometrical shapes. We derive expressions for the heat-release rate in the linear and weakly non-linear regimes.

5.1 Introduction

Several physical effects that occur in a combustion system act as sources of sound [Crighton et al., 1992, p.381]: unsteady combustion, viscosity (Obermeier [1985]), heat and mass diffusion (Kempton [1975]; Morfey [1973]; Obermeier [1975]), mean density variation (e.g. turbulent two-phase flow Crighton and Ffowcs Williams [1969]), and momentum changes of density inhomogeneities (Ffowcs Williams and Howe [1974]). By far the dominant source mechanism is the unsteady combustion. Variations in the heat-release rate produce temperature fluctuations, which in turn produce pressure fluctuations. These pressure fluctuations travel away from the combustion zone as a sound wave.

Unsteady combustion is a strong monopole source [Crighton et al., 1992, p.381]. The

prototype of a monopole source is a body with oscillating volume.

The governing equation for combustion-driven sound waves is Eq. (3.1.12), which is the wave equation for the acoustic pressure with a source term that is due to the unsteady heat release rate. To solve Eq. (3.1.12) we need to close the acoustic loop, i.e. to relate the volumetric heat-release rate Q' to the acoustic properties.

5.2 $\mathcal{G}$-Equation

5.2.1 Derivation of the $\mathcal{G}$-equation

In this thesis we consider premixed flames. If the fuel has been homogeneously mixed with the oxidizer and a heat source is supplied, it becomes possible for a flame to propagate. The gas behind the flame rapidly approaches the burnt gas state, while the mixture in front of the flame is in the unburnt state.

The flame can be considered as an interface, which separates the unburnt and burnt mixtures. The flame speed is the rate of propagation of the flame. Laminar flame speed is the speed at which a laminar flame propagates through a stationary unburnt mixture. The laminar flame speed is the property of the mixture only, but this does not hold for turbulent flames. As flow velocity and therefore turbulence increases, the flame begins to wrinkle, then corrugate and eventually the flame front breaks up. Therefore, the flame front of a turbulent flame propagates at a speed that does not only depend on the mixture's chemical properties, but also on the flow and on the turbulence. In this thesis we consider only laminar flames, and neglect the effects of turbulence.

We assume that the flame sheet is infinitely thin and the released heat is constant along the flame, therefore in our model the unsteady heat release rate depends on the instantaneous area of the flame sheet only. To represent an infinitely thin flame we apply the level set method (LSM), which is an analytical tool of mathematics for tracking interfaces and shapes. It is capable of tracking shapes which change the topology, for instance breaking down into two objects or the reverse of this process. Application of LSM to model the flame sheet is described in [Peters, 2000, pp.91-119].

Many authors have used this method, for example: Dowling [1997, 1999]; Ducruix et al. [2000]; Lee and Lieuwen [2003]; Lieuwen [2005]; Lieuwen and Zinn [1998]; Schuller et al. [2002, 2003].

The flame surface divides the region of the combustor into two separate zones. We introduce a scalar quantity, $\mathcal{G}$ which is negative ($\mathcal{G} < 0$) upstream of the flame in the unburnt region, and positive ($\mathcal{G} > 0$) downstream of the flame in the burnt region. This is shown in Figure (5.1). We can write the Lagrangian derivative of the scalar $\mathcal{G}$ along the flame surface as

$$\frac{\partial \mathcal{G}}{\partial t} + \nabla \mathcal{G} \cdot \frac{d\boldsymbol{x}}{dt} = 0 \ . \tag{5.2.1}$$

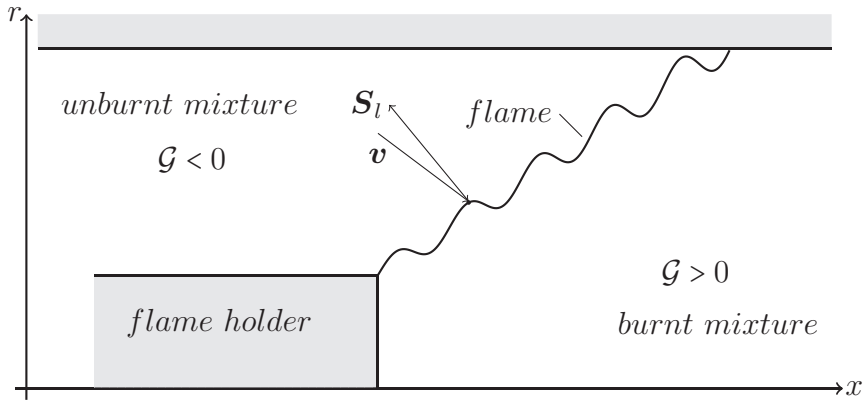

Figure 5.1: Schematic representation of the flame by the level set method

The mass conservation across the flame yields the relation between the flow velocity and the flame speed. The tangential component of the flow velocity is not affected by the combustion, the normal velocity component however changes due to the temperature jump across the flame sheet. Therefore we can write

$$\frac{d\boldsymbol{x}}{dt} = \boldsymbol{v} + \boldsymbol{n} \cdot S_l \ , \tag{5.2.2}$$

where S_l is the laminar flame speed, $\boldsymbol{v}$ is the flow velocity vector in the unburnt region and $\boldsymbol{n}$ is the normal vector pointing towards the unburnt mixture. The normal vector

is given by $\boldsymbol{n} = -\nabla\mathcal{G}/|\nabla\mathcal{G}|$, where $|\ldots|$ indicates the Euclidean norm, and therefore the equation which describes the flame sheet evolution is

$$\frac{\partial \mathcal{G}}{\partial t} + \boldsymbol{v} \cdot \nabla\mathcal{G} = S_l|\nabla\mathcal{G}| \ . \tag{5.2.3}$$

The R.H.S. of Eq. (5.2.3) is non-linear, this type of partial differential equations is called Eikonal.

5.2.2 Laminar flame speed

The laminar flame speed S_l depends on several parameters. From [Peters, 2000, p.101]

$$S_l = S_l^0 - \mathcal{L}S_l^0\kappa \ , \tag{5.2.4}$$

where S_l^0 is the flame speed of the uncurved flame and $\mathcal{L}$ is the Markstein length, which characterizes the effect of the curvature on the flame speed, and κ is the curvature. The flame curvature is defined in a standard mathematical way by $\kappa = \nabla \cdot \boldsymbol{n}$. Eq. (5.2.4) shows that the flame speed of a curved flame differs from that of the corresponding uncurved flame.

5.2.2.1 Dependence on temperature and pressure

Important factors that affect the uncurved laminar flame speed (S_l^0) are the temperature and the pressure [Turns, 2000, p.278]. It is convenient to introduce here the concept of 'equivalence ratio'. It is given by the expression

$$\Phi = \frac{(fuel/air)_{actual}}{(fuel/air)_{stoich}} \ , \tag{5.2.5}$$

where $(fuel/air)_{stoich}$ is the stoichiometric fuel/air ratio. The terms lean and rich refer to the case where $\Phi < 1$ and $\Phi > 1$ respectively. Adiabatic flame temperature is the

characteristic temperature of a combustion process. The constant pressure adiabatic flame temperature and constant volume adiabatic flame temperature are the temperature values that result from a complete combustion process which occurs without heat loss at constant pressure and volume respectively.

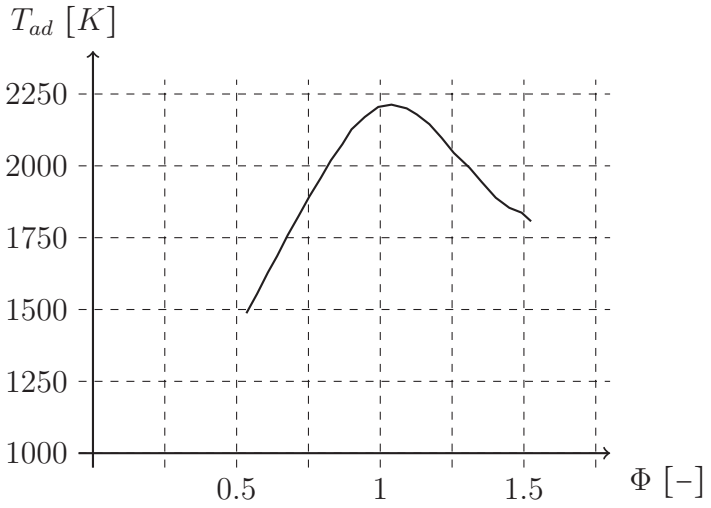

Figure 5.2: Adiabatic flame temperature of methane as function of the stoichiometric ratio measured at constant pressure of 1 atm. and 25 ^{o}C, from Law et al. [2006]

Figure (5.2) shows how the adiabatic flame temperature of methane (the fuel used in the LIMOUSINE burner) depends on the equivalence ratio. Using measurements empirical relationships were introduced to calculate the flame speed. Andrews and Bradley [1972] included only the effect of changing the temperature of the unburnt mixture, and derived Eq. (5.2.6a). Metghalchi and Keck [1982] provided Eq. (5.2.6b) which includes the effect of the equivalence ratio, the temperature of the unburnt mixture (T_u) and the pressure (p). In this case the laminar flame speed is calculated from a reference point $\left[S^0_{l,ref}; T_{u,ref}; p_{ref}\right]$ using the empirical coefficients α and β.

$$S^0_l = 10 + 3.71 \cdot 10^{-4} \left[T_u\right]^2 \ , \tag{5.2.6a}$$

$$S^0_l = S^0_{l,ref}(\Phi) \left(\frac{T_u}{T_{u,ref}}\right)^{\alpha} \left(\frac{p}{p_{ref}}\right)^{\beta} \ , \tag{5.2.6b}$$

where T_u is the temperature of the unburnt mixture and must be taken in Kelvin.

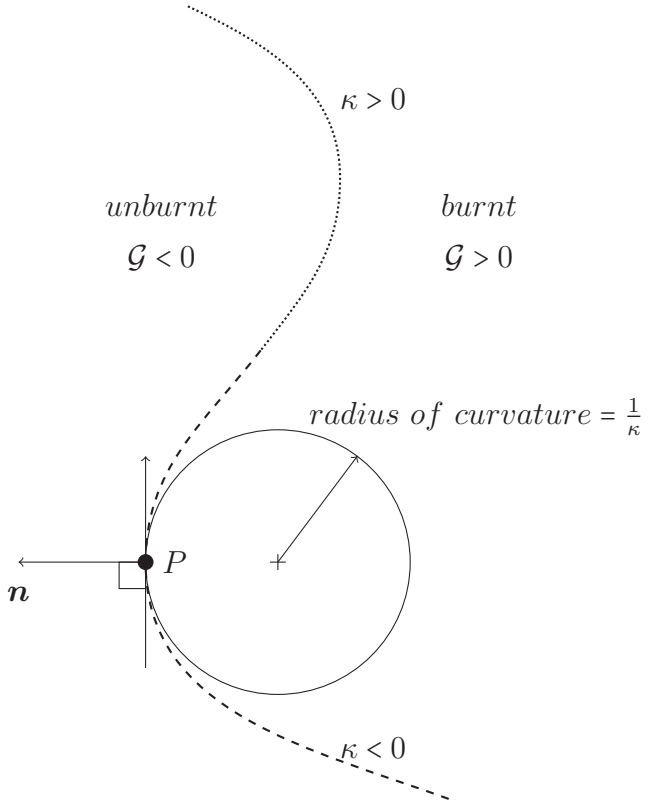

Figure 5.3: Curved flame front ($\cdots$: $\kappa < 0$, $- - -$: $\kappa > 0$)

5.2.2.2 Dependence on curvature

The flame speed also depends on the curvature (Markstein [1951]). Figure (5.3) shows a curved flame front. The curvature term adds a second order derivative to the kinematic $\mathcal{G}$-equation. This avoids the formation of cusps and non-unique solutions that would result from a constant value of the flame speed. The physical interpretation is that the curvature affects the flame speed along the flame surface, i.e. positive curvature results in smaller flame speed and vice versa.

5.2.2.3 Dependence on the Markstein length

The Markstein length is the product of the Markstein number (Mn) and the flame thickness (l_F). The exact formula to calculate the Markstein number can be found

in [Peters, 2000, p.90]. In the LIMOUSINE project methane is burnt in the test combustor. For methane flames the expression reduces to (Bechtold and Matalon [2001])

$$\mathrm{Mn} = \frac{\mathcal{L}}{l_F} = \frac{1}{\varphi} \ln \frac{1}{1-\varphi} \ , \tag{5.2.7}$$

where $\varphi = (T_b - T_u)/T_b$ is the gas expansion parameter, T_b and T_u is the temperature of the burnt and the unburnt gas respectively. The flame thickness can be calculated by using a one-dimensional approach based on conservation equations [Turns, 2000, pp.267-280]

$$l_F = 2\frac{k}{\rho_u c_p S_l^0} \ . \tag{5.2.8}$$

In the LIMOUSINE project using Eq. (5.2.8) the flame thickness is $l_F \approx 2.2$ mm, which is in excellent agreement with the result of the measurement of 2 mm (LIMOUSINE group [2011]). Using the measurement data of Table (4.2) $T_b = 1320$ K and $T_u = 400$ K, the Markstein length of our setup is $\mathcal{L} = 3.77$ mm. This result is going to be used later.

5.2.3 Non-linearities of the $\mathcal{G}$-Equation model

The $\mathcal{G}$-Equation involves two different types of non-linearities. This property is emphasized also by Lieuwen [2005]. In both cases, the nonlinearity is of geometric origin and is introduced by the orthogonal flame-front propagation and by calculation of the flame surface area.

1. orthogonal flame-front propagation, and

2. dependence of the flame area upon flame position gradient.

Figure (5.4) shows the non-linearities of the $\mathcal{G}$-Equation model.

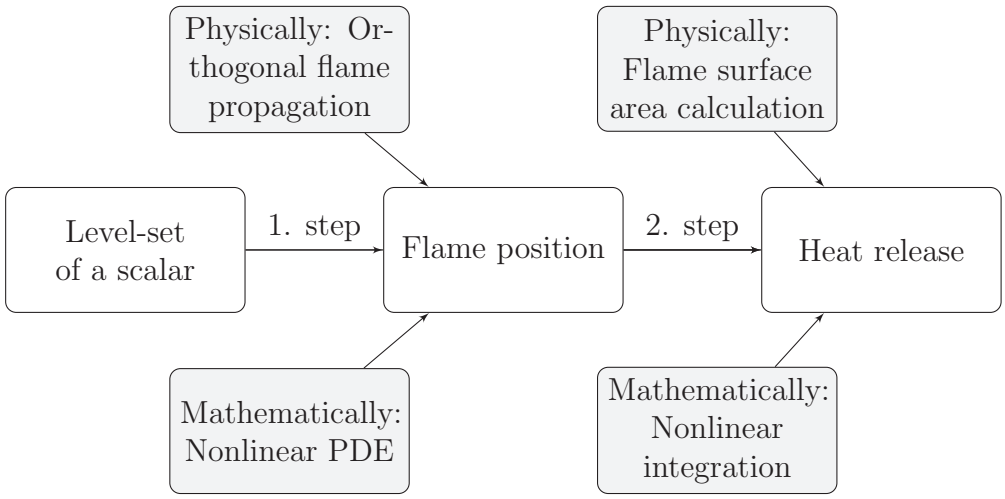

Figure 5.4: Non-linearities of the heat-release in the $\mathcal{G}$-Equation approach

5.3 Solutions of the $\mathcal{G}$-Equation

5.3.1 Curvature effects are neglected

We are going to solve the kinematic $\mathcal{G}$-Equation in a cylindrical coordinate system. At this stage we neglect the effect of the curvature. We consider two types of flames: ducted flames Figure (5.5(a)), which are attached to a flame holder and the open flames Figure (5.5(b)), in which case the flame is attached to the rim of a tube.

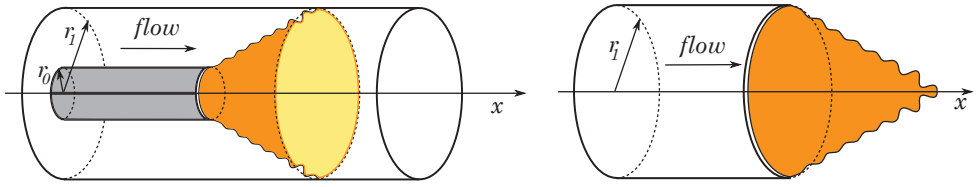

(a) Axisymmetric ducted flame (b) Axisymmetric open flame

Figure 5.5: (a) Axisymmetric ducted flame and (b) axisymmetric open flame

In a cylindrical coordinate system assuming rotational symmetry ($\partial/\partial\theta = 0$) the $\mathcal{G}$-Equation is of the following form

$$\frac{\partial \mathcal{G}}{\partial t} + u\frac{\partial \mathcal{G}}{\partial x} + v\frac{\partial \mathcal{G}}{\partial r} = S_l^0\sqrt{\left(\frac{\partial \mathcal{G}}{\partial x}\right)^2 + \left(\frac{\partial \mathcal{G}}{\partial r}\right)^2}\ , \tag{5.3.1}$$

where u is the velocity component parallel to the tube axis, and v is the radial one. We assume that the radial velocity component is negligible, i.e. $v = 0$. In the LIMOUSINE setup the width of the flame region is approximately two orders of magnitude smaller than the wavelength of the fundamental mode, therefore we assume that the spatial dependence of the fluctuating velocity component can be neglected inside the flame region, i.e. $\bar{u}(x) = \bar{u} = constant$ and $u'(x,t) = u'(t)$. Eq. (5.3.1) then simplifies to

$$\frac{\partial \mathcal{G}}{\partial t} + [\bar{u} + u'(t)]\frac{\partial \mathcal{G}}{\partial x} = S_l^0\sqrt{\left(\frac{\partial \mathcal{G}}{\partial x}\right)^2 + \left(\frac{\partial \mathcal{G}}{\partial r}\right)^2}\ . \tag{5.3.2}$$

5.3.1.1 Solution for the mean flame position

The mean component of Eq. (5.3.2) is

$$\bar{u}\frac{\partial \bar{\mathcal{G}}}{\partial x} = S_l^0\sqrt{\left(\frac{\partial \bar{\mathcal{G}}}{\partial x}\right)^2 + \left(\frac{\partial \bar{\mathcal{G}}}{\partial r}\right)^2}\ . \tag{5.3.3}$$

The boundary condition is that the flame is attached to the flame holder at the point $[x_0, r_0]$, i.e. $\bar{\mathcal{G}} = 0$ at $[x_0, r_0]$. We can write the solution in the following form

$$\bar{\mathcal{G}}(x,r) = (x - x_0) \pm (r - r_0)\sqrt{\left(\frac{\bar{u}}{S_l^0}\right)^2 - 1}\ . \tag{5.3.4}$$

This solution is shown in Figure (5.6).

Eq. (5.3.4) describes a conical shape, and shows that the mean flow velocity must be greater or equal than the laminar flame speed. Using implicit differentiation for $\bar{\mathcal{G}}$ we can see that $1/\sqrt{(\bar{u}/S_l^0)^2 - 1}$ is the tangent of the angle (denoted by α in Figure (5.6)) between the mean flame position and the tube axis. When $\bar{u} \to S_l^0$, the flame is very

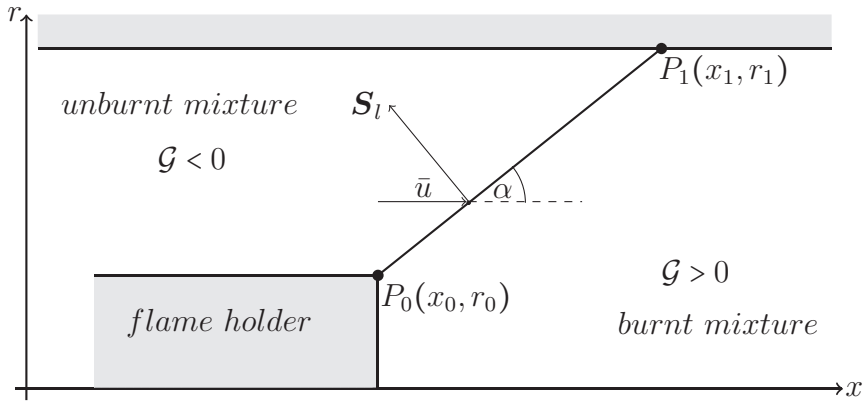

Figure 5.6: Mean position of a laminar flame for plug flow, i.e. $\bar{u}$=constant

short and its mean position is perpendicular to the tube axis. When $\bar{u} \gg S_l^0$, the flame is very long and its mean position is parallel to the tube axis. For the mean flame position to be stationary, S_l^0 must be balanced with the component of the velocity, which is perpendicular to the flame, i.e. $S_l^0 = \bar{u} \sin \alpha$.

5.3.1.2 Asymptotic solutions for the fluctuating flame position

In order to analyze Eq. (5.3.2) we introduce the following non-dimensional quantities

$$\begin{aligned} \tilde{x} &= \frac{x - x_0}{x_1 - x_0} \ , \\ \tilde{r} &= \frac{r - r_0}{r_1 - r_0} \ , \\ \tilde{t} &= t \frac{S_l^0}{\sqrt{(x_1 - x_0)^2 + (r_1 - r_0)^2}} \ , \\ \tilde{\mathcal{G}} &= \frac{\mathcal{G}}{\sqrt{(x_1 - x_0)^2 + (r_1 - r_0)^2}} \ . \end{aligned} \tag{5.3.5}$$

$[x_1, r_1]$ is the end point of the flame (see Figure (5.6)). $\mathcal{G}$ is divided by the mean length of the flame, t is divided by the time, which is needed for a perturbation to travel along the mean flame length with the flame speed S_l^0. Eq. (5.3.2) can therefore be written in the following form

$$\frac{\partial \tilde{\mathcal{G}}}{\partial \tilde{t}} + \frac{u'}{S_l^0}\frac{\partial \tilde{\mathcal{G}}}{\partial \tilde{x}} + \frac{\bar{u}}{S_l^0}\left[\sqrt{1+\left(\frac{r_1-r_0}{x_0-x_0}\right)^2}\right]\frac{\partial \tilde{\mathcal{G}}}{\partial \tilde{x}} =$$

$$= \sqrt{\left[1+\left(\frac{r_1-r_0}{x_1-x_0}\right)^2\right]\left(\frac{\partial \tilde{\mathcal{G}}}{\partial \tilde{x}}\right)^2 + \left[1+\left(\frac{x_1-x_0}{r_1-r_0}\right)^2\right]\left(\frac{\partial \tilde{\mathcal{G}}}{\partial \tilde{r}}\right)^2}\,. \quad (5.3.6)$$

We now use $\tan\alpha = (r_1 - r_0)/(x_1 - x_0)$, $S_l^0/\bar{u} = \sin\alpha$, and rewrite Eq. (5.3.6) as

$$\frac{\partial \tilde{\mathcal{G}}}{\partial \tilde{t}} + \frac{u'}{S_l^0}\frac{\partial \tilde{\mathcal{G}}}{\partial \tilde{x}} + \sqrt{\frac{1}{\sin^2\alpha} + \frac{1}{\cos^2\alpha}}\frac{\partial \tilde{\mathcal{G}}}{\partial \tilde{x}} = \sqrt{\left[1+\tan^2\alpha\right]\left(\frac{\partial \tilde{\mathcal{G}}}{\partial \tilde{x}}\right)^2 + \left[1+\frac{1}{\tan^2\alpha}\right]\left(\frac{\partial \tilde{\mathcal{G}}}{\partial \tilde{r}}\right)^2}\,. \quad (5.3.7)$$

We can see that in Eq. (5.3.7) the non-linearity is governed by $\tan^2\alpha$, i.e. by the gradient of the mean position. If $\tan^2\alpha$ is either larger or smaller than 1 by an order of magnitude, the non-linearity is weak. This is the case if the angle α is larger than approximately 70 degrees, or smaller than approximately 17 degrees. $\alpha = 70^o$ corresponds to $\bar{u}/S_l^0 = 1.05$ and $\alpha = 17^o$ to $\bar{u}/S_l^0 = 3$. These regions are shown in Figure (5.7). In a typical combustion rig the laminar flame speed is approximately 0.3 – 0.6 m/s, the mean flow velocity is larger than 1 m/s, which corresponds to region 2.

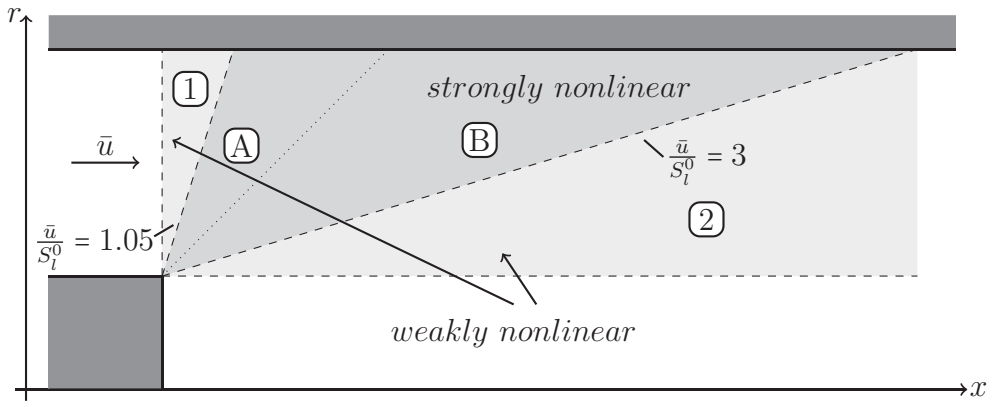

Figure 5.7: Non-linear regimes of a laminar flame (regions 1,2: weakly non-linear; A,B: strongly non-linear; $\cdots$: $\tan\alpha = 1$)

In regions 1 and 2 the $\mathcal{G}$-Equation exhibits weak non-linearity, i.e. to the leading order it is linear, and non-linear terms appear at higher orders. In regions A and B the $\mathcal{G}$-Equation is strongly non-linear, and this case is discussed in Appendix (B.1). In regions 1 and 2 we assume small amplitudes (i.e. $u' \ll \bar{u}$), therefore the dimensional form of the fluctuating component of Eq. (5.3.7) to the leading order is

$$\text{region 1}: \qquad \frac{\partial \mathcal{G}_1'}{\partial t} + (\bar{u} - S_l^0 \sin\alpha)\frac{\partial \mathcal{G}_1'}{\partial x} = u'(t) \ , \tag{5.3.8a}$$

$$\text{region 2}: \qquad \frac{\partial \mathcal{G}_2'}{\partial t} + \underline{\bar{u}\frac{\partial \mathcal{G}_2'}{\partial x}} + S_l^0 \cos\alpha \frac{\partial \mathcal{G}_2'}{\partial r} = u'(t) \ , \tag{5.3.8b}$$

where $\mathcal{G}_1'$ and $\mathcal{G}_2'$ are the fluctuating components of $\mathcal{G}$ in regions 1 and 2 respectively.

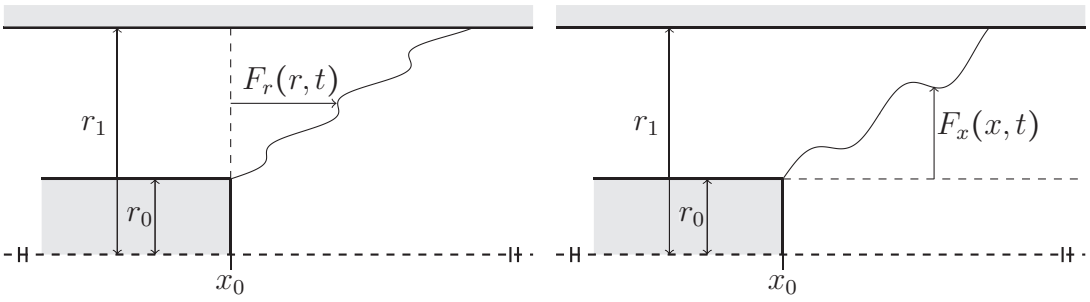

(a) $\mathcal{G} = x - x_0 - F_r(r,t)$ (b) $\mathcal{G} = r - r_0 - F_x(x,t)$

Figure 5.8: Schematic representation of the trial solutions

To solve Eq. (5.3.2) it is common to apply the trial solution of $\mathcal{G} = x - x_0 - F_r(r,t)$ or $\mathcal{G} = r - r_0 - F_x(x,t)$, which are shown in Figure (5.8). In the next section we will show that seeking the solution in the form of $\mathcal{G} = x - x_0 - F_r(r,t)$ results in loosing the underlined term in Eq. (5.3.8b).

5.3.1.3 Effects of the trial solutions

The advantage of seeking the solution of the $\mathcal{G}$-Equation in either form of $\mathcal{G} = x - x_0 - F_r(r,t)$ or $\mathcal{G} = r - r_0 - F_x(x,t)$ is that it gives solutions explicit in x or r respectively (see Figure (5.8)). The linearized fluctuating components of the flame front position are

$$\frac{\partial \mathcal{G}'}{\partial t} + \Big[\bar{u} + u'(t) - S_l^0 \sin\alpha\Big]\frac{\partial \mathcal{G}'}{\partial x} + S_l^0 \cos\alpha \frac{\partial \mathcal{G}'}{\partial r} = u'(t), \tag{5.3.9a}$$

$$\frac{\partial F_r'}{\partial t} + S_l^0 \cos\alpha \frac{\partial F_r'}{\partial r} = u'(t), \tag{5.3.9b}$$

$$\frac{\partial F_x'}{\partial t} + \Big[\bar{u} + u'(t) - S_l^0 \sin\alpha\Big]\frac{\partial F_x'}{\partial x} = u'(t), \tag{5.3.9c}$$

where Eq. (5.3.9a) is the linearized dimensional form of Eq. (5.3.7). Eq. (5.3.9b) and Eq. (5.3.9c) are the linearized dimensional fluctuating components of Eq. (5.3.7), if we seek the solution in the form of $\mathcal{G} = x - x_0 - F_r(r,t)$ or $\mathcal{G} = r - r_0 - F_x(x,t)$ respectively. Applying these trial solutions has the following consequences:

- Since F_r and F_x must be well defined, the effect of introducing trial solutions of these forms results in neglecting oscillations of the flame in the r or x directions respectively. This can be seen in Figure (5.8) and (5.9).

- Comparing Eq. (5.3.9c) with Eq. (5.3.8a) shows that introducing $\mathcal{G} = r - r_0 - F_x(x,t)$ yields no loss of accuracy to the leading order in region 1 for small values of $u'(t)$, i.e. if $u'(t) \ll \bar{u}$.

- Comparing Eq. (5.3.9b) with Eq. (5.3.8b) shows that using $\mathcal{G} = x - x_0 - F_r(r,t)$ results in neglecting the underlined term in Eq. (5.3.8b).

- Applying $\mathcal{G} = x - x_0 - F_r(r,t)$ is implicitly a small amplitude approximation, since the term $u' \cdot \partial \mathcal{G}'/\partial x$ is not represented in Eq. (5.3.9b).

- The partial time derivative and the forcing terms are independent of the trial

solutions (these are indicated by the dashed boxes in Eqs. 5.3.9a-5.3.9c).

- Eq. (5.3.9a) is valid to the leading order in region 1 and 2.
- Eq. (5.3.9c) is valid to the leading order in region 1.

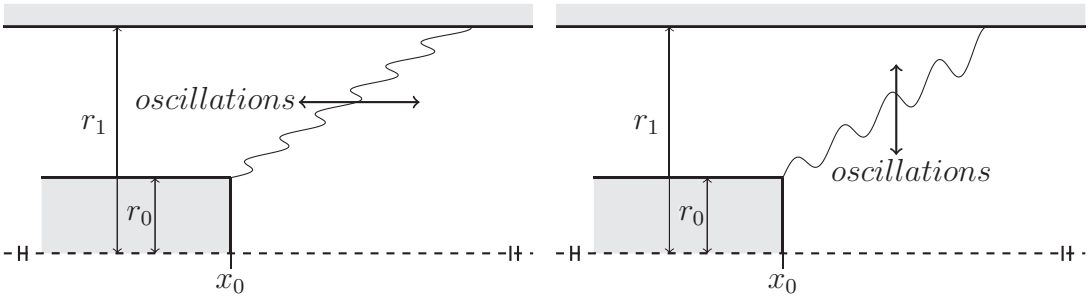

(a) $\mathcal{G} = x - x_0 - F_r(r,t)$ (b) $\mathcal{G} = r - r_0 - F_x(x,t)$

Figure 5.9: Effect of the trial solutions on the flame front behavior

5.3.1.4 Linear solution

To obtain a solution for the fluctuating component of the flame position, we assume small amplitudes ($u' \ll \bar{u}$), which simplifies Eq. (5.3.9a) to the following form

$$\frac{\partial \mathcal{G}'}{\partial t} + \frac{\partial \mathcal{G}'}{\partial x}\left(\bar{u} - S_l^0 \sin\alpha\right) + S_l^0 \cos\alpha \frac{\partial \mathcal{G}'}{\partial r} = u' \ . \tag{5.3.10}$$

Eq. (5.3.10) reduces to Eq. (5.3.8a) and to Eq. (5.3.8b) for large and small α respectively. The general solution of Eq. (5.3.10) can be obtained by performing a general coordinate system transformation and Laplace Transform (see Appendix (B.2)) to get

$$\begin{aligned}\mathcal{G}'(t,x,r) = \mathcal{G}'(t-\chi(x,r)) = H\Big[t-\chi(x,r)\Big]\mathcal{G}'(t-\chi(x,r),0) + \\ + H\Big[\chi(x,r)-t\Big]\mathcal{G}'(0,\chi(x,r)-t) + \int\limits_{t-\chi(x,r)}^{t} u'(\tau)d\tau \ ,\end{aligned} \tag{5.3.11}$$

where H is the Heaviside function, and $\chi(x,r)$ is a time-lag, i.e. it is the time required for a perturbation to travel from the attachment point $[x_0, r_0]$ to a point $[x, r]$ of the flame.

$$\chi(x,r) = \frac{\eta(x-x_0) - \epsilon(r-r_0)}{\eta\left(\bar{u} - S_l^0 \sin\alpha\right) - \epsilon S_l^0 \cos\alpha} \qquad \eta, \epsilon \in \mathbb{R} \ . \tag{5.3.12}$$

Any η and ϵ represents a solution. Eq. (5.3.10) is satisfied by (5.3.12) for any η and ϵ, i.e. Eq. (5.3.10) has an infinite number of travelling wave solutions. The first term on the R.H.S. of Eq. (5.3.11) is due to the boundary condition at the point of attachment, the second term is due to the initial condition. We can see that the second term vanishes if $t > \chi$, therefore neglecting the initial condition does not affect the physics of the solution. The boundary condition however plays an important role when solving the $\mathcal{G}$-Equation. This is reflected in Eq. (5.3.11) as well. In case of vanishing initial and boundary conditions the first two terms on the R.H.S. of Eq. (5.3.10) vanish. Any unsteadiness in the oncoming velocity $u'(t)$ forces perturbations to the flame front which propagate from the attachment of the flame. Unique solutions have been obtained by earlier researchers in two ways:

- Introducing either of the trial solutions ($\mathcal{G} = x - x_0 - F_r(r,t)$ or $\mathcal{G} = r - r_0 - F_x(x,t)$) yields a unique solution, which is equivalent to setting $\eta = 0$ or $\epsilon = 0$ respectively. This method was used in [Dowling, 1999; Ducruix et al., 2000; Lieuwen, 2005].

- Rotating the coordinate system in such a way that one of the rotated axis lies along the mean flame position. This method corresponds to setting $\eta = \cos\alpha$ and $\epsilon = -\sin\alpha$ (rotation by the angle $\pi/2 - \alpha$ clockwise) or to $\eta = \sin\alpha$ and $\epsilon = \cos\alpha$ (rotation by α anti-clockwise). The first case is shown in Figure (5.10). The rotation matrix is given by

$$\begin{pmatrix} w \\ z \end{pmatrix} = \begin{pmatrix} \cos\alpha & -\sin\alpha \\ \sin\alpha & \cos\alpha \end{pmatrix} \cdot \begin{pmatrix} x \\ r \end{pmatrix} \ . \tag{5.3.13}$$

Solving the $\mathcal{G}$-Equation in a rotated coordinate system was done by [Lieuwen et al., 2006; Schuller et al., 2003].

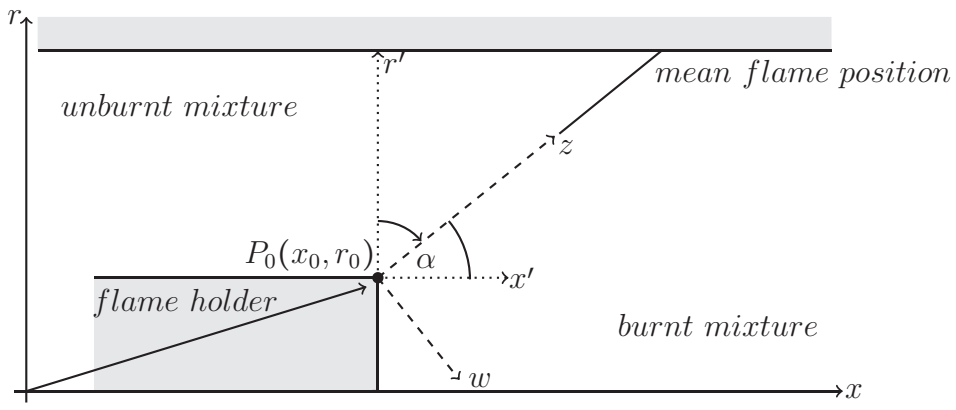

Figure 5.10: Transformation of the coordinate system to the mean flame position

5.3.2 Summary of the solutions of the $\mathcal{G}$-Equation without curvature effects

5.3.2.1 Solutions for the mean and linearized fluctuating components of the full $\mathcal{G}$-Equation

The solution for the mean position of the flame is given by Eq. (5.3.4), i.e.

$$\bar{\mathcal{G}} = (x - x_0) \pm (r - r_0)\sqrt{\left(\frac{\bar{u}}{S_l^0}\right)^2 - 1}\ . \tag{5.3.14}$$

The solution for the linearized fluctuating component for zero initial and boundary condition is

$$\mathcal{G}'(t, x, r) = \int_{t-\chi(x,r)}^{t} u'(\tau)d\tau\ , \tag{5.3.15}$$

where

$$\chi(x,r) = \frac{\eta(x-x_0) - \epsilon(r-r_0)}{\eta\left(\bar{u} - S_l^0 \sin\alpha\right) - \epsilon S_l^0 \cos\alpha} \qquad \eta, \epsilon \in \mathbb{R} \ . \tag{5.3.16}$$

5.3.2.2 Solutions in the form of $\mathcal{G} = r - r_0 - F_x(x,t)$

The solution for the mean flame position by applying $\mathcal{G} = r - r_0 - F_x(x,t)$ is

$$\bar{F}_x = \pm(x-x_0)\frac{1}{\sqrt{\left(\frac{\bar{u}}{S_l^0}\right)^2 - 1}} \ , \tag{5.3.17}$$

and the one for the linearized fluctuating component is

$$F_x'(x,t) = \int_{t-\chi_x}^{t} u'(\tau)d\tau \ , \quad \text{where} \quad \chi_x = \frac{x-x_0}{\bar{u} - S_l^0 \sin\alpha} \ . \tag{5.3.18}$$

5.3.2.3 Solutions in the form of $\mathcal{G} = x - x_0 - F_r(r,t)$

The solution for the mean flame position by applying $\mathcal{G} = x - x_0 - F_r(r,t)$ is

$$\bar{F}_r = \pm(r-r_0)\sqrt{\left(\frac{\bar{u}}{S_l^0}\right)^2 - 1} \ , \tag{5.3.19}$$

and the one for the linearized fluctuating component is

$$F_r'(r,t) = \int_{t-\chi_r}^{t} u'(\tau)d\tau \ , \quad \text{where} \quad \chi_r = \frac{r-r_0}{S_l^0 \cos\alpha} \ . \tag{5.3.20}$$

5.3.3 Curvature effects are considered

If we take curvature effects into account, the laminar flame speed is given by

$$S_l = S_l^0 - \mathcal{L} S_l^0 \kappa \ , \tag{5.3.21}$$

where S_l^0 is the laminar flame speed of the unwrinkled flame and $\mathcal{L}$ is the Markstein

length, which was calculated in Section (5.2.2). The curvature of the flame sheet κ can be calculated by $\nabla \cdot \boldsymbol{n}$. By assuming constant mean flow ($\bar{u}$=constant), vanishing radial velocity component ($v = 0$), and negligible spatial dependence of the acoustic velocity ($u' = u'(t)$) we can write the $\mathcal{G}$-Equation in a cylindrical coordinate system with curvature terms as

$$\frac{\partial \mathcal{G}}{\partial t} + u\frac{\partial \mathcal{G}}{\partial x} = S_l^0\sqrt{\left(\frac{\partial \mathcal{G}}{\partial x}\right)^2 + \left(\frac{\partial \mathcal{G}}{\partial r}\right)^2} - S_l^0\mathcal{L}\frac{2\frac{\partial \mathcal{G}}{\partial x}\frac{\partial \mathcal{G}}{\partial r}\frac{\partial^2 \mathcal{G}}{\partial x \partial r} - \left(\frac{\partial \mathcal{G}}{\partial r}\right)^2\frac{\partial^2 \mathcal{G}}{\partial x^2} - \left(\frac{\partial \mathcal{G}}{\partial x}\right)^2\frac{\partial^2 \mathcal{G}}{\partial r^2}}{\left(\frac{\partial \mathcal{G}}{\partial x}\right)^2 + \left(\frac{\partial \mathcal{G}}{\partial r}\right)^2} \ . \quad (5.3.22)$$

This is a second-order differential equation, in contrast to the case without curvature. The advantage of introducing $\mathcal{G} = x - x_0 - F_r(r,t)$ rather than $\mathcal{G} = r - r_0 - F_x(x,t)$ is that we can prescribe boundary conditions for specific r values, i.e. at $r = r_1$ or at $r = r_0$. For an open flame the tip of the flame is rounded, therefore in this case the second boundary condition is that $\partial \bar{F}_r/\partial r = 0$ at $r = 0$.

5.3.3.1 Effect of curvature on the mean flame position

If we introduce $\mathcal{G} = x - x_0 - F_r(r,t)$, we can write the mean component of Eq. (5.3.22) in terms of F_r in the following form

$$\frac{\bar{u}}{S_l^0} = \sqrt{1 + \left(\frac{\partial \bar{F}_r}{\partial r}\right)^2} - \mathcal{L}\frac{\frac{\partial^2 \bar{F}_r}{\partial r^2}}{1 + \left(\frac{\partial \bar{F}_r}{\partial r}\right)^2} \ . \quad (5.3.23)$$

The implicit solution of Eq. (5.3.23) can be obtained by introducing and integrating a new function for $\arctan \partial \bar{F}_r/\partial r$ (for details see Appendix (B.3))

$$\frac{r - c_0}{2\mathcal{L}}\frac{\bar{u}}{S_l^0} = \arctan\left[\frac{\frac{\partial \bar{F}_r}{\partial r}}{1 + \sqrt{1 + \left(\frac{\partial \bar{F}_r}{\partial r}\right)^2}}\right] + \frac{1}{\sqrt{\frac{\bar{u}^2}{S_l^2} - 1}}\operatorname{arctanh}\left[\sqrt{\frac{\frac{\bar{u}}{S_l} + 1}{\frac{\bar{u}}{S_l} - 1}}\frac{\frac{\partial \bar{F}_r}{\partial r}}{1 + \sqrt{1 + \left(\frac{\partial \bar{F}_r}{\partial r}\right)^2}}\right], \quad (5.3.24)$$

where c_0 is a constant to be determined from the boundary condition, by which we prescribe $\partial\bar{F}_r/\partial r$ in a certain point, e.g. $\partial\bar{F}_r/\partial r = 0$ at $r = 0$, which yields $c_0 = 0$ for an open flame. Eq. (5.3.24) shows that the solution is governed by 2 parameters, $\bar{u}/S_l^0$ and $(r - c_0)/2\mathcal{L}$. The solution given by Eq. (5.3.24) is plotted in Figure (5.12) with solid lines for certain values of $\bar{u}/S_l^0$. Eq. (5.3.24) also shows that

$$\lim_{\frac{r-c_0}{2\mathcal{L}} \to \pm\infty} \frac{\partial \bar{F}_r}{\partial r} = \pm\sqrt{\left(\frac{\bar{u}}{S_l^0}\right)^2 - 1}\ , \tag{5.3.25}$$

i.e. the gradient of the mean flame position of a curved flame tends to the one of an uncurved flame (given by the spatial derivative of Eq. (5.3.19)) as $(r - c_0)/2\mathcal{L}$ approaches infinity, i.e. either $\mathcal{L}$ tends to zero, or r to infinity. (see Figure (5.11)).

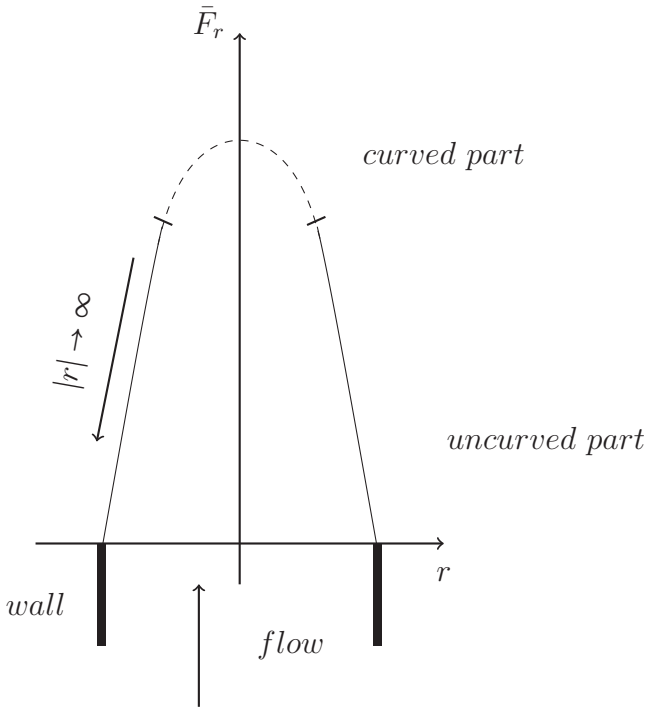

Figure 5.11: Schematic representation of an axisymmetric open curved flame (———: uncurved part, – – –: curved part)

arctan and arctanh can be linearized for small arguments

$$\arctan\left[\frac{\frac{\partial \bar{F}_r}{\partial r}}{1+\sqrt{1+\left(\frac{\partial \bar{F}_r}{\partial r}\right)^2}}\right]=\frac{\frac{\partial \bar{F}_r}{\partial r}}{1+\sqrt{1+\left(\frac{\partial \bar{F}_r}{\partial r}\right)^2}}\ , \tag{5.3.26a}$$

$$\operatorname{arctanh}\left[\sqrt{\frac{\frac{\bar{u}}{S_l}+1}{\frac{\bar{u}}{S_l}-1}}\frac{\frac{\partial \bar{F}_r}{\partial r}}{1+\sqrt{1+\left(\frac{\partial \bar{F}_r}{\partial r}\right)^2}}\right]=\sqrt{\frac{\frac{\bar{u}}{S_l}+1}{\frac{\bar{u}}{S_l}-1}}\frac{\frac{\partial \bar{F}_r}{\partial r}}{1+\sqrt{1+\left(\frac{\partial \bar{F}_r}{\partial r}\right)^2}}\ . \tag{5.3.26b}$$

The curved part of the flame corresponds to the near-origin region of Figure (5.12). We can see that in this regime the position gradient is linear. We substitute with Eq. (5.3.26a) and Eq. (5.3.26b) for the R.H.S. of Eq. (5.3.24) to get the following explicit approximation

$$\frac{\partial \bar{F}_r}{\partial r}=2\left[\frac{\bar{u}}{S_l^0}-1\right]\frac{\frac{r-c_0}{2\mathcal{L}}}{1-\left[\frac{r-c_0}{2\mathcal{L}}\left(\frac{\bar{u}}{S_l^0}-1\right)\right]^2}\ . \tag{5.3.27}$$

For large $(r-c_0)/2\mathcal{L}$ the solution in Eq. (5.3.24) is dominated by the function arctanh (since the maximum of arctan is $\pi/2$), therefore by using Eq. (5.3.25) we can see that

$$\lim_{\frac{r-c_0}{2\mathcal{L}}\to\infty}\arctan\left[\frac{\frac{\partial \bar{F}_r}{\partial r}}{1+\sqrt{1+\left(\frac{\partial \bar{F}_r}{\partial r}\right)^2}}\right]=\arctan\left(\sqrt{\frac{\frac{\bar{u}}{S_l^0}-1}{\frac{\bar{u}}{S_l^0}+1}}\right)\ . \tag{5.3.28}$$

By substituting with Eq. (5.3.28) for the first term on the R.H.S. of Eq. (5.3.24) we get the following asymptotic explicit solution for large $(r-c_0)/2\mathcal{L}$

$$\frac{\partial \bar{F}_r}{\partial r}=\frac{2\zeta}{1-\zeta^2}\ , \tag{5.3.29}$$

where ζ is given by

$$\zeta = \sqrt{\frac{\frac{\bar{u}}{S_l^0} - 1}{\frac{\bar{u}}{S_l^0} + 1}} \tanh\left\{\sqrt{\left(\frac{\bar{u}}{S_l^0}\right)^2 - 1}\left[\frac{\bar{u}}{S_l^0}\frac{r - c_0}{2\mathcal{L}} - \arctan\left(\sqrt{\frac{\frac{\bar{u}}{S_l^0} - 1}{\frac{\bar{u}}{S_l^0} + 1}}\right)\right]\right\} . \qquad (5.3.30)$$

$\partial \bar{F}_r/\partial r$ tends to $\sqrt{(\bar{u}/S_l^0)^2 - 1}$, hence large $(r - c_0)/2\mathcal{L}$ does not necessarily correspond to large $\partial \bar{F}_r/\partial r$. The exact implicit solution and the explicit approximations are shown in Figure (5.12). In the grey region the explicit solutions given by Eq. (5.3.27) and Eq. (5.3.29) yield more than 5 % error. The grey region in Figure (5.12) corresponds to the strongly non-linear region of Figure (5.7).

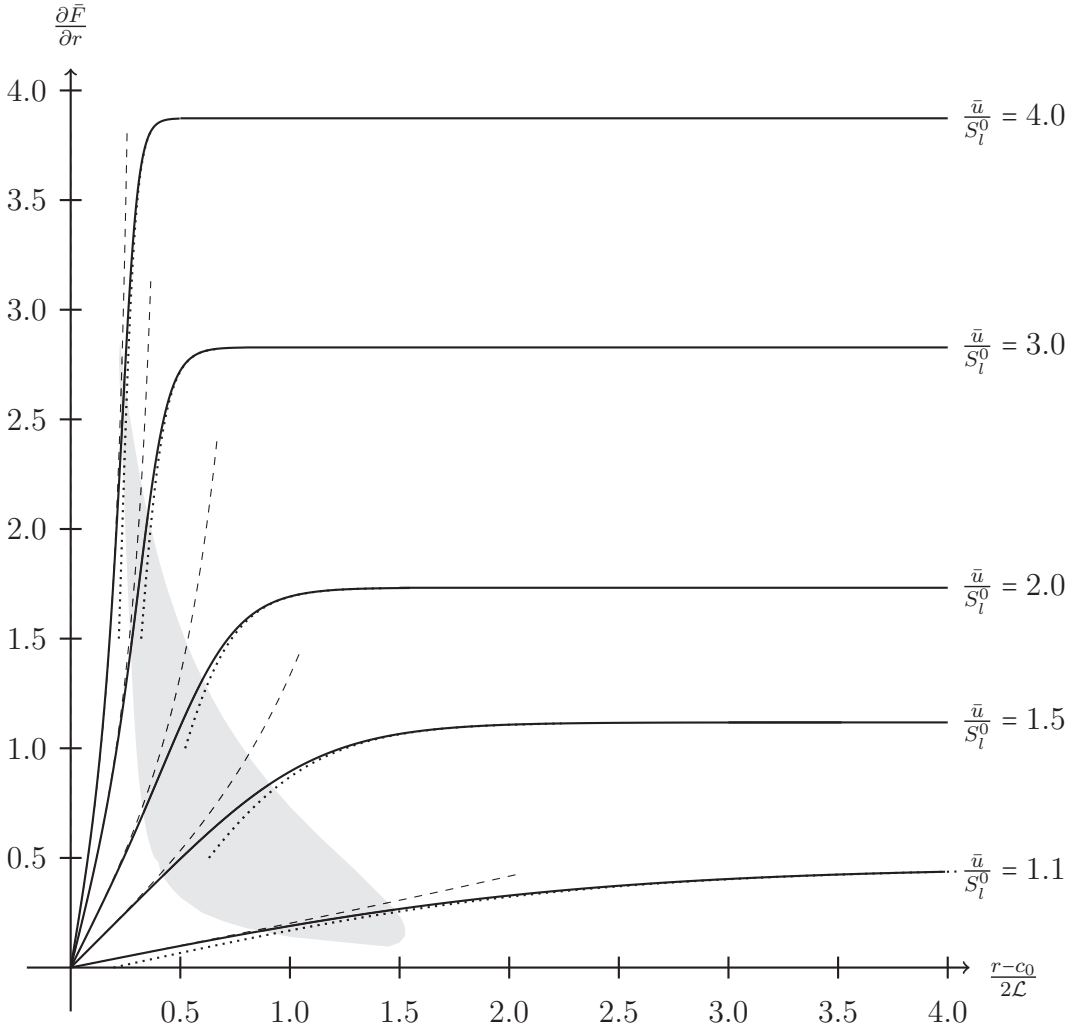

Figure 5.12: Gradient of the mean flame position as function of $(r - c_0)/2\mathcal{L}$ (——: exact implicit solution by Eq. (5.3.24), – – –: approximation given by Eq. (5.3.27), ·····: approximation given by Eq. (5.3.29))

Figure (5.12) shows that increasing $\bar{u}/S_l^0$ reduces the region, in which curvature is important.

To obtain the flame position in the curved region of the flame we perform the integration of Eq. (5.3.27), and write it in the following form

$$\frac{\bar{F}_r}{r_1 - r_0} = c_1 - \frac{2\mathcal{L}}{r_1 - r_0} \frac{1}{\frac{\bar{u}}{S_l^0} - 1} \ln\left\{1 - \left[\frac{r - c_0}{r_1 - r_0} \frac{r_1 - r_0}{2\mathcal{L}}\right]^2\right\} , \tag{5.3.31}$$

where c_1 is constant. $\tilde{r} = (r - c_0)/(r_1 - r_0)$ is a nondimensional radial coordinate, and lies in the interval of $[-1; 1]$. For an open flame $\partial \bar{F}_r/\partial r = 0$ at $r_0 = 0$, which gives $c_0 = 0$, and the nondimensional radial coordinate is $\tilde{r} = r/r_1$.
Integration of Eq. (5.3.29) yields the solution for the mean position far from the curved part of the flame

$$\frac{\bar{F}_r}{r_1 - r_0} = c_2 - \frac{2\mathcal{L}}{r_1 - r_0} \left[\frac{\bar{u}}{S_l^0}\left(\frac{\bar{u}}{S_l^0} + 1\right)\right]^{-1} \ln\left\{2\frac{\frac{\bar{u}}{S_l^0}}{\frac{\bar{u}}{S_l^0} + 1} + \frac{2}{\frac{\bar{u}}{S_l^0} + 1} \cosh 2\Lambda\right\} , \tag{5.3.32}$$

where c_2 is constant, and Λ is given by

$$\Lambda = \sqrt{\left(\frac{\bar{u}}{S_l^0}\right)^2 - 1}\left[\frac{\bar{u}}{S_l^0} \frac{r - c_0}{r_1 - r_0} \frac{r_1 - r_0}{2\mathcal{L}} - \arctan\left(\sqrt{\frac{\frac{\bar{u}}{S_l^0} - 1}{\frac{\bar{u}}{S_l^0} + 1}}\right)\right] . \tag{5.3.33}$$

Open flame shapes for different values of $\mathcal{L}/r_1$ and $\bar{u}/S_l^0$ are shown in Figure (5.13), and a schlieren image by Ducruix et al. [2000] with $\bar{u}/S_l^0 = 2$ and $\mathcal{L}/r_1 = 0.1$.

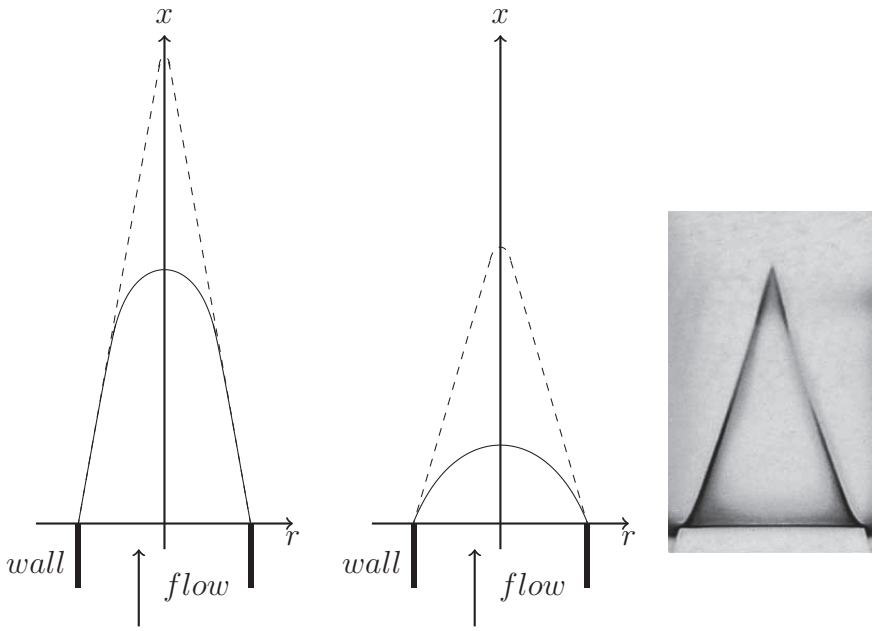

(a) $\frac{\bar{u}}{S_l^0} = 3$ (b) $\frac{\bar{u}}{S_l^0} = 2$ (c) Schlieren image, $\frac{\bar{u}}{S_l^0} = 2$, $\frac{\mathcal{L}}{r_1} = 0.1$

Figure 5.13: Axisymmetric open flame shapes using Eqs. (5.3.31) and (5.3.32) for (a) $\bar{u}/S_l^0 = 3$, (b) $\bar{u}/S_l^0 = 2$, (c) Schlieren image from Ducruix et al. [2000] with $\frac{\mathcal{L}}{r_1} = 0.1$ and $\frac{\bar{u}}{S_l^0} = 2$ (———: $\mathcal{L}/r_1 = 1$, − − −: $\mathcal{L}/r_1 = 0.1$)

Figure (5.12) and (5.13) shows that curvature is important, if

$$\frac{\mathcal{L}}{r_1 - r_0} = \frac{\mathcal{L}}{l_F}\frac{l_F}{r_1 - r_0} = \mathrm{Mn}\frac{l_F}{r_1 - r_0} \leq O(1) \ . \tag{5.3.34}$$

For methane combustion systems the Markstein number (Mn) is of the order of unity, therefore Eq. (5.3.34) shows that the condition for the curvature to contribute to the leading order solution is that the flame width is at least of the same order as the width between the wall and the flame holder. In the LIMOUSINE burner $\mathcal{L}/(r_1 - r_0)$ is of the order of 10^{-1}, therefore we neglect the effects of curvature.

5.4 Derivation of the heat release rate law

In our model the released heat is proportional to the flame surface area, which is described by the scalar $\mathcal{G}$

$$q_r(t) = \rho_u S_l^0 \Delta q_r A(t) \ , \tag{5.4.1}$$

where $q_r(t)$ is the total global heat-release in a cylindrical system, Δq_r is the heat released per unit mass by the chemical reaction, ρ_u is the density of the unburnt mixture, and $A(t)$ is the time-dependent flame surface area. The surface of the flame can be obtained by rotation of the function $F_x(x,t)$ around the x-axis or by rotation of the function $F_r(r,t)$ around $r = 0$, therefore it can be calculated by

$$A = \int_{x_0}^{x_1} 2\pi F_x \sqrt{1 + \left(\frac{\partial F_x}{\partial x}\right)^2}\, dx \ , \tag{5.4.2a}$$

$$= \int_{r_0}^{r_1} 2\pi r \sqrt{1 + \left(\frac{\partial F_r}{\partial r}\right)^2}\, dr \ . \tag{5.4.2b}$$

5.4.1 Mean heat release rate

The mean heat-release rate can be obtained from Eq. (5.4.1)

$$\bar{q}_r = \rho_u S_l^0 \Delta q_r \bar{A} \ , \tag{5.4.3}$$

where $\bar{q}_r$ denotes the mean component of the global heat-release rate. To obtain the mean flame surface area we substitute the equation for $\bar{\mathcal{G}}$ (Eq. (5.3.14)) into the mean of Eq. (5.4.2a) or Eq. (5.4.2b)

$$\bar{A} = \int_{x_0}^{x_1} 2\pi \left[r_0 + (x - x_0) \frac{1}{\sqrt{\left(\frac{\bar{u}}{S_l^0}\right)^2 - 1}} \right] \sqrt{1 + \left(\frac{1}{\left(\frac{\bar{u}}{S_l^0}\right)^2 - 1} \right)^2} \, dx \ , \tag{5.4.4}$$
$$= \frac{\bar{u}}{S_l^0} \left[\pi r_1^2 - \pi r_0^2 \right] \ .$$

We combine the expression (5.4.4) with Eq. (5.4.3) to get the mean global heat release rate in the following form

$$\bar{q}_r = \rho_u S_l^0 \Delta q_r \frac{\bar{u}}{S_l^0} \left[\pi r_1^2 - \pi r_0^2 \right] = \bar{m} \Delta q_r \ , \tag{5.4.5}$$

where $\bar{m}$ is the mean mass flow rate. This result shows that the mean heat-release rate is proportional to the mass flow rate of the mixture.

5.4.2 Fluctuating heat release rate

5.4.2.1 Analyzing the applicability of the solutions of the $\mathcal{G}$-Equation to derive a heat-release law

We have shown that a unique solution can be obtained for the $\mathcal{G}$-Equation if we either apply a trial solution ($\mathcal{G} = x - x_0 - F_r(r,t)$ or $\mathcal{G} = r - r_0 - F_x(x,t)$) or use rotation of the coordinate system. If we use $\mathcal{G} = r - r_0 - F_x(x,t)$, then to obtain the flame surface area we have to integrate to the point ($x = x_1$), where the oscillating flame sheet meets the wall (at $r = r_1$, see Figure (5.14)). The flame sheet oscillates, hence x_1 will be a function of time, and therefore its calculation requires one to find the inverse function of u'.

Applying the solution of the rotated coordinate system requires parametrization, which again involves finding the inverse function of u'. We can avoid making any assumption about u' a-priori by using $\mathcal{G} = x - x_0 - F_r(r,t)$, therefore we will apply the solution of the

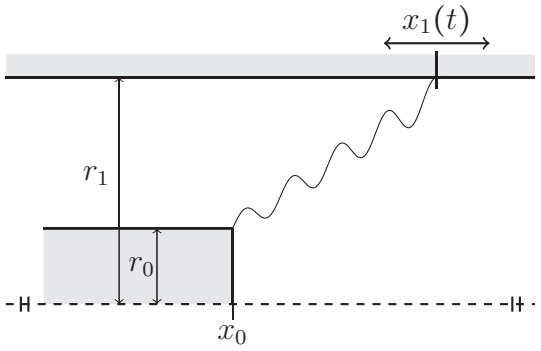

Figure 5.14: Time dependence of the integration limit when $\mathcal{G} = r - r_0 - F_x(x,t)$ is used

$\mathcal{G}$-Equation of this form. Figure (5.15) summarizes the solutions of the $\mathcal{G}$-Equation.

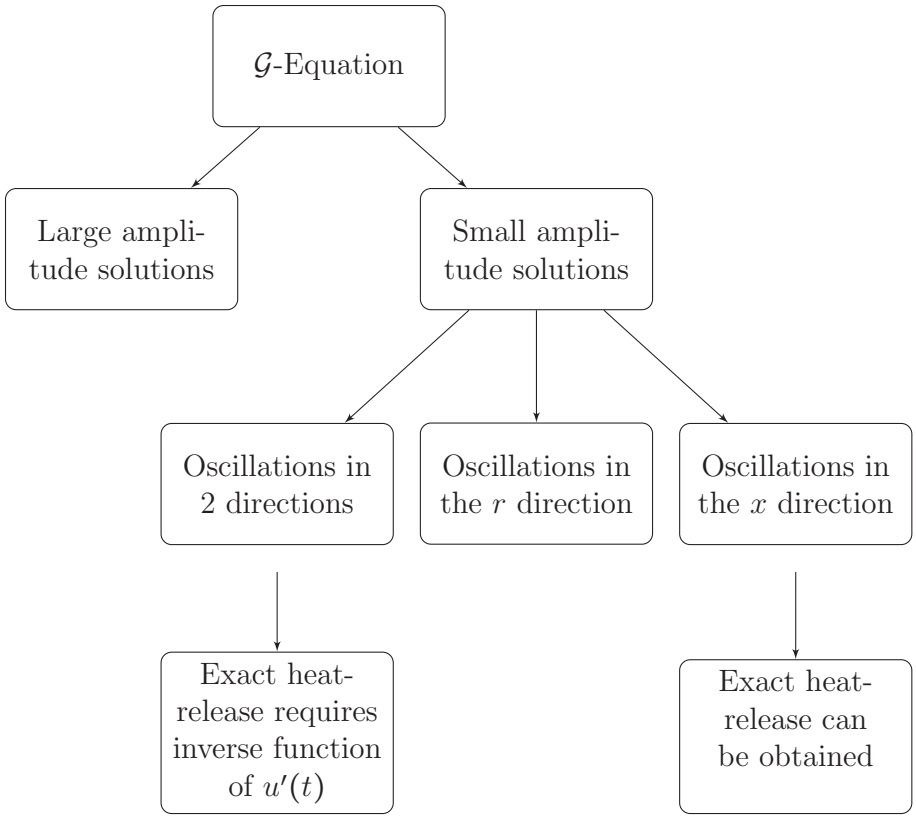

Figure 5.15: Summary of the solutions of the $\mathcal{G}$-Equation

5.4.2.2 Fluctuating heat release rate in cylindrical coordinate system

We use $\mathcal{G} = x - x_0 - F_r(r,t)$ to derive a heat-release rate law, by which we can treat u' as an arbitrary function. The fluctuating part of the heat release rate can be written in the following form

$$q_r'(t) = \rho_u S_l^0 \Delta q_r \int_{r_0}^{r_1} 2\pi r \sigma(r,t) dr \ , \tag{5.4.6}$$

where $\sigma(r,t)$ is given by

$$\sigma(r,t) = \sqrt{1 + \left(\frac{\partial \bar{F}_r}{\partial r} + \frac{\partial F_r'}{\partial r}\right)^2} - \sqrt{1 + \left(\frac{\partial \bar{F}_r}{\partial r}\right)^2} \ , \tag{5.4.7}$$

i.e. we express the fluctuating component of the flame surface area as the mean component subtracted from the total one. The source term in Eq. (3.1.12) requires the calculation of the partial time-derivative of the fluctuating heat release rate. We use Eq. (5.3.20) to write the time-derivative of $\sigma(r,t)$ as

$$\frac{\partial \sigma(r,t)}{\partial t} = -S_l^0 \cos\alpha \frac{\partial \sigma(r,t)}{\partial r} \ . \tag{5.4.8}$$

Using (5.4.8) and integration by parts we can rewrite Eq. (5.4.6) as

$$\frac{\partial}{\partial t} q_r'(t) = 2\pi \rho_u S_l^0 \Delta q_r S_l^0 \cos\alpha \frac{\partial}{\partial r} \int_{r_1}^{r_0} \left[r\sigma(r,t) + S_l^0 \cos\alpha \int \sigma(r,t) dt \right] dr \ . \tag{5.4.9}$$

By applying Eq. (5.4.5), introducing $\beta = r_0/r_1$ and $\chi_r = (r_1 - r_0)/S_l^0 \cos\alpha$, we can present the time-derivative of the non-dimensional heat-release rate fluctuation in the following form

$$\frac{\partial}{\partial t}\frac{q_r'}{\bar{q}} = \frac{2}{1+\beta}\frac{1}{\chi_r}\left\{\beta\Psi(t) - \Psi(t-\chi_r) + \frac{1-\beta}{\chi_r}\int \Psi(t) - \Psi(t-\chi_r)dt\right\} \ , \tag{5.4.10}$$

where the function $\Psi(t)$ is given by

$$\Psi(t) = \sqrt{\left[1 + \frac{u'(t)}{\bar{u}}\right]^2 + \tan^2\alpha\left[\frac{u'(t)}{\bar{u}}\right]^2} - 1 \ . \tag{5.4.11}$$

The axisymmetric open flame is in this case simply the limit of $\beta \to 0$. Eq. (5.4.11) shows that non-linearity of the heat-release is governed by $\tan^2\alpha(u'/\bar{u})^2$ in contrast to the non-linearity of the $\mathcal{G}$-Equation, which is governed by $\tan^2\alpha$. In the next chapter we will perform a weakly non-linear analysis. This requires powers of $u'/\bar{u}$, so we expand Eq. (5.4.10) up to cubic order and get

$$\begin{aligned}\frac{\partial}{\partial t}\frac{q_r'(t)}{\bar{q}} = \frac{2}{\chi_r}\frac{1}{1+\beta}\Bigg\{&\left[\beta\frac{u'}{\bar{u}} - \frac{u'(t-\chi_r)}{\bar{u}} + \frac{1-\beta}{\chi_r}\int \frac{u'}{\bar{u}} - \frac{u'(t-\chi_r)}{\bar{u}}dt\right] + \\ &+ \frac{1}{2}\tan^2\alpha\left[\beta\left(\frac{u'}{\bar{u}}\right)^2 - \left(\frac{u'(t-\chi_r)}{\bar{u}}\right)^2 + \frac{1-\beta}{\chi_r}\int \left(\frac{u'}{\bar{u}}\right)^2 - \left(\frac{u'(t-\chi_r)}{\bar{u}}\right)^2 dt\right] - \\ &- \frac{1}{2}\tan^2\alpha\left[\beta\left(\frac{u'}{\bar{u}}\right)^3 - \left(\frac{u'(t-\chi_r)}{\bar{u}}\right)^3 + \frac{1-\beta}{\chi_r}\int \left(\frac{u'}{\bar{u}}\right)^3 - \left(\frac{u'(t-\chi_r)}{\bar{u}}\right)^3 dt\right]\Bigg\} \ .\end{aligned} \tag{5.4.12}$$

5.4.2.3 Fluctuating heat release rate of a two-dimensional flame

Figure (5.16) shows the ducted and the open planar flames.

To obtain the heat release rate of a planar flame, similar derivation can be carried out (see Appendix B.4) to get

$$\frac{\partial}{\partial t}\frac{q_c'}{\bar{q}} = \frac{1}{\chi_c}\left\{\Psi(t) - \Psi(t-\chi_c)\right\} \ , \tag{5.4.13}$$

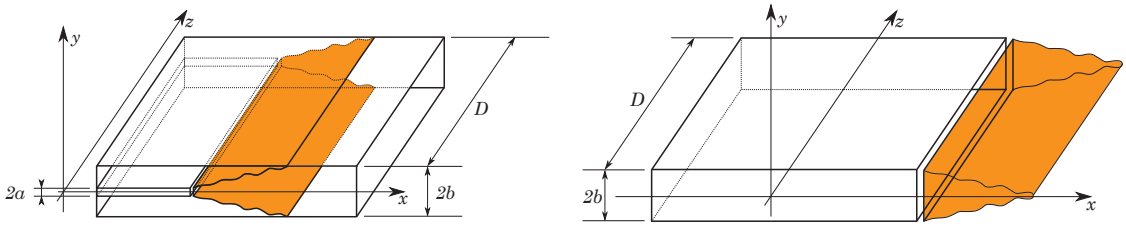

(a) Planar ducted flame (b) Planar open flame

Figure 5.16: (a) Planar ducted flame and (b) planar open flame

where Ψ is given by (5.4.11). Expanding Eq. (5.4.13) up to cubic terms yields

$$\frac{\partial}{\partial t}\frac{q_c'(t)}{\bar{q}/\chi_c} = \left[\frac{u'}{\bar{u}} - \frac{u'(t-\chi_c)}{\bar{u}}\right] + \frac{1}{2}\tan^2\alpha\left[\left(\frac{u'}{\bar{u}}\right)^2 - \left(\frac{u'(t-\chi_c)}{\bar{u}}\right)^2\right] - \\ - \frac{1}{2}\tan^2\alpha\left[\left(\frac{u'}{\bar{u}}\right)^3 - \left(\frac{u'(t-\chi_c)}{\bar{u}}\right)^3\right], \quad (5.4.14)$$

where $q_c'(t)$ denotes the fluctuating global heat release rate in a Cartesian coordinate system. As in case of a cylindrical coordinate system, the time-lag $\chi_c = (b-a)/S_l\cos\alpha$ is the time it takes for a perturbation to propagate along the flame front. Eq. (5.4.13) is the special case of Eq. (5.4.10) when $\beta \to 1$, i.e. the flame is radially very thin.

5.5 Conclusions

Laminar flame propagation and small amplitude perturbation was applied to derive the response of a ducted flame by the LSM. The weakly and strongly non-linear regions of the $\mathcal{G}$-Equation were analyzed and different solutions were presented. We have found that the linearized $\mathcal{G}$-Equation without curvature effects and trial solutions has an infinite number of solutions for the attached flame boundary condition. By applying trial solutions or rotation of the coordinate system we can get unique solutions for the $\mathcal{G}$-Equation, however, a trial solution neglects oscillations of the flame in one of the

axis directions. We have investigated and compared the solutions of the $\mathcal{G}$-Equation, and found that in order to calculate the flame surface area applying the trial solution of $\mathcal{G} = x - x_0 - F_r(r,t)$ requires no a-priori assumptions about the acoustic velocity. We derived a heat release law, which relates the rate of the released heat to the acoustic velocity. Summary of the chapter in keywords:

- the geometry has effect on the heat-release (described by β),
- the two-dimensional flame is the special case of a cylindrical flame ($\beta = 1$),
- weakly and strongly non-linear regions were identified,
- curvature is important only if the flame width is comparable to the distance between the wall and the flame holder,
- advantages and disadvantages of the trial solutions were presented,
- we derived a non-linear heat-release law,
- we found that non-linearity is governed by different parameters in the $\mathcal{G}$-Equation and in the heat-release rate law,
- we applied laminar flame propagation assumption, in contrast to the turbulent flame present in the LIMOUSINE burner.

Chapter 6

Stability regimes of the burner

In the present chapter we derive and solve the governing equation of the acoustic velocity of an active single mode, i.e. the feedback of the flame is included in the governing equation. We analyze the parameters and investigate their effects on the stability map of the LIMOUSINE burner. We will identify the weakly non-linear regions and by applying analytical tools we give predictions about the resulting amplitude of the oscillations.

6.1 Derivation of the governing equation for an active single mode

6.1.1 Derivation of the governing integral equation for the acoustic velocity

In the frequency domain Eq. (4.2.16) and Eq. (4.3.6) give the solution of the acoustic pressure in terms of the system's Green's function, i.e.

$$\hat{p}(x,\omega) = \int_0^L \hat{G}_T(x,\xi,\omega)\left[-\frac{\gamma-1}{\gamma\mathcal{R}\bar{T}(\xi)}i\omega\hat{Q}(\xi,\omega)\right]d\xi \ , \tag{6.1.1}$$

where $\hat{Q}$ is the local heat-release rate. In Eq. (6.1.1) we apply the linear momentum

equation (Eq. (3.1.8a)) to get the acoustic velocity in the frequency domain in the following form

$$\hat{u}(x,\omega) = -\frac{1}{\bar{\rho}(x)} \int_0^L \frac{\partial \hat{G}_T(x,\xi,\omega)}{\partial x} \frac{1}{c_p \bar{T}(\xi)} \hat{Q}(\xi,\omega) d\xi \ . \tag{6.1.2}$$

In Eq. (6.1.2) we used that $(\gamma - 1)/\gamma\mathcal{R} = 1/c_p$. We apply Inverse Fourier Transform to write the acoustic velocity in the time-domain as

$$u'(x,t) = -\frac{1}{\bar{\rho}(x)} \int_{-\infty}^{\infty} \int_0^L \frac{\partial G_T(x,\xi,t-\tau)}{\partial x} \frac{1}{c_p \bar{T}(\xi)} Q'(\xi,\tau) d\tau d\xi \ . \tag{6.1.3}$$

The Green's function of the burner is given by Eq. (4.3.51), i.e.

$$G_T(x,\xi,t-\tau) = \sum_{n=1}^{\infty} iH(t-\tau) e^{-i\omega_n(t-\tau)} \hat{g}(x,\xi,\omega_n) + C.C. \ . \tag{6.1.4}$$

Substitution with Eq. (6.1.4) into Eq. (6.1.3) yields

$$u'(x,t) = -\frac{1}{\bar{\rho}(x)} \int_0^t \int_0^L \sum_{n=1}^{\infty} ie^{-i\omega_n(t-\tau)} \frac{\partial \hat{g}(x,\xi,\omega_n)}{\partial x} \frac{1}{c_p \bar{T}(\xi)} Q'(\xi,\tau) d\tau \ d\xi + C.C. \ . \tag{6.1.5}$$

Eq. (6.1.3) describes the acoustic velocity field of the burner. We make the following assumptions:

1. The interaction between the modes is negligible. We can therefore consider a single mode isolated from the others, say mode n, i.e. drop the summation sign in Eq. (6.1.5).

2. The heat source is compact, i.e. the spatial dependence of the heat-release can be approximated by $\delta(x - x_q)$, where x_q is the position of the flame.

In Eq. (6.1.5) Q' is the heat-release rate per unit volume, in Eq. (5.4.12) q' is the global heat-release, therefore

$$Q' = \frac{\delta(x - x_q)}{\bar{A}} q_r' \ , \tag{6.1.6}$$

where $\bar{A}$ is the mean surface area. We substitute for $\bar{A}$ with Eq. (5.4.4), and then use Eq. (5.4.5) to rewrite the resulting expression,

$$\begin{aligned} Q'(x,t) =& \delta(x - x_q) \frac{S_l^0}{\bar{u}} \frac{1}{\pi(r_1^2 - r_0^2)} \bar{q} \frac{q_r'(t)}{\bar{q}} \ , & (6.1.7a) \\ =& \delta(x - x_q) \frac{S_l^0}{\bar{u}} \frac{1}{\pi(r_1^2 - r_0^2)} \bar{\rho}_u S_l^0 \Delta q_r \frac{\bar{u}}{S_l^0} \pi(r_1^2 - r_0^2) \frac{q_r'(t)}{\bar{q}} \ , & (6.1.7b) \\ =& \delta(x - x_q) \Delta q_r \bar{\rho}_u S_l^0 \frac{q_r'(t)}{\bar{q}} \ . & (6.1.7c) \end{aligned}$$

This is inserted for $Q'(\xi, \tau)$ in Eq. (6.1.5) to give the governing integral equation of mode n at the position of the heat-source ($x = x_q$)

$$\frac{u'(x_q,t)}{\bar{u}} = -\frac{S_l^0}{\bar{u}} \frac{\Delta q_r}{c_p \bar{T}(x_q)} \int_0^t i e^{-i\omega_n(t-\tau)} \frac{\partial \hat{g}(x, x_q, \omega_n)}{\partial x}\Big|_{x=x_q} \frac{q_r'(\tau)}{\bar{q}} d\tau + C.C. \ . \tag{6.1.8}$$

The heat-release rate can be obtained from Eq. (5.4.12), i.e.

$$\begin{aligned} F(t) = \frac{q_r'(t)}{\bar{q}} = \int \frac{2}{\chi_r} \frac{1}{1+\beta} \Bigg\{ & \left[\beta \frac{u'}{\bar{u}} - \frac{u'(t-\chi_r)}{\bar{u}} + \frac{1-\beta}{\chi_r} \int \frac{u'}{\bar{u}} - \frac{u'(t-\chi_r)}{\bar{u}} dt \right] + \\ & + \frac{1}{2} \tan^2 \alpha \left[\beta \left(\frac{u'}{\bar{u}} \right)^2 - \left(\frac{u'(t-\chi_r)}{\bar{u}} \right)^2 + \frac{1-\beta}{\chi_r} \int \left(\frac{u'}{\bar{u}} \right)^2 - \left(\frac{u'(t-\chi_r)}{\bar{u}} \right)^2 dt \right] - \\ & - \frac{1}{2} \tan^2 \alpha \left[\beta \left(\frac{u'}{\bar{u}} \right)^3 - \left(\frac{u'(t-\chi_r)}{\bar{u}} \right)^3 + \frac{1-\beta}{\chi_r} \int \left(\frac{u'}{\bar{u}} \right)^3 - \left(\frac{u'(t-\chi_r)}{\bar{u}} \right)^3 dt \right] \Bigg\} dt \ . \end{aligned} \tag{6.1.9}$$

Eq. (6.1.8) is an integral equation for the acoustic velocity at the position of the heat-source. The heat-release is given by Eq. (6.1.9), which involves instantaneous and time-lagged velocity both in linear and non-linear forms.

6.1.2 Derivation of the governing differential equation for a single active mode of the acoustic velocity

For a numerical approach Eq. (6.1.8) is useful, however, for analytical studies (both linear and non-linear) it is more useful to rewrite it into a differential equation. To this end we show that an integral equation of the form

$$u'(t) = A_1 I_1(t) + A_2 I_2(t), \quad \text{where} \quad I_1(t) = \int_0^t e^{\lambda_1 (t-\tau)} q d\tau \ , \quad I_2(t) = \int_0^t e^{\lambda_2 (t-\tau)} q d\tau \tag{6.1.10}$$

can be rewritten into a second order ordinary differential equation by differentiating it with respect to t two times, expressing I_1 and I_2 from Eq. (6.1.10) and from its time-derivative, and substituting them into the second order time-derivative of Eq. (6.1.10) (the derivation is shown in details in Appendix (C)). A similar method is applied in [Polyanin and Manzhirov, 2008, p.198]. Carrying out this procedure yields

$$\frac{d^2 u'}{dt^2} - (\lambda_1 + \lambda_2)\frac{du'}{dt} + \lambda_1 \lambda_2 u' = (A_1 + A_2)\frac{dq'}{dt} - (A_1 \lambda_2 + A_2 \lambda_1) q' \ . \tag{6.1.11}$$

Applying it to our integral equation (6.1.8) yields a second order ordinary differential equation, which describes the time-evolution of the acoustic velocity of a single mode

$$\frac{d^2}{dt^2}\frac{u'(x,t)}{\bar{u}} - 2\omega_i \frac{d}{dt}\frac{u'(x,t)}{\bar{u}} + (\omega_r^2 + \omega_i^2)\frac{u'(x,t)}{\bar{u}} =$$
$$= \frac{\bar{u}}{S_l^0}\frac{\Delta q_r}{c_p \bar{T}(x_q)} 2Im\left[\frac{\partial \hat{g}(x, x_q, \omega_n)}{\partial x}\right]\frac{dF}{dt} - \frac{\bar{u}}{S_l^0}\frac{\Delta q_r}{c_p \bar{T}(x_q)} 2\omega_r Re\left[\frac{\partial \hat{g}(x, x_q, \omega_n)}{\partial x}\right] F \ , \quad (6.1.12)$$

where ω_i and ω_r are the imaginary and real part of the eigenfrequency of the non-excited burner respectively, F is the heat-release rate given by Eq. (6.1.9). F and dF/dt contains all of the nonlinearities of the system. This ordinary differential equation describes the nondimensional acoustic velocity fluctuation in a certain observer position, furthermore it satisfies the boundary conditions through the tailored Green's function.

6.1.3 Calculation of the heat-release of the chemical reaction

The term $\Delta q_r / c_p \bar{T}(x_q)$ in Eq. (6.1.8) is a thermodynamic property, which describes the released heat by the chemical reaction of a unit mass of fuel-air mixture. We rewrite this parameter to

$$\frac{\Delta q_r}{c_p \bar{T}(x_q)} = \frac{\bar{T}_{ad}}{\bar{T}(x_q)}\frac{\Delta q_r}{c_p \bar{T}_{ad}} = \frac{1}{\eta_T}\frac{\Delta q_r}{c_p \bar{T}_{ad}} \ , \quad (6.1.13)$$

where $\bar{T}_{ad}$ is the adiabatic flame temperature at constant pressure. If no heat is lost during the operation of the combustor, the combustion process takes place at the adiabatic flame temperature. In the second part of Eq. (6.1.13) we separated $\Delta q_r / c_p \bar{T}(x_q)$ into two parameters: η_T and $\Delta q_r / c_p \bar{T}_{ad}$. η_T is a measure for the heat loss of the combustion system, $\Delta q_r / c_p \bar{T}_{ad}$ is a thermodynamic property of the fuel only.

The amount of heat release (Δq_r) from combustion of the fuel will depend on the phase of water in the products. If the water is in the gas phase, the value of the global

heat release is denoted as the lower heating value (LHV). If the water is in the liquid phase, additional energy can be extracted and the global energy release is called the higher heating value (HHV). The value of the LHV can be calculated from the HHV by subtracting the amount of energy released during the phase change of water from gas to liquid. In the LIMOUSINE burner water leaves the burner in gas phase, therefore we use the LHV. In Eq. (6.3.1) Δq_r is the heat released by a unit mass of fuel-air mixture, i.e.

$$\Delta q_r = \frac{\Delta Q_{r,fuel}}{m_{air} + m_{fuel}} = \frac{\Delta Q_{r,fuel}}{m_{fuel}} \frac{1}{1 + \frac{m_{air}}{m_{fuel}}} = \frac{1}{1 + AFR} \Delta q_{r,fuel} \ , \tag{6.1.14}$$

where $\Delta q_{r,fuel}$ is the heat released by a unit mass of fuel, m_{air} and m_{fuel} is the mass of the air and the fuel respectively, and AFR is the air-fuel-ratio. $1/(1 + AFR)$ is called the stoichiometric mixture fraction. Eq. (6.1.13) implicitly assumes that all of the released heat is available for conversion into mechanical energy, however, measurements showed that a fuel-air combustible mixture needs to be preheated for the chain-breaking mechanism and therefore the chemical reaction to start [Drysdale, 1999, p.90]. This critical temperature value is approximately 1000 K for a wide range of fuels, which shows that the mixture needs $\Delta T = 700K$ temperature increase from the standard conditions [Drysdale, 1999, p.90]. By taking this effect into account we can further improve our model by subtracting the heat of the preheating process, i.e.

$$\begin{aligned}
\Delta q_r =& \frac{\Delta Q_{r,fuel} - \Delta Q_{preheat}}{m_{air} + m_{fuel}} \ , \\
=& \frac{\Delta Q_{r,fuel} - c_{p,air} m_{air} \Delta T - c_{p,fuel} m_{fuel} \Delta T}{m_{air} + m_{fuel}} \ , \\
=& \frac{\frac{\Delta Q_{r,fuel}}{m_{fuel}} - c_{p,air} \frac{m_{air}}{m_{fuel}} \Delta T - c_{p,fuel} \Delta T}{1 + \frac{m_{air}}{m_{fuel}}} \ , \\
=& \frac{\Delta q_{r,fuel} - c_{p,air} \cdot AFR \cdot \Delta T - c_{p,fuel} \Delta T}{1 + AFR} \ ,
\end{aligned} \tag{6.1.15}$$

where ΔT is the temperature increase of the mixture from entering the combustion

chamber to starting the combustion process. The specific heat capacity can be calculated in the standard way of gas mixtures [Bird et al., 2002, p.582]

$$c_p = \frac{m_{air}c_{p,air} + m_{fuel}c_{p,fuel}}{m_{air} + m_{fuel}} = \frac{\frac{m_{air}}{m_{fuel}}c_{p,air} + c_{p,fuel}}{1 + \frac{m_{air}}{m_{fuel}}} = \frac{AFR \cdot c_{p,air} + c_{p,fuel}}{1 + AFR} \ . \qquad (6.1.16)$$

We can simplify Eq. (6.1.13), Eq. (6.1.15) and Eq. (6.1.16) using the facts that $1 \ll AFR$ (in Table (6.1)) and the specific heat capacity of air is of the same order as the one of the fuels. We introduce the equivalence ratio, i.e. $\Phi = AFR_{st}/AFR$, and therefore we can write that

$$\frac{\Delta q_r}{c_p \bar{T}_{ad}} = \Phi \frac{\Delta q_{r,fuel}}{AFR_{st} c_{p,air} \bar{T}_{ad}} - \frac{\Delta T}{\bar{T}_{ad}} \ . \qquad (6.1.17)$$

Eq. (6.1.17) is shown in Figure (6.1) assuming constant adiabatic flame temperature. The dependence of the adiabatic flame temperature on the stoichiometric ratio is shown in Figure (5.2). This model is valid in the range of $[\Phi_l; \Phi_h]$, where Φ_l and Φ_h are the lowest and highest value of the equivalence ratio, at which combustion occurs.

We compare some typical fuels by calculating their $\Delta q_r/c_p\bar{T}_{ad}$ values at stoichiometric conditions. Table (6.1) shows the thermodynamic properties of some common fuel types, and calculates $\Delta q_r/c_p\bar{T}_{ad}$ by using Eq. (6.1.13) and Eq. (6.1.17). The specific heat capacity of air was taken at 700 K as 1050 J/kgK. Table (6.1) shows that preheating the mixture significantly reduces the energy which is available for conversion into mechanical energy. It also indicates that the type of fuel applied for the combustion has an effect on the stability of the system.

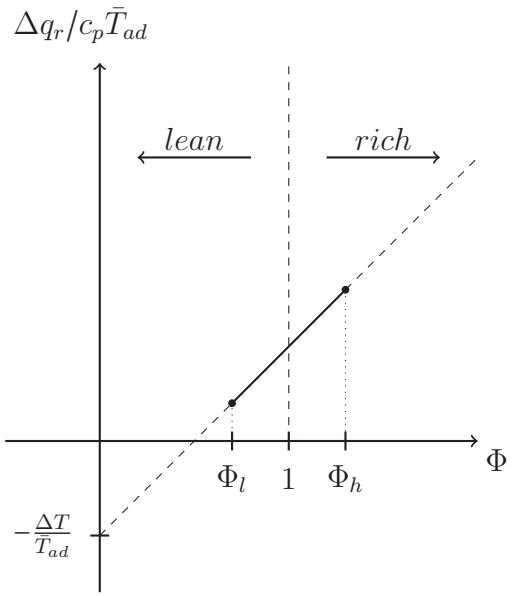

Figure 6.1: Specific heat release as function of the equivalence ratio for constant adiabatic flame temperature (The dependence of the adiabatic flame temperature on the stoichiometric ratio is shown in Figure (5.2))

6.2 The method of multiple scales

To solve Eq. (6.1.12) we apply the method of scale separation (which is described in [Mickens, 1981; Nayfeh and Mook, 1995; Zwillinger, 1998]), because it is applicable to the linear and weakly non-linear case (i.e. when non-linearity is small) as well. Another advantage of the multiple scales method is that it can treat damped systems conveniently [Nayfeh and Mook, 1995, p.57]. Since the magnitude of a dimensional constant or variable depends on the system of units, therefore to decide whether non-linearity is small, the first step is to put the underlying differential equation into a non-dimensional form. Discussion of units, dimensional and nondimensional constants is given by de St. Q. Isaacson and de St. Q. Isaacson [1975]. The next step is to identify a nondimensional small quantity, ϵ.

The idea of the multiple scales method is to assume that a periodic solution to Eq. (6.1.12) can be written as power series of the small parameter ϵ, and the expansion may be a function of multiple independent variables, or scales, instead of one single variable. In this case we may consider the dependent and independent variables (i.e.

fuel	AFR_{st}	LHV	$c_{p,fuel}$	T_{ad}	$(\Delta q_r/c_p\bar{T}_{ad})_{st}$	
	$[-]$	$[MJ/kg]$	$[J/kgK]$	$[K]$	$[-]$	$[-]$
					$\Delta T = 0K$	$\Delta T = 700K$
hydrogen	34.3	120.3	14300	2483	0.96	0.68
methane	17.2	50.3	2220	2223	1.11	0.79
ethane	16.1	47.8	1745	2228	1.15	0.84
propane	15.7	46.35	1669	2268	1.12	0.82
butane	15.4	45.75	1694	2243	1.14	0.83
natural gas	17.2	48.6	2340	2223	1.07	0.76

Table 6.1: Heating values of some common fuel types without and with preheating effects

$\tilde{u}$ and $\tilde{t}$) as

$$\tilde{u} = u_0(t_0, t_1, ..., t_n) + \epsilon u_1(t_0, t_1, ..., t_n) + \ldots + \epsilon^n u_n(t_0, t_1, ..., t_n) \ , \tag{6.2.1a}$$

$$\tilde{t} = \tilde{t}(t_0, \epsilon t_1, \ldots, \epsilon^n t_n) \ , \tag{6.2.1b}$$

$$\frac{d}{d\tilde{t}} = \frac{\partial}{\partial t_0} + \epsilon \frac{\partial}{\partial t_1} + \ldots + \epsilon^n \frac{\partial}{\partial t_n} \ , \tag{6.2.1c}$$

and solve the resulting equations of the different orders in the sequence of the orders separately. Since we require that higher terms in the expansion of (6.2.1a) provide smaller corrections, we have to eliminate those terms, which does not satisfy this criterion. They are usually referred to as secular terms and represent resonant forcing (sin t, cos t). By applying (6.2.1a) and (6.2.1b) we can separate second and higher order derivatives as well (see Appendix D.1). The number of the independent time scales needed depends on the order to which the expansion is performed. In non-linear analysis we carry out expansion up to $O(\epsilon^3)$, therefore three time scales (t_0, t_1 and t_2) are needed.

6.3 Stability analysis

As we discussed it in the previous section, in order to investigate the smallness of the parameters, we have to present Eq. (6.1.12) in a nondimensional form. To this end we introduce $\tilde{u} = u'/\epsilon_u \bar{u}$ and $\tilde{t} = \omega_r t$ to get

$$\frac{d^2\tilde{u}}{d\tilde{t}^2} - 2\frac{\omega_i}{\omega_r}\frac{d\tilde{u}}{d\tilde{t}} + \left(1 + \frac{\omega_i^2}{\omega_r^2}\right)\tilde{u} = \\ = \frac{\bar{u}}{S_l^0}\frac{1}{\eta_T}\frac{\Delta q_r}{c_p \bar{T}_{ad}} 2Im\left[\frac{1}{\omega_r}\frac{\partial \hat{g}(x, x_q, \omega_n)}{\partial x}\right]\frac{dF}{d\tilde{t}} - \frac{\bar{u}}{S_l^0}\frac{1}{\eta_T}\frac{\Delta q_r}{c_p \bar{T}_{ad}} 2Re\left[\frac{1}{\omega_r}\frac{\partial \hat{g}(x, x_q, \omega_n)}{\partial x}\right]F \ , \tag{6.3.1}$$

where the function F can be obtained by applying $\tilde{u}$ and $\tilde{t}$ in Eq. (5.4.12), i.e.

$$F(\tilde{t}) = \int \frac{2}{\chi_r \omega_r}\frac{1}{1+\beta}\Bigg\{\left[\beta\tilde{u} - \tilde{u}(\tilde{t} - \omega_r\chi_r) + \frac{1-\beta}{\omega_r\chi_r}\int \tilde{u} - \tilde{u}(\tilde{t} - \omega_r\chi)d\tilde{t}\right] + \\ + \epsilon_u \frac{1}{2}\tan^2\alpha\left[\beta\tilde{u}^2 - \tilde{u}^2(\tilde{t} - \omega_r\chi_r) + \frac{1-\beta}{\omega_r\chi_r}\int \tilde{u}^2 - \tilde{u}(\tilde{t} - \omega_r\chi_r)d\tilde{t}\right] - \\ - \epsilon_u^2 \frac{1}{2}\tan^2\alpha\left[\beta\tilde{u}^3 - \tilde{u}^3(\tilde{t} - \omega_r\chi_r) + \frac{1-\beta}{\omega_r\chi_r}\int \tilde{u}^3 - \tilde{u}^2(\tilde{t} - \omega_r\chi_r)d\tilde{t}\right]\Bigg\}d\tilde{t} \ . \tag{6.3.2}$$

In the linear stability analysis we consider the linear terms of the heat-release only (first line in Eq. (6.3.2)), in the non-linear analysis we will include non-linear terms up to cubic order as well.

6.3.1 Linear stability analysis

Linear stability analysis is capable to predict the stable and unstable regions of a thermoacoustic system, however it gives no information about the amplitude of the oscillation, since it tends exponentially either to infinity or to zero by time. In the linear stability analysis we solve Eq. (6.3.1) by neglecting the non-linear terms in the

heat-release rate, i.e.

$$\frac{d^2\tilde{u}}{d\tilde{t}^2} - 2\frac{\omega_i}{\omega_r}\frac{d\tilde{u}}{d\tilde{t}} + \left(1 + \frac{\omega_i^2}{\omega_r^2}\right)\tilde{u} = \\ = \frac{\bar{u}}{S_l^0}\frac{1}{\eta_T}\frac{\Delta q_r}{c_p\bar{T}_{ad}} 2Im\left[\frac{1}{\omega_r}\frac{\partial\hat{g}(x, x_q, \omega_n)}{\partial x}\right]\frac{dF}{d\tilde{t}} - \frac{\bar{u}}{S_l^0}\frac{1}{\eta_T}\frac{\Delta q_r}{c_p\bar{T}_{ad}} 2Re\left[\frac{1}{\omega_r}\frac{\partial\hat{g}(x, x_q, \omega_n)}{\partial x}\right]F \ , \tag{6.3.3}$$

where F contains only the linear terms

$$F = \int \frac{2}{\chi_r\omega_r}\frac{1}{1+\beta}\left[\beta\tilde{u} - \tilde{u}(\tilde{t} - \omega_r\chi_r) + \frac{1-\beta}{\omega_r\chi_r}\int \tilde{u} - \tilde{u}(\tilde{t} - \omega_r\chi_r)d\tilde{t}\right]d\tilde{t} \ . \tag{6.3.4}$$

We substitute with Eq. (6.3.4) for F in Eq. (6.3.3), and differentiate with respect to $\tilde{t}$ two times to get

$$\frac{d^4\tilde{u}}{d\tilde{t}^4} - 2\epsilon_\omega\frac{d^3\tilde{u}}{d\tilde{t}^3} + (1+\epsilon_\omega^2)\frac{d^2\tilde{u}}{d\tilde{t}^2} = \\ = 2\epsilon_i\frac{1}{\chi_r\omega_r}\frac{2}{1+\beta}\left\{\beta\frac{d^2\tilde{u}}{d\tilde{t}^2} - \frac{d^2}{d\tilde{t}^2}\tilde{u}(\tilde{t} - \omega_r\chi_r) + \frac{1-\beta}{\omega_r\chi_r}\left[\frac{d\tilde{u}}{d\tilde{t}} - \frac{d}{d\tilde{t}}\tilde{u}(\tilde{t} - \omega_r\chi)\right]\right\} - \\ - 2\epsilon_r\frac{1}{\chi_r\omega_r}\frac{2}{1+\beta}\left\{\beta\frac{d\tilde{u}}{d\tilde{t}} - \frac{d}{d\tilde{t}}\tilde{u}(\tilde{t} - \omega_r\chi_r) + \frac{1-\beta}{\omega_r\chi_r}\left[\tilde{u} - \tilde{u}(\tilde{t} - \omega_r\chi_r)\right]\right\} \quad . \tag{6.3.5}$$

The following abbreviations have been introduced in Eq. (6.3.5)

$$\epsilon_\omega = \frac{\omega_i}{\omega_r} \ , \tag{6.3.6a}$$

$$\epsilon_r = \frac{\bar{u}}{S_l^0}\frac{1}{\eta_T}\frac{\Delta q_r}{c_p \bar{T}_{ad}} Re\left[\frac{1}{\omega_r}\frac{\partial \hat{g}(x, x_q, \omega_n)}{\partial x}\right], \tag{6.3.6b}$$

$$\epsilon_i = \frac{\bar{u}}{S_l^0}\frac{1}{\eta_T}\frac{\Delta q_r}{c_p \bar{T}_{ad}} Im\left[\frac{1}{\omega_r}\frac{\partial \hat{g}(x, x_q, \omega_n)}{\partial x}\right]. \tag{6.3.6c}$$

Based on the magnitude of the reflection coefficients (given in Table (E.2)) we assume small damping (see Figure (4.5)), i.e. $|\omega_i| \ll |\omega_r|$, which has the following consequences.

- The relative damping rate, given by Eq. (6.3.6a), is small, $|\epsilon_\omega| \ll 1$.
- Since the imaginary part of the eigenfrequency is much smaller than the real part, therefore we assume that the imaginary part of $\partial \hat{g}/\partial x$ is much smaller than its real part, i.e. $|\epsilon_i| \ll |\epsilon_r|$.

An estimate for ϵ_ω, ϵ_r and ϵ_i (calculated in Appendix (E.2) for the LIMOUSINE burner with parameters listed in Appendix (E.1)) shows that ϵ_i is indeed much smaller than ϵ_r and ϵ_ω, therefore we can simplify Eq. (6.3.5) by dropping the first term on the R.H.S..

We introduce two time scales ($t_0 = \tilde{t}$, $t_1 = \epsilon_r \tilde{t}$) and transform the terms in Eq. (6.3.5). We then seek a solution in the form $\tilde{u} = u_0 + \epsilon_r u_1$, substitute it into Eq. (6.3.5) and collect the coefficients of equal powers of ϵ_r.

To the leading order (at $O(\epsilon_r^0)$) we have a harmonic oscillation, i.e.

$$\frac{\partial^4 u_0}{\partial t_0^4} + \frac{\partial^2 u_0}{\partial t_0^2} = 0 \ , \tag{6.3.7}$$

which has the solution

$$u_0 = A(t_1)\exp(-it_0) + C.C.\ . \tag{6.3.8}$$

At the order of $O(\epsilon_r^1)$ we get

$$\begin{aligned}
&\epsilon_r \frac{\partial^4 u_1}{\partial t_0^4} + 4\epsilon_r \frac{\partial^4 u_0}{\partial t_0^3 \partial t_1} - 2\epsilon_\omega \frac{\partial^3 u_0}{\partial t_0^3} + \epsilon_r \frac{\partial^2 u_1}{\partial t_0^2} + 2\epsilon_r \frac{\partial^2 u_0}{\partial t_0 \partial t_1} = \\
&= -2\epsilon_r \frac{1}{\chi_r \omega_r} \frac{2}{1+\beta} \left[\beta \frac{\partial u_0}{\partial t_0} - \frac{\partial u_0(t_0 - \chi_r \omega_r)}{\partial t_0} \right] - 2\epsilon_r \frac{1}{\chi_r \omega_r} \frac{2}{1+\beta} \frac{1-\beta}{\chi_r \omega_r} \Big[u_0 - u_0(t_0 - \chi_r \omega_r) \Big] \ .
\end{aligned} \tag{6.3.9}$$

We rearrange Eq. (6.3.9) and eliminate the secular terms to obtain the following equation for $A(t_1)$

$$\frac{\partial A}{\partial t_1} = A \left[\frac{\epsilon_\omega}{\epsilon_r} + (\varphi_i - i\varphi_r) \right] \ , \tag{6.3.10}$$

where

$$\varphi_i(\beta, \chi_r \omega_r) = \frac{\beta \chi_r \omega_r - \chi \omega_r \cos(\chi_r \omega_r) + (1-\beta)\sin(\chi_r \omega_r)}{\frac{1+\beta}{2}(\chi_r \omega_r)^2} \ , \tag{6.3.11a}$$

$$\varphi_r(\beta, \chi_r \omega_r) = \frac{\chi_r \omega_r \sin(\chi_r \omega_r) - (1-\beta)[1 - \cos(\chi_r \omega_r)]}{\frac{1+\beta}{2}(\chi_r \omega_r)^2} \ . \tag{6.3.11b}$$

Eq. (6.3.10) is of first order and linear in A. The solution is

$$A(t_1) = c_0 \exp\left\{ t_1 \left[\frac{\epsilon_\omega}{\epsilon_r} + (\varphi_i - i\varphi_r) \right] \right\} \ , \tag{6.3.12}$$

where c_0 is a complex constant, and with Eq. (6.3.8) we obtain

$$u_0 = a_0 \exp\left[t_0\left(\epsilon_\omega + \epsilon_r \varphi_i\right)\right] \sin\left[\zeta_0 + t_0\left(1 + \epsilon_r \varphi_r\right)\right] \ , \tag{6.3.13}$$

where a_0 and ζ_0 are the initial conditions.

The growth rate in Eq. (6.3.13) $(\epsilon_\omega + \epsilon_r \varphi_i)$ has to be positive to get instability. We substitute with Eqs. (6.3.6a)-(6.3.6b) for ϵ_ω and ϵ_r in Eq. (6.3.13) to get the linear instability condition

$$\frac{\omega_i}{\omega_r} + \frac{\bar{u}}{S_l^0} \frac{1}{\eta_T} \frac{\Delta q_r}{c_p T_{ad}} Re\left[\frac{1}{\omega_r} \frac{\partial \hat{g}(x, x_q, \omega_n)}{\partial x}\right] \varphi_i(\beta, \chi_r \omega_r) > 0 \ . \tag{6.3.14}$$

φ_i and φ_r are plotted in Figure (6.2). Calculation, which includes ϵ_i is given in Appendix (D.2).

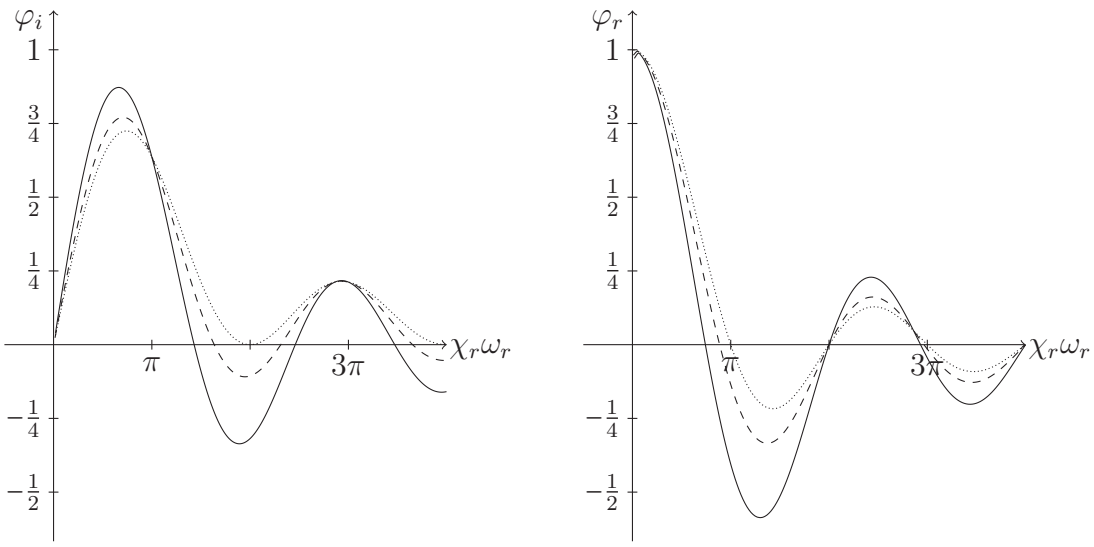

Figure 6.2: Representation of (a) φ_i and (b) φ_r as function of the phase lag, $\chi_r\omega_r$ (——— : $\beta = 0$, − − − : $\beta = 0.5$, ····· : $\beta = 1.0$)

Eq. (6.3.14) shows that the negative growth rate due to the losses (ω_i/ω_r) must be balanced by the positive growth rate due to heating to get instability.

It also shows that lean mixtures are more susceptible to thermoacoustic instabilities: the primary effect of reducing the equivalence ratio is lower combustion temperature

(see Figure (5.2)), which increases the magnitude of ϵ_r (through $\Delta q_r / c_p T_{ad}$), and therefore a stable system can turn into an unstable one.

The unstable frequency can be smaller or larger than the stable one, which depends on the sign of $\epsilon_r \varphi_r$.

It is interesting to see that for $\beta = 1$, i.e. for planar flames φ_i is always non-negative, therefore instability does not depend on the phase-lag, but only on the geometry and on the boundary conditions. This finding suggests that the planar flame model is not realistic. To resolve this problem one might adopt the concept of the 'equivalent hydraulic radius', often used in fluid dynamics: for non-circular geometries an equivalent radius can be calculated by dividing the cross sectional area with the wetted perimeter [Bird et al., 2002, p.190], which gives $\beta = 0.56$ for the LIMOUSINE setup.

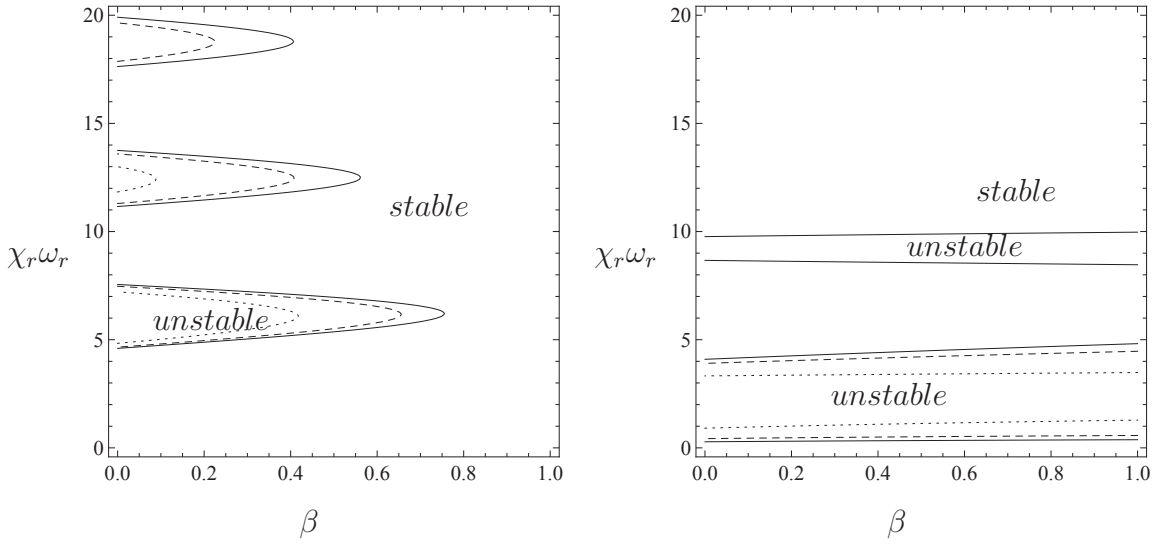

(a) first mode

(b) second mode

Figure 6.3: Linear stability map of the LIMOUSINE burner for $\Phi = 1$ and various phase-lag, β and $\bar{u}/S_l^0$ (———:$\bar{u}/S_l^0 = 3$, – – –: $\bar{u}/S_l^0 = 2$, ·····: $\bar{u}/S_l^0 = 1$)

Figure (6.3) shows the linear stability map of the LIMOUSINE burner for different $\bar{u}/S_l^0$ values as function of β and $\chi_r\omega_r$. It clearly indicates that for larger frequencies the unstable regimes get smaller, which reflects the low-pass filter property of our flame model.

We can also see that there is a minimum of the mean flow velocity to get instability. This feature was also found for setups with gauze heating in Neuringer and Hudson

[1951].

Our linear model predicts instability above a critical fuel-air ratio, which was observed by others as well [Dowling, 1999; Langhorne, 1987].

From Eq. (6.3.14) and Figure (6.3) we can see that some fuel types are more susceptible to thermoacoustic instabilities than others. This property was measured by Allison et al. [2012].

Figure (6.3) shows significant difference in the stability of the first two modes. They can be explained by comparing $|\epsilon_\omega|$ with $|\epsilon_r|$: in case of the first mode $|\epsilon_\omega| \ll |\epsilon_r|$, therefore the stability map is mostly affected by φ_i. In case of the second mode, however, $|\epsilon_\omega| \sim |\epsilon_r|$ therefore the stabilizing effect of ϵ_ω is reflected in the stability map. There is a potential error in the results of the second mode, since we assumed frequency independence of the reflection coefficients.

In order to meet emission regulations increasing the stoichiometric ratio is not in the focus of industrial research. However, our model indicates that for rich mixtures we get similar instability effects as for lean mixtures. This was shown by measurements, e.g. Allison et al. [2012].

6.3.2 Non-linear stability analysis

In this section we perform a non-linear stability analysis, therefore include the non-linear terms of the heat-release rate in the calculation of Eq. (6.3.1). The frequency of a nonlinear system is not constant and it is coupled to the amplitude, in contrast to a linear system. In the this case we have to substitute the heat-release rate in the following form

$$F = \frac{2}{\chi_r\omega_r}\frac{1}{1+\beta}\int\Bigg\{\Bigg[\beta\tilde{u} - \tilde{u}(\tilde{t}-\chi\omega_r) + \frac{1-\beta}{\chi_r\omega_r}\int \tilde{u} - \tilde{u}(\tilde{t}-\chi\omega_r)d\tilde{t}\Bigg] + \\ + \epsilon_u\frac{1}{2}\tan^2\alpha\Bigg[\beta\tilde{u}^2 - \big(\tilde{u}(\tilde{t}-\chi\omega_r)\big)^2 + \frac{1-\beta}{\chi_r\omega_r}\int \tilde{u}^2 - \big(\tilde{u}(\tilde{t}-\chi\omega_r)\big)^2 d\tilde{t}\Bigg] - \\ - \epsilon_u^2\frac{1}{2}\tan^2\alpha\Bigg[\beta\tilde{u}^3 - \big(\tilde{u}(\tilde{t}-\chi\omega_r)\big)^3 + \frac{1-\beta}{\chi_r\omega_r}\int \tilde{u}^3 - \big(\tilde{u}(\tilde{t}-\chi\omega_r)\big)^3 d\tilde{t}\Bigg]\Bigg\}d\tilde{t}\ . \quad (6.3.15)$$

Substituting Eq. (6.3.15) in Eq. (6.3.1) yields

$$\frac{d^2\tilde{u}}{d\tilde{t}^2} - 2\epsilon_\omega\frac{d\tilde{u}}{d\tilde{t}} + \tilde{u} = 2\epsilon_i\frac{1}{\chi\omega_r}\frac{2}{1+\beta}\Bigg\{\Bigg[\beta\tilde{u} - \tilde{u}(\tilde{t}-\chi_r\omega_r) + \frac{1-\beta}{\chi_r\omega_r}\int \tilde{u} - \tilde{u}(\tilde{t}-\chi_r\omega_r)d\tilde{t}\Bigg] + \\ + \epsilon_\Phi\epsilon_u\Bigg[\beta\tilde{u}^2 - \big(\tilde{u}(\tilde{t}-\chi_r\omega_r)\big)^2 + \frac{1-\beta}{\chi_r\omega_r}\int \tilde{u}^2 - \big(\tilde{u}(\tilde{t}-\chi_r\omega_r)\big)^2 d\tilde{t}\Bigg] - \\ - 3\epsilon_\Phi\epsilon_u^2\Bigg[\beta\tilde{u}^3 - \big(\tilde{u}(\tilde{t}-\chi_r\omega_r)\big)^3 + \frac{1-\beta}{\chi_r\omega_r}\int \tilde{u}^3 - \big(\tilde{u}(\tilde{t}-\chi_r\omega_r)\big)^3\Bigg]\Bigg\} - \\ - 2\epsilon_r\frac{1}{\chi_r\omega_r}\frac{2}{1+\beta}\int\Bigg\{\Bigg[\beta\tilde{u} - \tilde{u}(\tilde{t}-\chi_r\omega_r) + \frac{1-\beta}{\chi_r\omega_r}\int \tilde{u} - \tilde{u}(\tilde{t}-\chi_r\omega_r)d\tilde{t}\Bigg] + \\ + \epsilon_\Phi\epsilon_u\Bigg[\beta\tilde{u}^2 - \big(\tilde{u}(\tilde{t}-\chi_r\omega_r)\big)^2 + \frac{1-\beta}{\chi_r\omega_r}\int \tilde{u}^2 - \big(\tilde{u}(\tilde{t}-\chi_r\omega_r)\big)^2 d\tilde{t}\Bigg] - \\ - \epsilon_\Phi\epsilon_u^2\Bigg[\beta\tilde{u}^3 - \big(\tilde{u}(\tilde{t}-\chi_r\omega_r)\big)^3 + \frac{1-\beta}{\chi_r\omega_r}\int \tilde{u}^3 - \big(\tilde{u}(\tilde{t}-\chi_r\omega_r)\big)^3 d\tilde{t}\Bigg]\Bigg\}d\tilde{t}\ . \quad (6.3.16)$$

Similarly to the linear case, we have introduced the following abbreviations

$$\epsilon_u \sim O\left(\frac{u'}{\bar{u}}\right) , \tag{6.3.17a}$$

$$\epsilon_\omega = \frac{\omega_i}{\omega_r} , \tag{6.3.17b}$$

$$\epsilon_r = \frac{\bar{u}_u}{S_l}\frac{\Delta q_r}{c_p \bar{T}(x_q)} Re\left[\frac{1}{\omega_r}\frac{\partial \hat{g}(x, x_q, \omega_n)}{\partial x}\right] , \tag{6.3.17c}$$

$$\epsilon_i = \frac{\bar{u}_u}{S_l}\frac{\Delta q_r}{c_p \bar{T}(x_q)} Im\left[\frac{1}{\omega_r}\frac{\partial \hat{g}(x, x_q, \omega_n)}{\partial x}\right] , \tag{6.3.17d}$$

$$\epsilon_\Phi = \frac{1}{2}\tan^2\alpha = \frac{1}{2}\frac{1}{\left(\frac{\bar{u}}{S_l^0}\right)^2 - 1} . \tag{6.3.17e}$$

The assumptions of the linear analysis hold, and in order to obtain a weakly non-linear regime, additional constrains have to be satisfied:

1. We assumed small amplitudes during the derivation of the heat-release law $\rightarrow$ $\epsilon_u \ll 1$.

2. Cubic terms must be of the same order as the linear ones $\rightarrow \epsilon_\Phi \epsilon_u^2 \sim O(1)$.

3. Quadratic terms must not appear in the leading order $\rightarrow \epsilon_r \epsilon_\Phi \epsilon_u \ll 1$.

Figure (6.4) shows the relationships between the small parameters, which identifies region 1 of Figure (5.7).

Figure (6.4) shows that in the non-linear analysis we should apply $\epsilon = \epsilon_r/\epsilon_u$ for our small quantity in the power expansion. In the linear analysis we have seen that ϵ_i can be neglected compared to ϵ_r, therefore we solve the following equation

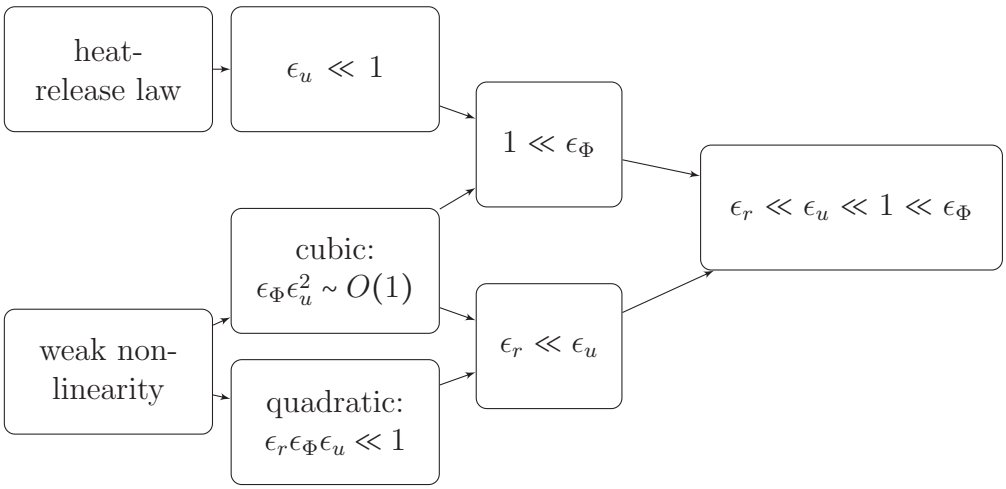

Figure 6.4: Necessary conditions of the weakly non-linear regime which identifies region 1 in Figure (5.7)

$$\frac{d^2\tilde{u}}{d\tilde{t}^2} - 2\epsilon_\omega \frac{d\tilde{u}}{d\tilde{t}} + \tilde{u} = -2\epsilon_r \frac{1}{\chi_r\omega_r}\frac{2}{1+\beta}\int \Bigg\{ \Bigg[\beta\tilde{u} - \tilde{u}(\tilde{t}-\chi_r\omega_r) + \frac{1-\beta}{\chi_r\omega_r}\int \tilde{u} - \tilde{u}(\tilde{t}-\chi_r\omega_r)d\tilde{t}\Bigg] + \\ + \epsilon_\Phi\epsilon_u\Bigg[\beta\tilde{u}^2 - \big(\tilde{u}(\tilde{t}-\chi_r\omega_r)\big)^2 + \frac{1-\beta}{\chi_r\omega_r}\int \tilde{u}^2 - \big(\tilde{u}(\tilde{t}-\chi_r\omega_r)\big)^2 d\tilde{t}\Bigg] - \\ - \epsilon_\Phi\epsilon_u^2\Bigg[\beta\tilde{u}^3 - \big(\tilde{u}(\tilde{t}-\chi_r\omega_r)\big)^3 + \frac{1-\beta}{\chi_r\omega_r}\int \tilde{u}^3 - \big(\tilde{u}(\tilde{t}-\chi_r\omega_r)\big)^3 d\tilde{t}\Bigg]\Bigg\} d\tilde{t}\ . \quad (6.3.18)$$

To eliminate the integrals we perform differentiation with respect to $\tilde{t}$ two times to obtain

$$\frac{d^4\tilde{u}}{d\tilde{t}^4} - 2\epsilon_\omega\frac{d^3\tilde{u}}{d\tilde{t}^3} + \frac{d^2\tilde{u}}{d\tilde{t}^2} = -2\epsilon_r\frac{1}{\chi_r\omega_r}\frac{2}{1+\beta}\Bigg[\beta\frac{d}{d\tilde{t}}\tilde{u} - \frac{d}{d\tilde{t}}\tilde{u}(\tilde{t}-\chi_r\omega_r) + \frac{1-\beta}{\chi_r\omega_r}\big(\tilde{u} - \tilde{u}(\tilde{t}-\chi_r\omega_r)\big)\Bigg] - \\ - 2\epsilon_\Phi\epsilon_u\epsilon_r\frac{1}{\chi_r\omega_r}\frac{2}{1+\beta}\Bigg[\beta\frac{d}{d\tilde{t}}\tilde{u}^2 - \frac{d}{d\tilde{t}}\big(\tilde{u}(\tilde{t}-\chi_r\omega_r)\big)^2 + \frac{1-\beta}{\chi_r\omega_r}\Big[\tilde{u}^2 - \big(\tilde{u}(\tilde{t}-\chi_r\omega_r)\big)^2\Big]\Bigg] + \\ + 2\epsilon_\Phi\epsilon_u^2\epsilon_r\frac{1}{\chi_r\omega_r}\frac{2}{1+\beta}\Bigg[\beta\frac{d}{d\tilde{t}}\tilde{u}^3 - \frac{d}{d\tilde{t}}\big(\tilde{u}(\tilde{t}-\chi_r\omega_r)\big)^3 + \frac{1-\beta}{\chi_r\omega_r}\Big[\tilde{u}^3 - \big(\tilde{u}(\tilde{t}-\chi_r\omega_r)\big)^3\Big]\Bigg]\ . \quad (6.3.19)$$

We introduce three time scales ($t_0 = \tilde{t}$, $t_1 = \epsilon\tilde{t}$, $t_2 = \epsilon^2\tilde{t}$) and transform the terms in Eq.

(6.3.19). We then seek a solution in the form $\tilde{u} = u_0 + \epsilon u_1 + \epsilon^2 u_2$, substitute it into Eq. (6.3.19) and collect the coefficients of equal powers of ϵ.

To the leading order we have a harmonic oscillation

$$\frac{\partial^4 u_0}{\partial t_0^4} + \frac{\partial^2 u_0}{\partial t^2} = 0 \ , \tag{6.3.20}$$

which has the solution

$$u_0 = A(t_1, t_2)e^{-it_0} + C.C. \ . \tag{6.3.21}$$

At the next order (ϵ^1) we get

$$\begin{aligned} &\frac{\partial^4 u_1}{\partial t_0^4} + 4\frac{\partial^4 u_0}{\partial t_0^3 \partial t_1} + \frac{\partial^2 u_1}{\partial t_0^2} + 2\frac{\partial^2 u_0}{\partial t_0 \partial t_1} = \\ &= -2\frac{1}{\chi_r \omega_r}\frac{2}{1+\beta}\epsilon_\Phi \epsilon_u^2 \left[\beta \frac{\partial}{\partial t_0} u_0^2 - \frac{\partial}{\partial t_0}\left(u_0(t_0 - \chi_r\omega_r)\right)^2 + \frac{1-\beta}{\chi_r\omega_r}\left[u_0^2 - \left(u_0(t_0-\chi_r\omega_r)\right)^2\right]\right] \ . \end{aligned} \tag{6.3.22}$$

At this order (ϵ^1) only the quadratic terms appear, which means that there are no secular terms to eliminate, i.e. A doesn't depend on t_1, and $\partial/\partial t_1 = 0$. For u_1 we get therefore a non-zero particular solution, which is

$$u_1 = \frac{1}{6}\epsilon_\Phi \epsilon_u^2 \frac{1}{\chi_r\omega_r}\frac{2}{1+\beta} A^2 e^{-2it_0}\left[2i\left(e^{2i\chi_r\omega_r} - \beta\right) + \frac{1-\beta}{\chi_r\omega_r}\left(1 - e^{2i\chi_r\omega_r}\right)\right] + C.C. \ . \tag{6.3.23}$$

We write Eq. (6.3.23) in the following compact form:

$$u_1 = \delta A^2 e^{-2it_0} + C.C. \ . \tag{6.3.24}$$

δ is defined by

$$\delta = -\frac{2}{3}\epsilon_\Phi \epsilon_u^2 \Big[\varphi_r(\beta, 2\chi_r\omega_r) + i\varphi_i(\beta, 2\chi_r\omega_r) \Big] \,, \tag{6.3.25}$$

where φ_r and φ_i are given in Eq. (6.3.11b) and (6.3.11a).

At ϵ^2 order we get

$$\begin{aligned}
&\epsilon^2 \left[\frac{\partial^4 u_2}{\partial t_0^4} + 4\frac{\partial^4 u_0}{\partial t_0^3 \partial t_2} \right] - 2\epsilon_\omega \frac{\partial^3 u_0}{\partial t_0^3} + \epsilon^2 \left[2\frac{\partial^2 u_0}{\partial t_0 \partial t_2} + \frac{\partial^2 u_2}{\partial t_0^2} \right] = \\
&\quad = -2\epsilon_r \frac{1}{\chi_r\omega_r} \frac{2}{1+\beta} \left[\beta \frac{\partial}{\partial t_0} u_0 - \frac{\partial}{\partial t_0} u_0(t_0 - \chi_r\omega_r) + \frac{1-\beta}{\chi_r\omega_r} \left(u_0 - u_0(t_0 - \chi_r\omega_r) \right) \right] - \\
&\qquad - 2\epsilon_\Phi \epsilon_u^2 \epsilon^2 \frac{1}{\chi_r\omega_r} \frac{2}{1+\beta} \Bigg\{ 2\beta \frac{\partial}{\partial t_0} u_0 u_1 - 2\frac{\partial}{\partial t_0} u_0(t_0 - \chi_r\omega_r) u_1(t_0 - \chi_r\omega_r) + \\
&\qquad\quad + \frac{1-\beta}{\chi_r\omega} \Big[2u_0 u_1 - 2u_0(t_0 - \chi_r\omega_r) u_1(t_0 - \chi_r\omega_r) \Big] \Bigg\} + \\
&+ 2\epsilon_r \epsilon_\Phi \epsilon_u^2 \frac{1}{\chi_r\omega_r} \frac{2}{1+\beta} \left[\beta \frac{\partial}{\partial t_0} u_0^3 - \frac{\partial}{\partial t_0} \left(u_0(t_0 - \chi_r\omega_r) \right)^3 + \frac{1-\beta}{\chi_r\omega_r} \left[u_0^3 - \left(u_0(t_0 - \chi_r\omega_r) \right)^3 \right] \right] \,,
\end{aligned} \tag{6.3.26}$$

with the following quadratic and cubic terms

$$u_0 u_1 = \delta A^3 e^{-3it_0} + \delta A^2 A^* e^{-it_0} + C.C. \,, \tag{6.3.27a}$$

$$u_0(t_0 - \chi\omega) u_1(t_0 - \chi\omega) = \delta A^3 e^{3i\chi\omega} e^{-3it_0} + \delta A^2 A^* e^{i\chi\omega} e^{-it_0} + C.C. \,, \tag{6.3.27b}$$

$$u_0^3 = A^3 e^{-3it_0} + 3A^2 A^* e^{-it_0} + C.C. \,, \tag{6.3.27c}$$

$$[u_0(t_0 - \chi\omega)]^3 = A^3 e^{3i\chi\omega} e^{-3it_0} + 3A^2 A^* e^{i\chi\omega} e^{-it_0} + C.C. \,. \tag{6.3.27d}$$

We substitute with Eqs. (6.3.27a)-(6.3.27d) in Eq. (6.3.26) and introduce a polar

representation for A, i.e. $A = ae^{i\zeta}$. Eliminating the secular terms yields

$$\frac{\partial a}{\partial t_2} + ia\frac{\partial \zeta}{\partial t_2} = a\left[\frac{\epsilon_\omega}{\epsilon^2} + \frac{\epsilon_r}{\epsilon^2}(\varphi_i - i\varphi_r)\right] - a^3\epsilon_\Phi\epsilon_u^2\left[\left(3\frac{\epsilon_r}{\epsilon^2} - 2\delta\right)(\varphi_i - i\varphi_r)\right] . \tag{6.3.28}$$

The real part of Eq. (6.3.28) gives a non-linear ordinary differential equation of Bernoulli-type for the amplitude evolution

$$\frac{\partial a}{\partial t_2} = a\theta_1^r - a^3\theta_3^r , \tag{6.3.29}$$

where

$$\theta_1^r = \frac{\epsilon_\omega}{\epsilon^2} + \varphi_i\frac{\epsilon_r}{\epsilon^2} , \tag{6.3.30a}$$

$$\theta_3^r = 3\epsilon_\Phi\epsilon_u^2\left[\frac{\epsilon_r}{\epsilon^2}\varphi_i + \frac{4}{9}\epsilon_\Phi\epsilon_u^2\sigma_\varphi^r\right] , \tag{6.3.30b}$$

$$\sigma_\varphi^r = \varphi_r(\beta, 2\chi_r\omega_r)\varphi_i(\beta, \chi_r\omega_r) + \varphi_i(\beta, 2\chi_r\omega_r)\varphi_r(\beta, \chi_r\omega_r) . \tag{6.3.30c}$$

Eq. (6.3.29) shows that neglecting cubic terms ($\theta_3^r = 0$) yields the linear solution. The second term in Eq. (6.3.30b) is the contribution of the higher order quadratic terms. We write the solution of Eq. (6.3.29) in the following form

$$a(t_0) = \frac{a_0 e^{(\epsilon_\omega + \epsilon_r\varphi_i)t_0}}{\sqrt{1 + a_0^2\frac{\theta_3^r}{\theta_1^r}\left[e^{2(\epsilon_\omega + \epsilon_r\varphi_i)t_0} - 1\right]}} , \tag{6.3.31}$$

where a_0 is the initial condition for the amplitude. We get the following values for $a(t_0)$ for small and large times

$$a(t) = \begin{cases} a_0 & \text{if} \quad t = 0 \\ 0 & \text{if} \quad \epsilon_\omega + \epsilon_r \varphi_i < 0 \quad \text{for} \quad t \to \infty \\ \sqrt{\theta_1^r / \theta_3^r} & \text{if} \quad \epsilon_\omega + \epsilon_r \varphi_i > 0 \quad \text{for} \quad t \to \infty \ . \end{cases} \tag{6.3.32}$$

Eq. (6.3.32) shows that the amplitude of a limit cycle is $\sqrt{\theta_1^r/\theta_3^r}$. The growth rate is $\epsilon_\omega + \epsilon_r \varphi_i$, and its sign is an indicator for stability behavior. If it is positive , the oscillation is unstable. The non-linear instability criterion is identical to the linear one.

Figure (6.5) compares the evolution of the amplitude for the linear and non-linear cases. It shows that non-linearity is of threshold nature, i.e. below a critical value of the acoustic velocity the effects of nonlinear combustion are not present. This was confirmed experimentally by Ma et al. [1991].

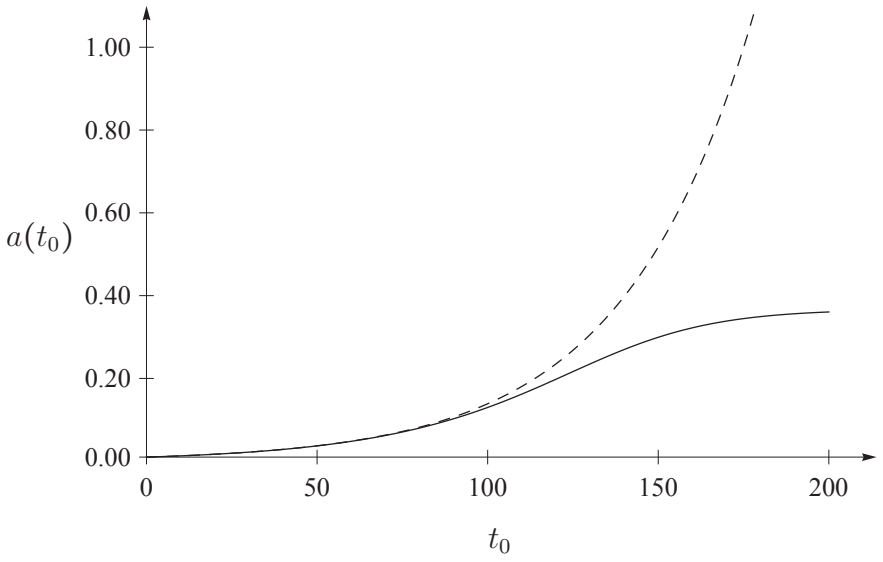

Figure 6.5: Schematic representation of the evolution of the amplitude as function of time in case of an instability (———:non-linear, – – –: linear)

The imaginary part of Eq. (6.3.28) gives a non-linear ordinary differential equation of Bernoulli-type for the phase evolution

$$\frac{\partial \zeta}{\partial t_2} = -\theta_1^i + \theta_3^i a^2 \ , \tag{6.3.33}$$

where

$$\theta_1^i = \frac{\epsilon_r}{\epsilon^2}\varphi_r \ , \tag{6.3.34a}$$

$$\theta_3^i = 3\epsilon_\Phi \epsilon_u^2 \left[\frac{\epsilon_r}{\epsilon^2}\varphi_r + \frac{4}{9}\epsilon_\Phi \epsilon_u^2 \sigma_\varphi^i \right] \ , \tag{6.3.34b}$$

$$\sigma_\varphi^i = \varphi_i(\beta, 2\chi_r\omega_r)\varphi_i(\beta, \chi_r\omega_r) - \varphi_r(\beta, 2\chi_r\omega_r)\varphi_r(\beta, \chi_r\omega_r) \ . \tag{6.3.34c}$$

The solution of Eq. (6.3.33) is

$$\zeta(t_0) = \zeta_0 - \epsilon_r\varphi_r t_0 + \frac{\theta_3^i}{\theta_3^r} \ln \sqrt{1 + a_0^2 \frac{\theta_3^r}{\theta_1^r}\left[e^{2(\epsilon_\omega + \epsilon_r\varphi_i)t_0} - 1\right]} \ , \tag{6.3.35}$$

where ζ_0 is the initial condition of the phase.

Using Eq. (6.3.31) and Eq. (6.3.35) we can write the solution of Eq. (6.3.18) to the leading order in the following form

$$u_0 = a_0 \exp\left\{ t_0\Big[\epsilon_\omega + \epsilon_r\varphi_i\Big] - \Sigma(t_0) \right\} \cdot \sin\left\{ \zeta_0 + t_0\Big[1 + \epsilon_r\varphi_r\Big] - \frac{\theta_3^i}{\theta_3^r}\Sigma(t_0) \right\} \ , \tag{6.3.36}$$

where

$$\Sigma(t_0) = \ln \sqrt{1 + a_0^2 \frac{\theta_3^r}{\theta_1^r}\Big[e^{2t_0(\epsilon_\omega + \epsilon_r\varphi_i)} - 1\Big]} \ . \tag{6.3.37}$$

Eq. (6.3.36) is of the form

$$u_0 = a_0 e^{t_0 \Omega_i(t_0)} \sin\left[\zeta_0 + t_0 \Omega_r(t_0)\right] \ , \tag{6.3.38}$$

where

$$\Omega_i(t) = \epsilon_\omega + \epsilon_r \varphi_i - \Lambda(t) \ , \tag{6.3.39a}$$

$$\Omega_r(t) = 1 + \epsilon_r \varphi_r - \frac{\theta_3^i}{\theta_3^r} \Lambda(t) \ , \tag{6.3.39b}$$

with

$$\Lambda(t) = \frac{\Sigma(t)}{t} = \frac{1}{t} \ln \sqrt{1 + a_0^2 \frac{\theta_3^r}{\theta_1^r} \left[e^{2(\epsilon_\omega + \epsilon_r \varphi_i)t} - 1 \right]} \ . \tag{6.3.40}$$

Ω_i and Ω_r are the non-linear growth rate and frequency respectively. They both evolve with time. Eq. (6.3.39a) shows that $\Lambda(t) = \epsilon_\omega + \epsilon_r \varphi_i$ for $t \to \infty$. In case of an instability for $t \to \infty$ we get

$$\Omega_i \Big|_{t \to \infty} = 0 \ , \tag{6.3.41a}$$

$$\Omega_r \Big|_{t \to \infty} = 1 + \epsilon_r \varphi_r - \frac{\theta_3^i}{\theta_3^r} \left[\epsilon_\omega + \epsilon_r \varphi_i \right] = 1 + \epsilon_r \varphi_r + \Delta\Omega_r \ . \tag{6.3.41b}$$

Figure (6.6) shows the linear and non-linear growth rates and frequencies as function of time for an unstable system.

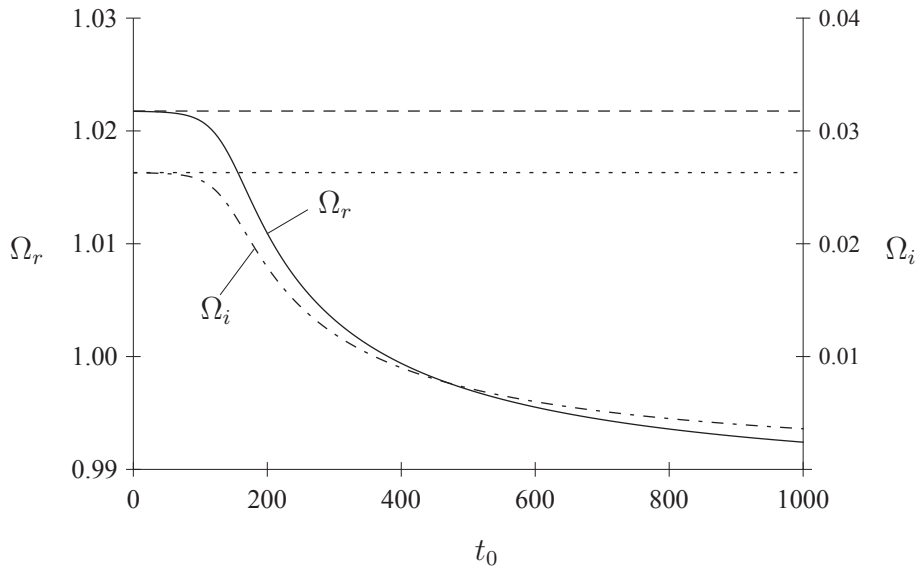

Figure 6.6: Time evolution of the nonlinear frequency $\Omega_r(t)$ and growth rate $\Omega_i(t)$ of the first mode for $\beta = 0.1$ and $\chi_r\omega_r = 6$ (———:nonlinear frequency, − − −: linear frequency, − · −: nonlinear growth rate ·····: linear growth rate)

Figure (6.6) reflects that the non-linear growth rate and frequency are governed by the same function, $\Lambda(t)$. Figure (6.7) represents the non-linear growth rate Ω_i as function of the non-linear frequency Ω_r, where time is a parameter: (a) shows a general scenario, (b) shows the first mode of the LIMOUSINE setup for different values of the stoichiometric ratio and phase-lag with $\beta = 0.1$. The adiabatic flame temperature for certain values of Φ were taken from Figure (5.2).

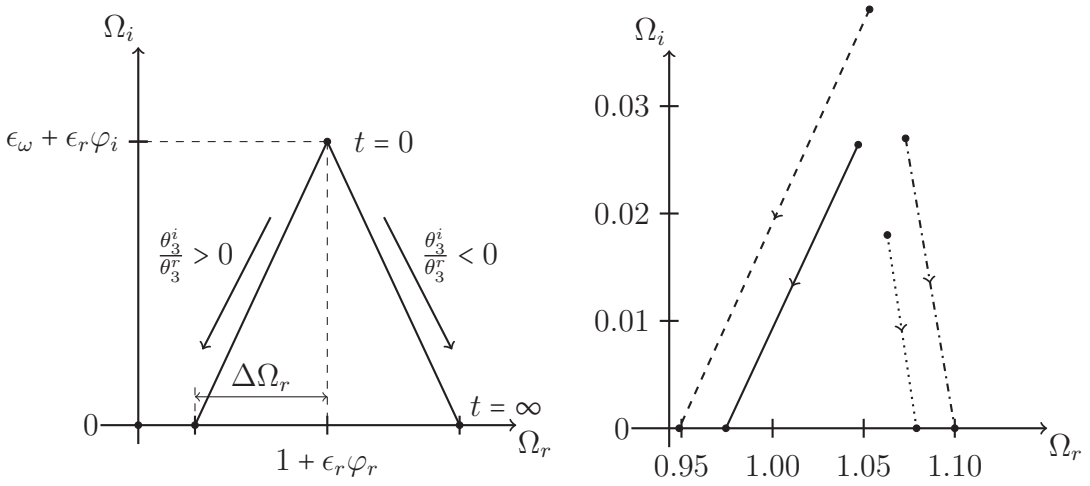

(a) general setup

(b) LIMOUSINE setup

Figure 6.7: Time evolution of the damping and the eigenfrequency: (a) general setup, (b) first mode of LIMOUSINE setup, $\beta = 0.1$ (———:$\Phi = 1.00$,$\chi_r\omega_r = 6$; − − −: $\Phi = 0.75$,$\chi_r\omega_r = 6$; ·····: $\Phi = 1.00$,$\chi_r\omega_r = 5.5$; − · −: $\Phi = 0.75$,$\chi_r\omega_r = 5.5$)

Figure (6.7) shows that lean systems are more susceptible to instabilities (higher initial growth rate), and the frequency of the non-linear system can be lower or larger (even by 5-10 %) than the one of the corresponding linear system, depending on the system properties. Dhanuka et al. [2011] performed measurements at very low frequencies in a premixed combustor and found that decreasing the stoichiometric ratio reduces the frequency of the instabilities in their setup. Figure (6.8) shows the phase plot of the first mode for stable and unstable cases.

6.3.2.1 Effect of the parameters on the resulting limit-cycle amplitudes

The amplitude of the solution given by Eq. (6.3.36) is $\sqrt{\theta_1^r/\theta_3^r}$ (see Eq. (6.3.32)), i.e.

$$\left|\frac{u'}{\bar{u}}\right|_{t\to\infty} = \sqrt{\frac{2}{3}} \cdot \sqrt{\left(\frac{\bar{u}}{S_l^0}\right)^2 - 1} \cdot \sqrt{\frac{\epsilon_\omega + \epsilon_r\varphi_i}{\epsilon_r\varphi_i + \frac{4}{9}\epsilon_\Phi\epsilon_r^2\sigma_\varphi}} \,. \tag{6.3.42}$$

We can see that if we do not include losses in our model ($\epsilon_\omega = 0$) and neglect the quadratic terms ($\sigma = 0$), then the amplitude is given by the following simple form

$$\left|\frac{u'}{\bar{u}}\right|_{\substack{t\to\infty \\ \epsilon_\omega=0 \\ \sigma=0}} = \sqrt{\frac{2}{3}} \cdot \sqrt{\left(\frac{\bar{u}}{S_l^0}\right)^2 - 1} \ . \tag{6.3.43}$$

We plot the amplitudes as function of $\bar{u}/S_l^0$ for different values of β, χ and $\Delta q_r/c_p\bar{T}_{ad}$ at stoichiometric conditions, i.e. we investigate the effect of the type of fuel used in the combustion chamber on the instabilities.

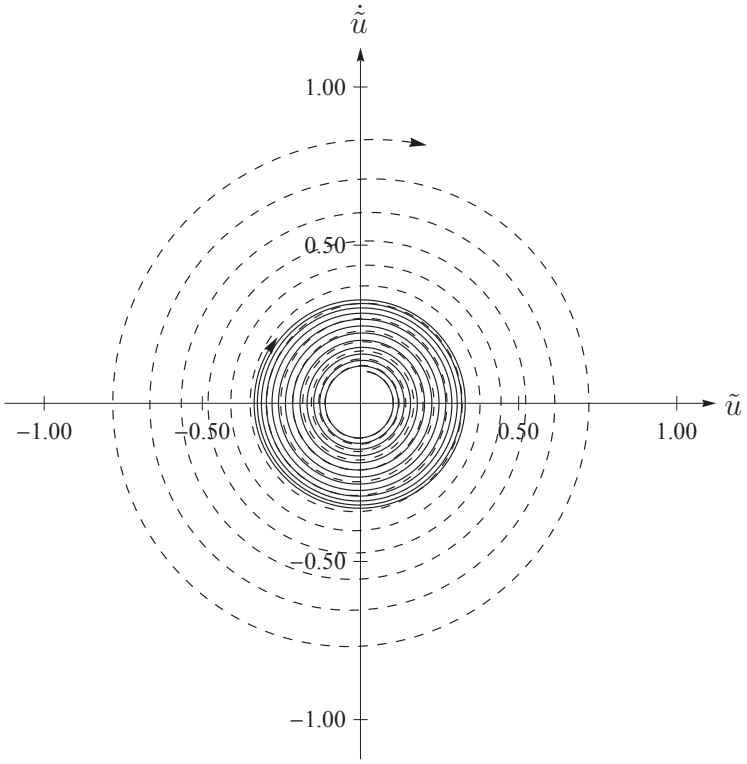

(a) unstable system ($\chi_r\omega_r = 6$)

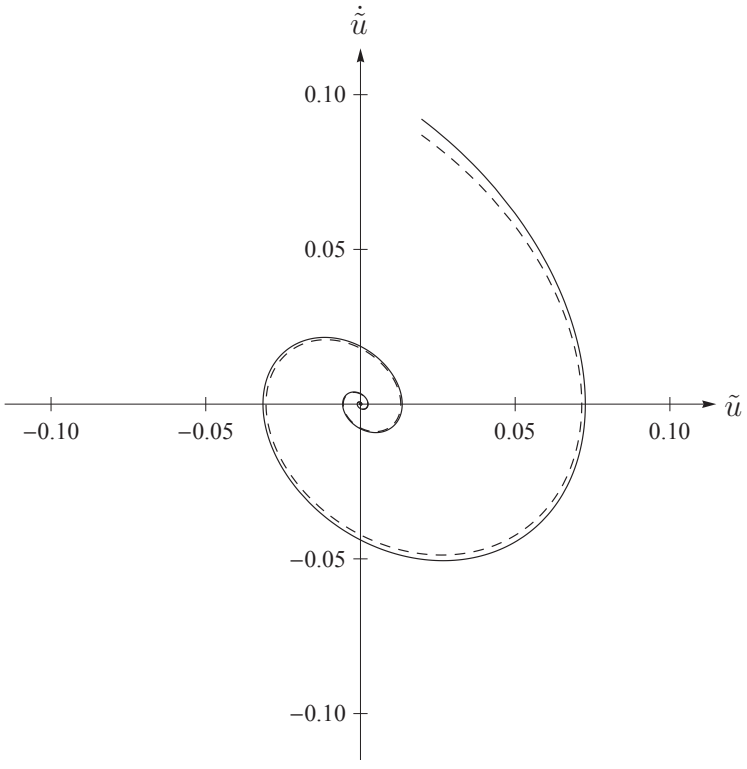

(b) stable system ($\chi_r\omega_r = 2$)

Figure 6.8: Phase plot of (a) an unstable and (b) of a stable system for $\beta = 0.1$ (———:nonlinear, − − −: linear)

Figure (6.9) shows the resulting amplitudes of the first mode as function of $\bar{u}/S_l^0$ for the phase-lag of 6, and for $\beta = 0.1, 0.2, 0.3$. Figure (6.10) shows the resulting amplitudes of the second mode as function of $\bar{u}/S_l^0$ for the phase-lag of 2, and for $\beta = 0.1, 0.2, 0.3$. They both indicate that decreasing β increases the amplitude in case of an instability.

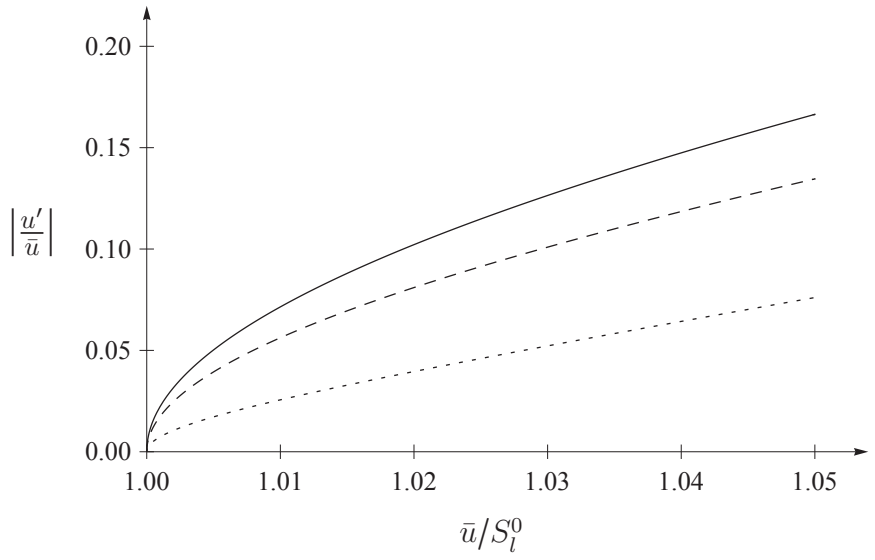

Figure 6.9: Amplitude of the first mode as function of $\bar{u}/S_l^0$ for $\chi_r\omega_r = 6$ (———:$\beta = 0.1$, – – –: $\beta = 0.2$, ·····: $\beta = 0.3$)

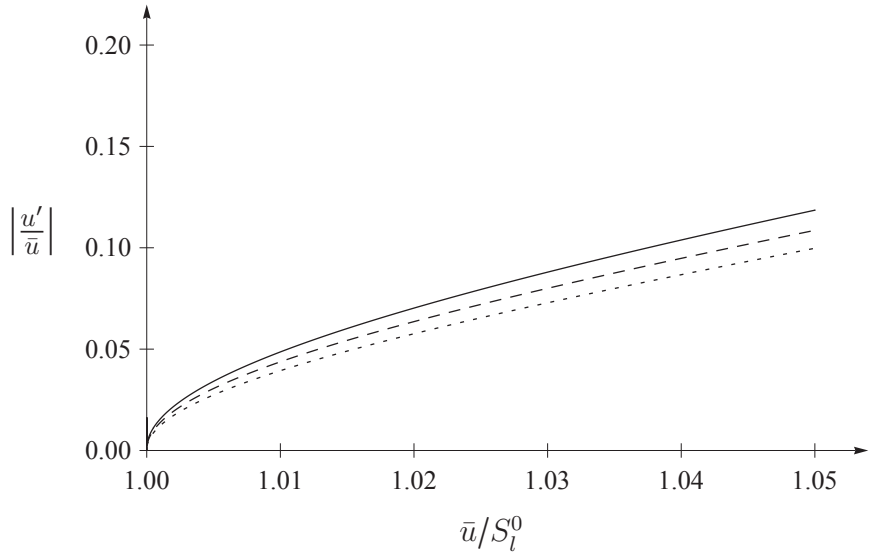

Figure 6.10: Amplitude of the second mode as function of $\bar{u}/S_l^0$ for $\chi_r\omega_r = 2$ (———:$\beta = 0.1$, – – –: $\beta = 0.2$, ·····: $\beta = 0.3$)

Figure (6.11) shows the resulting amplitudes of the first mode as function of $\bar{u}/S_l^0$ for β = 0.1 and phase-lags of 5.5,6.0,6.5. Figure (6.12) shows the resulting amplitudes of the second mode as function of $\bar{u}/S_l^0$ for β = 0.1 and phase-lags of 1.5,2.0,2.5. They confirm that there is critical range of the phase-lag, where instability can be triggered. This property can be also seen in the linear stability map.

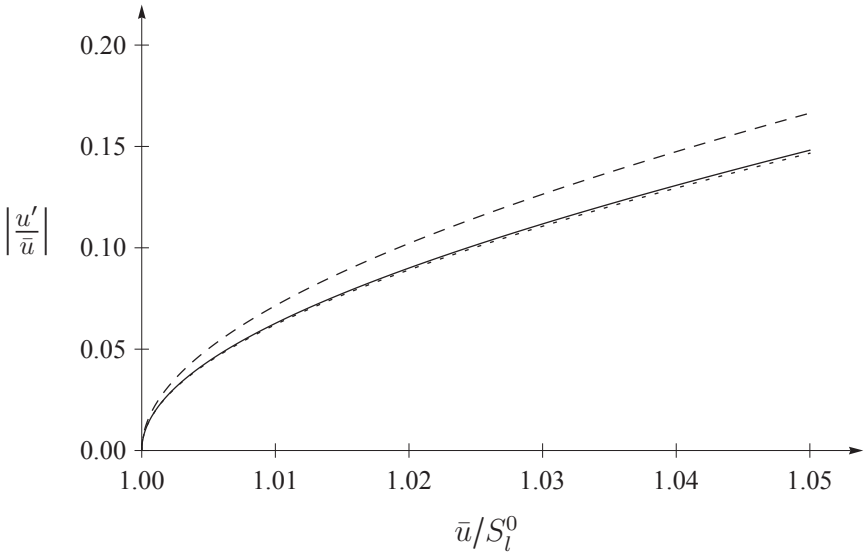

Figure 6.11: Amplitude of the first mode as function of $\bar{u}/S_l^0$ for β = 0.1 (———:$\chi_r\omega_r$ = 5.5, – – –: $\chi_r\omega_r$ = 6.0, ·····: $\chi_r\omega_r$ = 6.5)

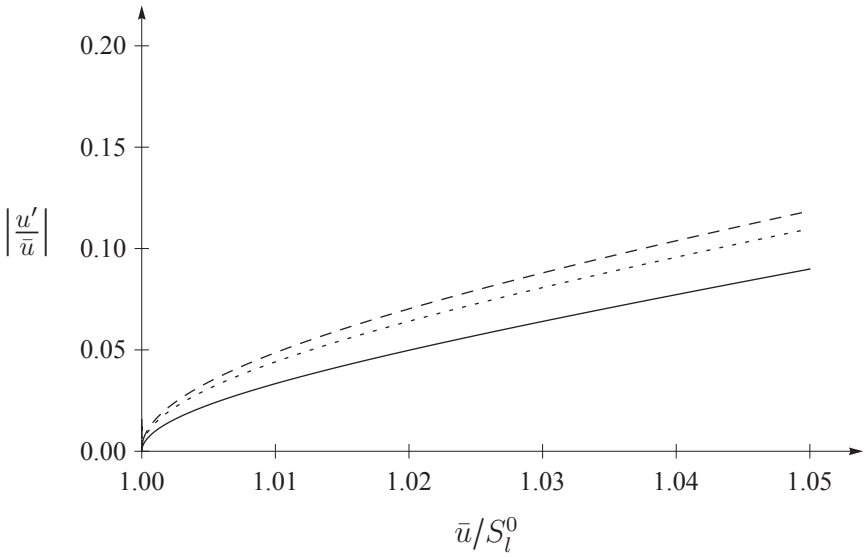

Figure 6.12: Amplitude of the second mode as function of $\bar{u}/S_l^0$ for β = 0.1 (———:$\chi_r\omega_r$ = 1.5, – – –: $\chi_r\omega_r$ = 2.0, ·····: $\chi_r\omega_r$ = 2.5)

Figure (6.13) shows the amplitudes of the first mode of certain fuel types as function of $\bar{u}/S_l^0$ for $\beta = 0.1$ and phase-lag of 6. Figure (6.14) shows the amplitudes of the second mode of certain fuel types as function of $\bar{u}/S_l^0$ for $\beta = 0.1$ and phase-lag of 2.

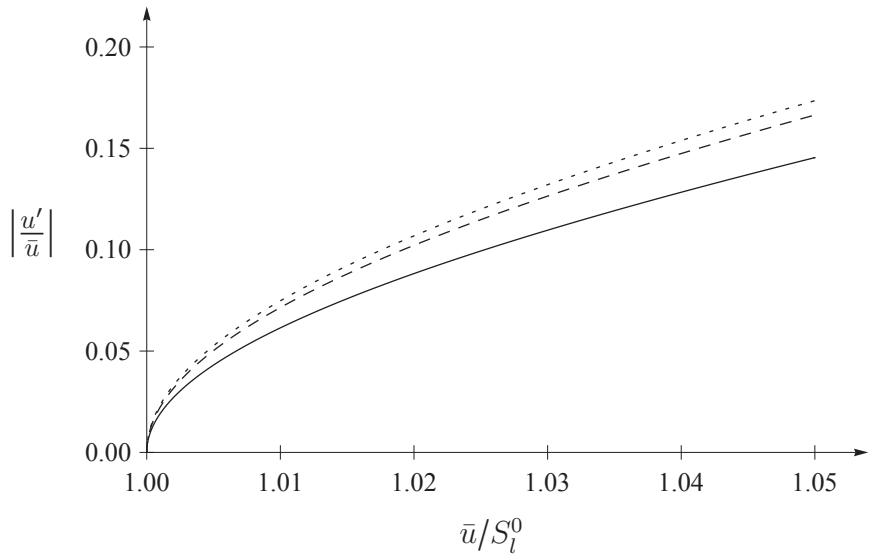

Figure 6.13: Amplitude of the first mode of certain fuel types as function of $\bar{u}/S_l^0$ for $\chi_r\omega_r = 6$ and $\beta = 0.1$ (———:hydrogen, – – –: methane, ·····: ethane)

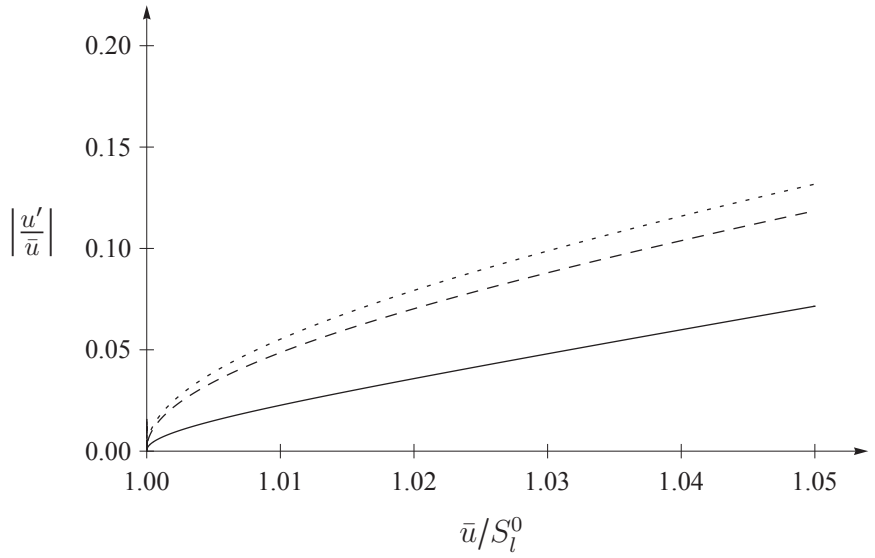

Figure 6.14: Amplitude of the second mode of certain fuel types as function of $\bar{u}/S_l^0$ for $\chi_r\omega_r = 2$ and $\beta = 0.1$ (———:hydrogen, – – –: methane, ·····: ethane)

The figures clearly show that close to a transition point a small change in any of the parameters can result in large change of the amplitude, which explains the difficulty of predicting the amplitudes of thermoacoustic oscillations.

6.4 Conclusions

In this chapter we derived the governing differential equation of an active single mode by including the response of the flame into the model. We have identified important parameters, which affects the instability of the system. We calculated the transition points of the burner using linear theory. By applying non-linear theory we found that weakly non-linear regime exists where the mean flow velocity tends to the laminar flame speed. We have shown that the heat-release rate of the flame must be of correct phase and magnitude in order to balance the losses of the system. We found that we can get limit-cycles in the weakly non-linear regime, however, this regime exists in a very narrow interval of $\bar{u}/S_l^0$. We calculated and studied the resulting limit-cycle amplitudes and frequencies of instabilities for various parameters.
The summary of the chapter in keywords:

- we derived the governing differential equation for a general heat-release model,
- by applying linear theory stable and unstable regions were identified,
- we predicted the limit-cycle amplitudes for many system parameters,
- some fuel types are more susceptible to thermoacoustic instabilities than others,
- lean conditions increase the unstable regions,
- a weakly non-linear region exists where the mean flow velocity tends to the laminar flame speed,
- most of the non-linear regimes are strongly non-linear, i.e. the acoustic velocity is of the same order as the mean flow velocity.

Chapter 7

Conclusions and future work

7.1 Conclusions

Here the short summary of the major results is presented:

1. **Effects of the mean temperature profile**

   The governing differential equation of the acoustic pressure with axial mean temperature gradient was derived in the time-domain from first principles and studied in details. By using this more general form of the wave equation the effect of the temperature increase on the wave propagation and wave reflection was included into the mathematical model. By applying more, increasingly complex configurations of the mathematical model the *preheating and cooling effects of the wall were analyzed*.

2. **Experimentally validated Green's function**

   The Green's function approach has been used to solve the wave equation with a heat source and mean temperature gradient. The Green's function of the laboratory burner has been derived and compared to measurements, which showed excellent agreement. In this way an *experimentally validated tailored Green's function* has been obtained. *Using perturbation techniques we have showed when the increase in the mean temperature can be neglected or modeled as a jump.*

3. **Kinematics of a premixed ducted flame**

The kinematics of a ducted premixed flame was studied analytically by applying the level-set method ($\mathcal{G}$-Equation). The weakly and strongly non-linear regions were identified in the parameter space. The importance of the boundary condition of the flame was also demonstrated, and different solutions of the $\mathcal{G}$-Equation were analyzed. The curvature effects of the flame were also investigated: *solutions were provided for the mean flame position, and conditions were obtained for neglecting curvature effects in the $\mathcal{G}$-Equation.*

4. **Non-linear heat-release model**

   A new non-linear heat-release rate law has been derived and applied to the laboratory burner, in which it was assumed that the instantaneous global heat-release is proportional to the instantaneous flame surface area. A region of the parameter space has been identified in which cubic terms are of the same order as the linear ones.

5. **Governing equation of the acoustic velocity of an active single mode for arbitrary heat-release model and boundary conditions**

   The governing differential equation of an active single velocity mode has been derived for an arbitrary heat-release model, i.e. the feedback of the flame was included in the equation. The interaction of the modes was neglected. *The acoustic velocity obtained in this way satisfies the boundary conditions through the tailored Green's function.*

6. **Stability analysis**

   The stable and unstable regions in the parameter space of the burner were identified by using linear theory. In the applied model the instability criteria for the linear and weakly non-linear cases are identical. By applying weakly non-linear analysis the limit-cycle amplitudes and frequencies were predicted. *The model confirmed that lean combustion systems are more susceptible to thermoacoustic oscillations and that the type of fuel burned in the rig affects thermoacoustic instabilities.* It has been shown that the difference between the limit-cycle frequency

and the passive (when there is no feedback of the flame) frequency can be as large as 5-10 % (see Figure (6.7)).

7. **Flexibility of the model**

   The range of the parameters of the developed mathematical model covers a wider range than the one of the LIMOUSINE burner. Thus, we believe that it can be applied to a wide range of thermoacoustic problems.

7.2 Future work

Here we outline different ways to improve the mathematical model by considering the following open questions.

- The non-linear heat-release model, which was derived in §5, needs to be validated by comparing it to measurements.

- In the derivation of the $\mathcal{G}$-Equation it was found that non-linearities of this model can be of kinematic and geometric origin. The kinematic non-linearity was neglected by taking the linear solution of the $\mathcal{G}$-Equation in the weakly non-linear regime of the parameter space. Only the geometric non-linearity has been included in the model by calculating the exact flame surface area of the linear solution of the $\mathcal{G}$-Equation. This approach can be extended by including non-linear terms up to cubic order in the weakly non-linear regimes of the $\mathcal{G}$-Equation.

- We found that weakly non-linear regime of the acoustic velocity exists in the parameter space only in a very narrow interval of $\bar{u}/S_l^0$, and in most of the cases the acoustic velocity is comparable to the mean flow velocity, i.e. $u' \sim \bar{u}$. This property does not affect the Green's function calculation, but it needs to be considered in the heat-release model by taking appropriate boundary conditions: when the acoustic velocity is comparable to the mean flow velocity, the flame is not attached. There is no agreement on the appropriate boundary condition of the flame for large amplitude oscillations. Dowling [1997] used non-linear boundary

conditions numerically, and obtained flow reversal. The numerical results show good agreement with practical observations, however, a theoretical justification of the results is still lacking.

- We applied laminar flame assumption for deriving our heat-release rate law. Measurements clearly indicated the existence of turbulence in the flow, accurate modelling of the system would therefore require including the effects of turbulence. It would be also very interesting to compare our analytical heat-release law to a turbulent one.

- In the thesis we worked with low frequencies. The model can be extended to higher frequencies as well, which would be necessary when investigating the interaction of the modes. In this case one should consider 2D acoustics, careful consideration of the temperature profile, and the acoustical boundary conditions, since the applied reflection coefficients were measured at the first unstable frequency.

- The interactions of the modes were neglected in the derivation of the governing differential equation of the acoustic velocity. There might be regimes of the parameter space in which modes interact. Thus, the theory can be extended by considering the interactions of n modes, which will lead to a differential equation of order $2n$ in this model.

- During the derivation of the heat-release law we used plug-flow assumption, i.e. the velocity was uniform in the cross-section. Works of [Schuller et al., 2002, 2003] showed the importance of the convective character of a perturbation. Our heat-release rate law can be therefore improved by including an axially propagating wave.

References

P.M. Allison, J.F. Driscoll, and M. Ihme. Acoustic behavior of a partially-premixed gas turbine model combustor. In *AIAA Aerospace Sciences Meeting*, Nashville, Tennessee, 2012.

G.E. Andrews and D. Bradley. The burning velocity of methane-air mixtures. *Combustion and flame*, 19:275–288, 1972.

K. Balasubramanian and R.I. Sujith. Thermoacoustic instability in a Rijke tube: Non-normality and nonlinearity. *Physics of Fluids*, 20(4), 2008.

J.K. Bechtold and M. Matalon. The dependence of the Markstein length on stoichiometry. *Combustion and flame*, 127:1906–1913, 2001.

W.G. Berl. Technical panel on solid propellant instability of combustion, the johns hopkins university applied physics laboratory. *Scientific Papers*, 1963.

J.F. Bird, F.T. McClure, and R.W. Hart. Acoustic instability in the transverse modes of solid propellants. *12th International Astronautical Congress Proceedings*, pages 459–473, 1963.

R.B. Bird, W.E. Steward, and E.N. Lightfoot. *Transport phenomena*. John Wiley and Sons, Inc., 2nd edition, 2002. ISBN 0-471-41077-2.

P.L. Blackshear. Driving standing waves by heat addition. *4th symphosium (international) on combustion*, 4(1):553–566, 1953.

D.T. Blackstock. *Fundamentals of physical acoustics*. John Wiley and Sons, Inc., 1st edition, 2000. ISBN 0-471-31979-1.

W. Bohl and W. Elmendorf. *Strömungsmaschinen 1.* Vogel Fachbuch, 9th edition, 2004. ISBN 3-8023-1980-X.

J. Bosscha and P. Riess. Das Anblasen offener Röhren durch eine Flamme. *Annalen der Physik und Chemie*, 108(2):653–656, 1859.

S.M. Candel. Combustion instabilities coupled by pressure waves and their active control. In *24th Symposium (International) on Combustion*, pages 1277–1296, 1992.

R.H. Cantrell and R.W. Hart. Interaction between sound and flow in acoustic cavities: Mass, momentum and energy considerations. *The Journal of the Acoustical Society of America*, 36:697–706, 1964.

G.F. Carrier. The mechanics of the Rijke tube. *Quarterly of Applied Mathemathics*, 12(4):383–395, 1955.

S.I. Cheng. High frequency combustion instability in solid propellant rockets. *Jet Propulsion*, 24:27–32, 1954.

S.I. Cheng. Unstable combustion in solid propellant rocket motors. *9th (International) Symposium in Combustion*, pages 81–90, 1962.

B.T. Chu. Stability of systems containing a heat source - the Rayleigh criterion. *NACA Research memorandum NACA RM 56D27*, 1956.

B.T. Chu. Analysis of a self-sustained thermally driven nonlinear vibration. *Physics of Fluids*, 6(11):1638–1645, 1963.

B.T. Chu and S.J. Ying. Thermally driven nonlinear oscillations in a pipe with traveling shock waves. *Physics of Fluids*, 6(11):1625–1638, 1963.

A.A. Collyer and D.J. Ayres. The generation of sound in a Rijke tube using two heating coils. *Journal of Physics*, 5:73–75, 1972.

S.M. Correa. Power generation and aeropropulsion gas turbines: from combustion science to combustion technology. In *27th Symposium on combustion*, 1998.

D.G. Crighton and J.E. Ffowcs Williams. Sound generation by turbulent two-phase flow. *Journal of Fluid Mechanics*, 36(3):585–603, 1969.

D.G. Crighton, A.P. Dowling, J.E. Ffowcs Williams, M. Heckl, and F.G. Leppington. *Modern Methods in Analytical Acoustics*. Springer-Verlag, 1st edition, 1992. ISBN 3-540-19737-0.

L. Crocco. Aspects of combustion instability in liquid propellant rocket motors. part 1. *Journal of the American Rocket Society*, 21:163–178, 1951.

L. Crocco. Aspects of combustion instability in liquid propellant rocket motors. part 2. *Journal of the American Rocket Society*, 22:7–16, 1952.

L. Crocco. Research on combustion instability in liquid propellant rockets. *12th Symposium (International) on Combustion*, 12(1):85–99, 1969.

F.E.C. Culick. Stability of high-frequency pressure oscillations in rocket combustion chambers. *AAIA Journal*, 1(5):1097–1104, 1963.

F.E.C. Culick. Nonlinear behvaiour of acoustic waves in combustion chambers. part i. *Acta Astronautica*, 3(9-10):715–734, 1976.

F.E.C. Culick. A note on Rayleigh's criterion. *Combustion Science and Technology*, 56:159–166, 1987.

F.E.C. Culick. Some recent results for nonlinear acoustics in combustion chambers. *American Institute of Aeronautics and Astronautics*, 90:3927, 1990.

F.E.C. Culick. Some recent results for nonlinear acoustics in combustion chambers. *AIAA Journal*, 32(1):146–169, 1994.

F.E.C. Culick. Unsteady Motions in Combustion Chambers for Propulsion Systems. Technical Report RTO AGARDograph AG-AVT-039, The Research and Technology Organisation (RTO) of NATO, 2006.

D. de St. Q. Isaacson and M. de St. Q. Isaacson. *Dimensional methods in engineering and physics*. John Wiley and Sons, 1st edition, 1975. ISBN 978-0470428665.

S.K. Dhanuka, J.E. Temme, and J.F. Driscoll. Lean-limit combustion instabilities of a lean premixed prevaporized gas turbine combustor. *Proceedings of the Combustion Institute*, 33:2961–2966, 2011.

J.H.M. Disselhorst and L. van Wijngaarden. Flow in the exit of open pipes during acoustic resonance. *Journal of Fluid Mechanics*, 99(2):293–319, 1979.

A.P. Dowling. Nonlinear self-excited oscillations of a ducted flame. *Journal of Fluid Mechanics*, 346:271–290, 1997.

A.P. Dowling. A kinematic model of a ducted flame. *Journal of Fluid Mechanics*, 394: 51–72, 1999.

A.P. Dowling and J.E. Ffowcs Williams. *Sound and sources of sound*. Ellis Horwood series in engineering science, 1st edition, 1983. ISBN 0-85312-400-0.

D. Drysdale. *An introduction to fire dynamics*. John Wiley and Sons, 2nd edition, 1999. ISBN 0-471-97290-8.

S. Ducruix, D. Durox, and S. Candel. Theoretical and experimental determinations of the transfer function of a laminar premixed flame. *Proceedings of the Combustion Institute*, 28:765–773, 2000.

S. Ducruix, T. Schuller, D. Durox, and S. Candel. Combustion dynamics and instabilities: Elementary coupling and driving mechanisms. *Journal of Propulsion and Power*, 19(5):722–734, 2003.

D.G. Duffy. *Green's functions with Applications*. CRC Press, 1st edition, 2001. ISBN 1-58488-110-0.

D. Durox, T. Schuller, and S. Candel. Combustion dynamics of inverted conical flames. *Proceedings of the Combustion Institute*, 30:1717–1724, 2005.

F. Fahy. *Foundations of engineering acoustics*. Elsevier Academic Press, 4th edition, 2001. ISBN 0-12-247665-4.

J.J. Fang. Application of combustion time-lag theory to combustion stability analysis of liquid and gaseous propellant rocket engines. *22nd AIAA Aerospace Sciences Meeting, AIAA-84-0510*, 1984.

K.T. Feldman. Review of the literature on Rijke thermoacoustic phenomena. *Journal of Sound and Vibration*, 7(1):83–89, 1968.

J.E. Ffowcs Williams and M.S. Howe. The generation of sound by density inhomogeneities in low Mach number nozzle flows. *Journal of Fluid Mechanics*, 70(3): 605–622, 1974.

M. Fleifil, A.M. Annaswamy, Z.A. Ghoneim, and A.F. Ghoniem. Response of a laminar premixed flame to flow oscillations: A kinematic model and thermoacoustic instability results. *Combustion and Flame*, 106:487–510, 1996.

J. Göttgens, F. Mauss, and N. Peters. Analytic approximations of burning velocities and flame thicknesses of lean hydrogen, methane, ethylene, ethane, acetylene, and propane flames. In *24th Symposium on Combustion*, 1992.

P. Green. *Perrys chemical engineers handbook*. McGraw-Hill, Inc., 7th edition, 1999. ISBN 0-07-115448-5.

C.C. Hantschk and D. Vortmeyer. Numerical simulation of self-excited thermoacoustic instabilities in a Rijke tube. *Journal of Sound and Vibration*, 277(3):511–522, 1999.

D.T. Harrje and F.H. Reardon. *Liquid propellant rocket combustion instability*. Scientific and Technical Information Office, National Aeronautics and Space Administration, 1972.

R.W. Hart and F.T. McClure. Combustion instability: Acoustic interaction with a burning surface. *The Journal of Chemical Physics*, 30:1501–1414, 1959.

R.W. Hart and F.T. McClure. Theory of acoustic instability in solid-propellant rocket combustion. *10th (International) Symposium on Combustion*, 24:1047–1065, 1965.

M.A. Heckl. Active control of the noise from a Rijke tube. *Journal of Sound and Vibration*, 124(1):117–133, 1988.

M.A. Heckl. Non-linear acoustic effects in the Rijke tube. *Acustica*, 72:63–71, 1990.

M.A. Heckl and M.S. Howe. Stability analysis of the Rijke tube with a Green's function approach. *Journal of sound and vibration*, 305:672–688, 2007.

B. Higgins. On the sound produced by a current of hydrogen gas passing through a tube. *Journal of Natural Philosophy and Chemical Arts*, 1:129, 1802.

R.C. Jensen. A mathematical model for the amplitude of acoustic pressure oscillation in solid rocket motors. *8th JANNAF Combustion Meeting*, 1(220), 1971.

R.C. Jensen and M.B. Beckstead. Analysis of combustion instability data. *10th JANNAF Combustion Meeting*, 2(231):163–177, 1972.

M.P. Juniper. Triggering in the horizontal Rijke tube: non-normality, transient growth and bypass transition. *Journal of fluid mechanics*, 667:272–308, 2011a.

M.P. Juniper. Transient growth and triggering in the horizontal Rijke tube. *International journal of spray and combustion dynamics*, 3(3):209–224, 2011b.

D.M. Kang, F.E.C. Culick, and A. Ratner. Combustion dynamics of a low-swirl combustor. *Combustion and Flame*, 151:412–425, 2007.

W.E. Kaskan. The dependence of flame temperature on mass burning velocity. *6th symphosium (international) on combustion*, 6(1):134–143, 1957.

Y. Katto and A. Sajiki. Onset of oscillation of a gas-column in a tube due to the existence of heat-conduction field : A problem of generating mechanical energy from heat. *Bulletin of JSME*, 20(147):1161–1168, 1977.

K.S. Kedia, S.B. Nagaraja, and R.I. Sujith. Impact of linear coupling on thermoacoustic instabilities. *Combustion Science and Technology*, 180(9):1588–1612, 2008.

J.J. Keller. Thermoacoustic oscillations in combustion chambers of gas turbines. *The American Institute of Aeronautics and Astronautics*, 33(12):2280–2287, 1995.

A.J. Kempton. Heat diffusion as a source of aerodynamic sound. *Journal of Fluid Mechanics*, 78:1–31, 1975.

L.V. King. Some recent results for nonlinear acoustics in combustion chambers. *Proceedings of the Royal Society of London. Series A, Containing Papers of a Mathematical and Physical Character*, 90(622):563–570, 1914.

B. Kosztin, M.A. Heckl, R. Müller, and J. Hermann. Instabilities in a model gas turbine combustor: theory and experiment. In *17th International Congress on Sound and Vibration*, Cairo, Egypt, 2010.

B. Kosztin, M.A.Heckl, R. Müller, and J. Hermann. Instabilities in a model gas turbine combustor with different mean-temperature profiles. In *18th International Congress on Sound and Vibration*, Rio de Janeiro, Brazil, 2011.

B. Kosztin, M.A. Heckl, R. Müller, and J. Hermann. Thermo-acoustic properties of a burner with axial temperature gradient: Theory and experiment. *International journal of spray and combustion dynamics*, 5(1):67–84, 2013.

Y.P. Kwon and B.H. Lee. Stability of the Rijke thermoacoustic oscillation. *Journal of Acoustical Society of America*, 78(4):1414–1420, 1985.

P.K. Kythe. *Green's functions and linear differential equations*. CRC Press, 1st edition, 2011. ISBN 978-1-4398-4008-5.

P.J. Langhorne. Reheat buzz: an acoustically coupled combustion instability. Part 1. Experiment. *Journal of Fluid Mechanics*, 193:417–443, 1987.

C.K. Law, A.Makino, and T.F. Lu. On the off-stoichiometric peaking of adiabatic flame temperature. *Combustion and flame*, 145:808–819, 2006.

D.H. Lee and T. Lieuwen. Acoustic near-field characteristics of a conical, premixed flame. *Journal of the acoustical society of America*, 113(1):167–177, 2003.

K.O. Lehmann. Über die Theory der Netztone. *Annalen der Physik*, 29:527–555, 1937.

H. Levine and J. Schwinger. On the radiation of sound from an unflanged circular pipe. *Physical Review*, 73(4):383–406, 1948.

P.Y. Liang, S. Fisher, and Y.M. Chang. Comprehensive modeling of a liquid rocket combustion chamber. *Journal of Propulsion*, 2:97–104, 1986.

P.Y. Liang, S. Fisher, and Y.M. Chang. Numerical analysis of ssme preburner injector atomization and combustion processes. *Journal of Propulsion*, 3:508–513, 1987.

T. Lieuwen. Modeling premixed combustion-acoustic wave interactions: A Review. *Journal of Propulsion and Power*, 19(5):765–781, 2003.

T. Lieuwen. Nonlinear kinematic response of premixed flames to harmonic velocity disturbances. *Proceedings of the Combustion Institute*, 30:1725–1732, 2005.

T. Lieuwen. *Unsteady combustor physics*. Cambridge University Press, 1st edition, 2012. ISBN 978-1-107-01599-9.

T. Lieuwen and B.T. Zinn. The role of equivalence ratio oscillations in driving combustion instabilities in low NOx gas turbines. In *27th Symposium on combustion*, pages 1809–1816, 1998.

T. Lieuwen, S. Mohan, R. Rajaram, and Preetham. Acoustic radiation from weakly wrinkled premixed flames. *Combustion and Flame*, 144:360–369, 2006.

M.J. Lighthill. *On sound generated aerodynamically: II. Turbulence as a source of sound*. Proc. Roy. Soc. London, 1954.

LIMOUSINE group. Limit cycles of thermo-acoustic oscillations in gas turbine combustors. Brno, Czech Republic, 2011.

Y. Ma, W.K. van Moorhem, and R.W. Shorthill. Experimental investigation of velocity coupling in combustion instability. *Journal of Propulsion and Power*, 7(5):692–699, 1991.

L. Magri, K. Balasubramanian, R.I. Sujith, and M.P. Juniper. Non-normality in combustion-acoustic interaction in diffusion flames: a critical revision. *Journal of Fluid Mechanics*, 773:681–683, 2013.

G.C. Mailing. Simplified analysis of the Rijke phenomenon. *Journal of Fluid Mechanics*, 99(2):1058–1060, 1963.

S. Mariappan. *Theoretical and experimental investigation of the non-normal nature of thermoacoustic interactions*. Indian Institute of Technology Madras, PhD Thesis, 2012.

G.H. Markstein. Experimental and theoretical studies of flame-front stability. *Journal of the Aeronautical Sciences (Institute of the Aeronautical Sciences)*, 18(3):199–209, 1951.

K.I. Matveev and F.E.C. Culick. Modeling of unstable regimes in a Rijke tube. In *5th International Symposium on Fluid-Structure Interactions*, New Orleans, LA, USA, 2002.

K.I. Matveev and F.E.C. Culick. A study of the transition to instability in a Rijke tube with axial temperature gradient. *Journal of Sound and Vibration*, 264:689–706, 2003a.

K.I. Matveev and F.E.C. Culick. Limit-cycle properties of a Rijke tube. *Technical Acoustics*, 12, 2003b.

H.J. Merk. Analysis of heat-driven oscillations of gas flows. *Applied Scientific Research, Section A*, 6(4):317–336, 1957a.

H.J. Merk. Analysis of heat-driven oscillations of gas flows. *Applied Scientific Research, Section A*, 6(5-6):402–420, 1957b.

H.J. Merk. Analysis of heat-driven oscillations of gas flows. *Applied Scientific Research, Section A*, 7(2-3):175–191, 1958.

H.J. Merk. Analysis of heat-driven oscillations of gas flows. *Applied Scientific Research, Section A*, 8(1):1–27, 1959.

M. Metghalchi and J.C. Keck. Burning velocities of mixtures of air with methanol, isooctane and indolene at high pressures and temperatures. *Combustion and flame*, 48:191–210, 1982.

K. Meyberg and P. Vachenauer. *Höhere Mathematik*. Springer-Verlag, 4th edition, 2001. ISBN 3-540-41851-2.

R.E. Mickens. *An introduction to nonlinear oscillations*. Cambridge University Press, 1st edition, 1981. ISBN 0-521-22208-9.

C.E. Mitchell, D.J. Howell, and J.J. Fang. An improved predictive model for injector face baffies. *24th JANNAF Combustion Meeting*, 1987.

C.L. Morfey. Amplification of aerodynamic noise by convected flow inhomogeneities. *Journal of Sound and Vibration*, 31:391–397, 1973.

B.D. Mugridge. Combustion driven oscillations. *Journal of sound and vibrations*, 70 (3):437–452, 1980.

A.H. Nayfeh and D.T. Mook. *Nonlinear oscillations*. John Wiley and Sons, Inc., 1st edition, 1995. ISBN 0-471-12142-8.

J.L. Neuringer and G.E. Hudson. An investigation of sound vibrations in a tube containing a heat source. *Journal of the Acoustical Society of America*, 24(6):667–674, 1951.

T.V. Nguyen. An improved high-frequency combustion stability model. *AIAA/ASME/SAE/ASEE 24th Joint Propulsion Conference, AIAA-88-2853*, 1988.

C. Nicoli and P. Pelce. One-dimensional model for the Rijke tube. *Journal of Fluid Mechanics*, 202:83–96, 1987.

F. Nicoud and T. Poinsot. Thermoacoustic instabilities: Should the Rayleigh criterion be extended to include entropy changes? *Combustion and Flame*, 142:153–159, 2005.

F. Nicoud and T. Poinsot. Acoustic modes in combustors with complex impedances and multidimensional active flames. *AAIA Journal*, 45:426–441, 2007.

F. Obermeier. Sound generation by heated subsonic jets. *Journal of Sound and Vibration*, 41:463–472, 1975.

F. Obermeier. Aerodynamic sound generation caused by viscous processes. *Journal of Fluid Mechanics*, 99(1):111–120, 1985.

A.D. Osborne. *Complex variables*. Addison Wesley Longman Limited, 1st edition, 1999. ISBN 0-201-34290-1.

K.S. Peat. The acoustical impedance at discontinuities of ducts in the presence of a mean flow. *Journal of sound and vibration*, 127:123–132, 1988.

N. Peters. Laminar flamelet concepts in turbulent combustion. In *21th Symposium on Combustion*, pages 1231–1250, 1986.

N. Peters. Kinetic foundation of thermal flame theory. *Progress in Astronautics and Aeronautics*, 173:73–91, 1997.

N. Peters. *Turbulent combustion*. Cambridge University Press, 4th edition, 2000. ISBN 0-521-66082-3.

K.D. Philippart. Stability characteristics and analysis of liquid oxygen/methane injectors. *24th JANNAF Combustion Meeting*, 1987.

K.D. Philippart and M.D. Moser. Stability analysis of liquid oxygen/methane injectors using currently available analytical tools. *24th AIAA/ASME/SAE/ASEE Joint Propulsion Conference, AIAA-88-2851*, 1988.

T. Poinsot, C.L. Chatelier, S.M. Candel, and E. Esposito. Experimental determination of the reflection coefficient of a premixed flame in a duct. *Journal of sound and vibration*, 107(2):265–278, 1986.

A.D. Polyanin. *Handbook of linear partial differential equations for scientiscts and engineers*. CRC Press, 1st edition, 2002. ISBN 1-58488-299-9.

A.D. Polyanin and A.V. Manzhirov. *Handbook of Integral Equations*. CRC Press, 2nd edition, 2008. ISBN 1-58488-507-6.

A.D. Polyanin and V.F. Zaitsev. *Handbook of exact solutions for ordinary differential equations*. CRC Press, 1st edition, 1995. ISBN 0-8493-9438-4.

E.A. Powell and B.T. Zinn. A single mode approximation in the solution of nonlinear combustion instability problems. *Combustion Science and Technology*, 3:121–132, 1971.

A.A. Putnam. *Combustion-driven oscillations in industry*. American Elsevier Publishing Company Inc., New York, 1st edition, 1971. ISBN 0-444-00101-8.

A.A. Putnam and W.R. Dennis. A study of burner oscillations of the organ-pipe type. *Transactions of ASME*, 75:15–28, 1953.

A.A. Putnam and W.R. Dennis. Burner oscillations of the gauze-tone type. *Journal of the Acoustical Society of America*, 26(5):716–725, 1954.

A.A. Putnam and W.R. Dennis. Organ-pipe oscillations in a burner with deep ports. *Journal of the Acoustical Society of America*, 28(2):260–269, 1956.

R.L. Raun, M.W. Beckstead, J.C. Finlinson, and K.P. Brooks. A review of Rijke tubes, Rijke burners and related devices. *Progress in Energy and Combustion Science*, 19: 313–364, 1993.

Lord Rayleigh. The explanation of certain acoustical phenomena. *Nature*, 18:319–321, 1878.

R.H. Reardon. An investigation of transverse mode combustion instability in liquid propellant rocket motors. *Princeton University Aeronautical Engineering Report No. 550.*, 1961.

E.G. Richardson. The theory of the singing flame. *Proceedings of the Physical Society of London*, 35:47, 1922.

P.L. Rijke. Notiz ber eine neue Art, die Luft in einer an beiden Enden offenen Röhre in Schwingungen zu verstehen. *Annalen der Physik*, 107:339–343, 1859.

G.F. Roach. *Green's Functions*. Cambridge University Press, 2nd edition, 1982. ISBN 0-531-28288-8.

T.D. Rossing. *Springer handbook of acoustics*. Springer Verlag, 2007. ISBN 978-0-387-30446-5.

N. Rott. Thermoacoustics. *Advances in applied mechanics*, 20:135–175, 1980.

T. Saito. Vibrations of air columns excited by heat supply. *Bulletin of JSME*, 8(32): 651–659, 1965.

H. Schimmer and D. Vortmeyer. Acoustical oscillation in a combustion system with a flat flame. *Combustion and Flame*, 28:17–24, 1977.

T. Schuller, S. Ducruix, D. Durox, and S. Candel. Modeling tools for the prediction of premixed flame transfer functions. *Proceedings of the Combustion Institute*, 29: 107–113, 2002.

T. Schuller, D. Durox, and S. Candel. A unified model for the prediction of laminar flame transfer functions: comparisons between conical and V-flame dynamics. *Combustion and Flame*, 134:21–34, 2003.

A.F. Seybert. Two-sensor methods for the measurement of sound intensity and acoustic properties of ducts. *Journal of the Acoustical Society of America*, 83:2233–2239, 1988.

W.A. Sirignano. A theory of axial-mode shock-wave oscillations in a solid rocket combustor. *10th (International) Symposium on Combustion*, 1964.

W.A. Sirignano and L. Crocco. A shock wave model of unstable rocket combustors. *The American Institute of Aeronautics and Astronautics*, 2:1285–1296, 1964.

Sondhauss. Über die Schallschwingungen der Luft in erhitzten Glasröhren und in gedeckten Pfeifen von ungleicher Weite. *Annalen der Physik und Chemie*, 79(2): 1–34, 1850.

P. Subramanian and R.I. Sujith. Non-normality and internal flame dynamics in premixed flameacoustic interaction. *Journal of fluid mechanics*, 679:315–342, 2011.

R.I. Sujith. Exact solutions for modeling sound propagation through a combustion zone. *Acoustical Society of America*, 110(4):1839–1844, 2001.

R.I. Sujith, G.A. Waldherr, and B.T. Zinn. An exact solution for one-dimensional acoustic fields in ducts with an axial temperature gradient. *Journal of Sound and Vibration*, 184(3):389–402, 1995.

M. Summerfield, L.H. Caveny, R.A. Battista, N. Kubota, Y.A. Gostintsev, and H. Isoda. Theory of dynamic extinguishment of solid propellants with special reference to nonsteady heat feedback law. *Journal of Spacecraft and Rockets*, 8:251–258, 1951.

H. Tsuji and T. Takeno. An experimental investigation on high-frequency combustion oscillations. *Tenth Symposium (International) on Combustion*, 10(1):1327–1335, 1965.

S.R. Turns. *An introduction to Combustion: Concepts and Applications*. McGraw-Hill, 2nd edition, 2000. ISBN 0-07-230096-5.

M. Valk. Acoustic power measurements of oscillating flames. *Combustion and Flame*, 41:251–260, 1981.

K. Wieczorek, C. Sensiau, W. Polifke, and F. Nicoud. Assessing non-normal effects in thermoacoustic systems with mean flow. *Physics of Fluids*, 23, 2011.

F.A. Williams. *The Mathematics of combustion (ed. J.D. Buckmaster)*. Society for Industrial & Applied Mathematics, 1985. ISBN 0-89871-053-7.

X. Wu, M. Wang, and P. Moin. Combustion instability due to the nonlinear interaction between sound and flame. *Center for Turbulence Research, Annual Research Briefs 2001*, 2001.

H.G. Yoon, J. Peddieson, and K.R. Purdy. Non-linear response of a generalized Rijke tube. *International Journal of Engineering Science*, 39:1707–1723, 2001.

B.T. Zinn. A theoretical study of nonlinear combustion instability in liquid propellant rocket engines. *The American Institute of Aeronautics and Astronautics*, 6:1966–1972, 1968.

B.T. Zinn and T. Lieuwen. Combustion instability: basic concepts. 2005.

B.T. Zinn and M.E. Lores. Application of the galerkin method in the solution of nonlinear and axial combustion instability problems in liquid rockets. *Combustion Science and Technology*, 4:269–278, 1972.

B.T. Zinn and E.A. Powell. Application of the galerkin method in the solution of combustion instability problems. *Proceedings of the 19th International Astronautical Congress*, 3:59–73, 1970a.

B.T. Zinn and E.A. Powell. Nonlinear combustion instability in liquid-propellant rocket engines. *13th (International) Symposium on Combustion, The Combustion Institute*, 3:491–503, 1970b.

D. Zwillinger. *Handbook of differential equations*. Academic Press, 3rd edition, 1998. ISBN 0-12-784396-5.

Appendix A

Energy equation

Assuming negligible viscous dissipation and thermal conduction the general form of the one-dimensional energy equation is

$$\rho c_p \left(\frac{\partial T}{\partial t} + u \frac{\partial T}{\partial x} \right) = Q + \left(\frac{\partial p}{\partial t} + u \frac{\partial p}{\partial x} \right). \tag{A.0.1}$$

By using the state equation of a perfect gas ($p = \rho \mathcal{R} T$) we can write the temporal and spatial derivatives of the temperature in the following forms

$$\frac{\partial T}{\partial t} = \frac{1}{\rho \mathcal{R}} \frac{\partial p}{\partial t} - \frac{p}{\rho \mathcal{R}} \frac{1}{\rho} \frac{\partial \rho}{\partial t} \ , \tag{A.0.2a}$$

$$\frac{\partial T}{\partial x} = \frac{1}{\rho \mathcal{R}} \frac{\partial p}{\partial x} - \frac{p}{\rho \mathcal{R}} \frac{1}{\rho} \frac{\partial \rho}{\partial x} \ . \tag{A.0.2b}$$

Substituting with Eq. (A.0.2a) and Eq. (A.0.2b) for the terms on the L.H.S. of Eq. (A.0.1) yields

$$\frac{\rho c_p}{\rho \mathcal{R}} \frac{\partial p}{\partial t} - \frac{c_p p}{\mathcal{R}} \frac{1}{\rho} \frac{\partial \rho}{\partial t} + u \frac{c_p}{\mathcal{R}} \frac{\partial p}{\partial x} - u \frac{c_p p}{\mathcal{R}} \frac{1}{\rho} \frac{\partial \rho}{\partial x} = Q + \frac{\partial p}{\partial t} + u \frac{\partial p}{\partial x} \ . \tag{A.0.3}$$

We rearrange the terms to get

$$\left(\frac{c_p}{\mathcal{R}}-1\right)\frac{\partial p}{\partial t}-\frac{c_p p}{\mathcal{R}\rho}\left(\frac{\partial \rho}{\partial t}+u\frac{\partial \rho}{\partial x}\right)+u\frac{\partial p}{\partial x}\left(\frac{c_p}{\mathcal{R}}-1\right)=Q\ . \tag{A.0.4}$$

Using the momentum equation we substitute $-\rho\,\partial u/\partial x$ for the terms in the second bracket of the L.H.S. of Eq. (A.0.4)

$$\frac{c_p-\mathcal{R}}{\mathcal{R}}\frac{\partial p}{\partial t}+\frac{c_p p}{\mathcal{R}\rho}\rho\frac{\partial u}{\partial x}+u\frac{\partial p}{\partial x}\frac{c_p-\mathcal{R}}{\mathcal{R}}=Q\ . \tag{A.0.5}$$

We multiply Eq. (A.0.5) by $\mathcal{R}$ and divide it by $c_p-\mathcal{R}$ to get

$$\frac{\partial p}{\partial t}+\frac{c_p}{c_p-\mathcal{R}}p\frac{\partial u}{\partial x}+u\frac{\partial p}{\partial x}=\frac{\mathcal{R}}{c_p-\mathcal{R}}Q\ . \tag{A.0.6}$$

We introduce the ratio of the specific heats ($\gamma=c_p/c_v$) to write

$$\begin{aligned}\frac{c_p}{c_p-\mathcal{R}}&=\frac{c_p}{c_p-(c_p-c_v)}=\gamma\ ,\\ \frac{\mathcal{R}}{c_p-\mathcal{R}}&=\frac{c_p-c_v}{c_v}=\gamma-1\ ,\end{aligned} \tag{A.0.7}$$

which leads to the following form of the energy equation

$$\frac{\partial p}{\partial t}+\gamma p\frac{\partial u}{\partial x}+u\frac{\partial p}{\partial x}=(\gamma-1)Q\ . \tag{A.0.8}$$

Appendix B

Heat-release

B.1 Strongly non-linear regions of the $\mathcal{G}$-Equation

In regions A and B of Figure (5.7) the $\mathcal{G}$-Equation is strongly non-linear. In Eq. (5.3.7) $\partial\tilde{\mathcal{G}}/\partial\tilde{x}$ and $\partial\tilde{\mathcal{G}}/\partial\tilde{r}$ are of order 1, therefore to have $\tilde{\mathcal{G}}$ explicit in $\tilde{r}$ or $\tilde{x}$ it is common to introduce the following trial solutions [Ducruix et al., 2000; Schuller et al., 2003]: $\tilde{\mathcal{G}} = \tilde{r} + \tilde{F}_A(\tilde{x},\tilde{t})$ and $\tilde{\mathcal{G}} = \tilde{x} + \tilde{F}_B(\tilde{r},\tilde{t})$. They are shown in Figure (5.8). Subscripts A and B refer to the regions A and B respectively. If we use $\tilde{F}_A = F_A/(r_1 - r_0)$ and $\tilde{F}_B = F_B/(x_1 - x_0)$, we can write Eq. (5.3.2) in region A and B in the following forms

$$\text{region A}: \qquad \frac{\partial F_A}{\partial t} + u\frac{\partial F_A}{\partial x} = S_l^0\sqrt{\left(\frac{\partial F_A}{\partial x}\right)^2 + 1}\ , \tag{B.1.1a}$$

$$\text{region B}: \qquad \frac{\partial F_B}{\partial t} + u = S_l^0\sqrt{\left(\frac{\partial F_B}{\partial r}\right)^2 + 1}\ . \tag{B.1.1b}$$

We can see that Eq. (B.1.1a) reduces to Eq. (5.3.8a) for large α, and Eq. (B.1.1b) reduces to Eq. (5.3.8b) for small α. Eq. (B.1.1a) and (B.1.1b) can be solved by taking their spatial derivatives, and introducing a new function for the spatial gradients. In this way we obtain homogeneous quasilinear PDEs. Implicit solutions can be obtained

by the method of characteristics, which are

$$\frac{\partial F_A}{\partial x} = \left[\varphi \left(t - \frac{x - x_0}{\bar{u} - S_l^0 \frac{\frac{\partial F_A}{\partial x}}{\sqrt{\left(\frac{\partial F_A}{\partial x}\right)^2 + 1}}} \right) \right]^{-1} , \tag{B.1.2a}$$

$$\frac{\partial F_B}{\partial r} = \varphi \left(t - \frac{r - r_0}{S_l^0 \frac{\frac{\partial F_B}{\partial r}}{\sqrt{\left(\frac{\partial F_B}{\partial r}\right)^2 + 1}}} \right) . \tag{B.1.2b}$$

The function φ generally is given by the boundary condition at $[r_0, x_0]$: $\partial F_A/\partial x(t, x = x_0) = 1/\varphi(t)$ and $\partial F_B/\partial r(t, r = r_0) = \varphi(t)$ respectively. A similar solution was presented for region B by Lieuwen [2005]. The general solutions Eq. (B.1.2a) and Eq. (B.1.2b) do not contain u' since we assumed that it has no spatial dependence.

B.1.1 Non-linear boundary conditions

Measurements indicated that at low acoustic velocity amplitudes the flame is attached to the flame-holder. Since the flame does not move in the point of attachment, Lieuwen [2005] proposed that $\partial F/\partial t = 0$ at the point of attachment. This leads to the following boundary conditions: $\partial F_A/\partial t = 0$ at $x = x_0$ and $\partial F_B/\partial t = 0$ at $r = r_0$ in Eq. (B.1.1a) and Eq. (B.1.1b) respectively. Performing the substitution yields the following for $\varphi(t)$

$$\left.\frac{\partial F_A}{\partial x}\right|_{x=x_0} = \varphi^{-1}(t) = \left[\sqrt{\left(\frac{\bar{u} + u'(t)}{S_l^0} \right)^2 - 1} \right]^{-1} , \tag{B.1.3a}$$

$$\left.\frac{\partial F_B}{\partial r}\right|_{r=r_0} = \varphi(t) = \sqrt{\left(\frac{\bar{u} + u'(t)}{S_l^0} \right)^2 - 1} . \tag{B.1.3b}$$

Eq. (B.1.3a) and (B.1.3b) also indicate that the flame cannot be attached when the amplitude of the oscillation is comparable to the mean flow velocity. They also indicate

that only implicit solutions can be obtained, however, we need solutions explicit in u' to derive a heat-release law, which will be therefore also explicit in u'.

B.2 Solution of the linearized $\mathcal{G}$-Equation without curvature

To solve Eq. (5.3.10) we introduce new coordinates

$$x - x_0 = a_1 w + a_2 z \ , \tag{B.2.1a}$$

$$r - r_0 = a_3 w + a_4 z \ , \tag{B.2.1b}$$

and we write the spatial derivatives in the following forms

$$\frac{\partial}{\partial x} = \frac{-a_2}{a_1 a_4 - a_2 a_3}\frac{\partial}{\partial w} + \frac{a_1}{a_1 a_4 - a_2 a_3}\frac{\partial}{\partial z} \ , \tag{B.2.2a}$$

$$\frac{\partial}{\partial x} = \frac{a_4}{a_1 a_4 - a_2 a_3}\frac{\partial}{\partial w} + \frac{-a_3}{a_1 a_4 - a_2 a_3}\frac{\partial}{\partial z} \ . \tag{B.2.2b}$$

We substitute the coordinate transformation into Eq. (5.3.10) to get

$$\begin{aligned}\frac{\partial \mathcal{G}'}{\partial t} + \left[(\bar{u} - S_l^0 \sin\alpha)\frac{-a_2}{a_1 a_4 - a_2 a_3} + S_l^0 \cos\alpha \frac{a_4}{a_1 a_4 - a_2 a_3}\right]\frac{\partial \mathcal{G}'}{\partial w} + \\ + \left[(\bar{u} - S_l^0 \sin\alpha)\frac{a_1}{a_1 a_4 - a_2 a_3} + S_l^0 \cos\alpha \frac{-a_3}{a_1 a_4 - a_2 a_3}\right]\frac{\partial G'}{\partial z} = u'(t) \ .\end{aligned} \tag{B.2.3}$$

The boundary condition is given in a point, therefore we eliminate one of the spatial

derivatives. This can be done in 2 ways:

$$\frac{\bar{u} - S_l^0 \sin\alpha}{S_l^0 \cos\alpha} = \frac{a_2}{a_4} \ , \text{ or} \tag{B.2.4a}$$

$$\frac{\bar{u} - S_l^0 \sin\alpha}{S_l^0 \cos\alpha} = \frac{a_1}{a_3} \ . \tag{B.2.4b}$$

We use the fact that $\bar{u} = S_l^0/\sin\alpha$, and write $\bar{u} - S_l^0 \sin\alpha/S_l^0 \cos\alpha = \cos\alpha/\sin\alpha$. By applying either of (B.2.4a) or (B.2.4b) Eq. (5.3.10) can be reduced to

$$\frac{\partial \mathcal{G}'}{\partial t} + c_0 \frac{\partial \mathcal{G}'}{\partial p} = u'(t) \ , \tag{B.2.5}$$

where p is a spatial coordinate (w or z), and c_0 is a constant. We apply Laplace Transform to transform Eq. (B.2.5) into the following ODE

$$s\hat{\mathcal{G}}' + c_0 \frac{\partial \hat{\mathcal{G}}'}{\partial p} = u'(s) + f(p) \ , \tag{B.2.6}$$

where s is the Laplace variable and $f(p)$ is the initial condition. The solution in the (s, p) domain is given by

$$\mathcal{G}'(t,p) = H\Big[t - p/c_0\Big]\mathcal{G}'(t,p)\Big|_{\substack{t=t-p/c_0 \\ p=0}} + H\Big[p - c_0 t\Big]\mathcal{G}'(t,p)\Big|_{\substack{t=0 \\ p=p-c_0 t}} + \int_{t-p/c_0}^{t} u'(\tau)d\tau \ . \tag{B.2.7}$$

B.3 Solution for the mean position of the $\mathcal{G}$-Equation with curvature

To solve Eq. (5.3.23) we introduce a new variable for the gradient of the mean position, i.e. $\Lambda = \arctan(\partial \bar{F}_r/\partial r)$. We can write Eq. (5.3.23) in terms of Λ as

$$\frac{\bar{u}}{S_l^0} = \frac{1}{\cos\Lambda} - \mathcal{L}\frac{\partial \Lambda}{\partial r} \ . \tag{B.3.1}$$

We express $\partial r/\partial\Lambda$ and perform integration with respect to Λ to get the following implicit solution

$$r = c_0 - \frac{\mathcal{L}S_l^0}{\bar{u}}\Lambda - 2\frac{\mathcal{L}S_l^0}{\bar{u}}\frac{1}{\sqrt{\frac{\bar{u}^2}{S_l^2}-1}}\operatorname{arctanh}\left[\sqrt{\frac{\frac{\bar{u}}{S_l}+1}{\frac{\bar{u}}{S_l}-1}}\tan\left(\frac{1}{2}\Lambda\right)\right] , \tag{B.3.2}$$

where c_0 is a constant to be determined from a boundary condition. We are going to use the following trigonometric identities:

$$\tan\left(\frac{1}{2}\Lambda\right) = \frac{\tan\Lambda}{1+\sqrt{1+\tan^2\Lambda}} = \frac{\frac{\partial \bar{F}_r}{\partial r}}{1+\sqrt{1+\left(\frac{\partial \bar{F}_r}{\partial r}\right)^2}} \ , \tag{B.3.3a}$$

$$\arctan\left(\frac{\partial \bar{F}_r}{\partial r}\right) = 2\arctan\left(\frac{\frac{\partial \bar{F}_r}{\partial r}}{1+\sqrt{1+\left(\frac{\partial \bar{F}_r}{\partial r}\right)^2}}\right) \ . \tag{B.3.3b}$$

We substitute with (B.3.3a) and (B.3.3b) for the R.H.S. of Eq. (B.3.2) to get

$$\frac{r-c_0}{2\mathcal{L}}\frac{\bar{u}}{S_l^0} = \arctan\left[\frac{\frac{\partial \bar{F}_r}{\partial r}}{1+\sqrt{1+\left(\frac{\partial \bar{F}_r}{\partial r}\right)^2}}\right] + \frac{1}{\sqrt{\frac{\bar{u}^2}{S_l^2}-1}}\operatorname{arctanh}\left[\sqrt{\frac{\frac{\bar{u}}{S_l}+1}{\frac{\bar{u}}{S_l}-1}}\frac{\frac{\partial \bar{F}_r}{\partial r}}{1+\sqrt{1+\left(\frac{\partial \bar{F}_r}{\partial r}\right)^2}}\right] . \tag{B.3.4}$$

B.4 Fluctuating heat release rate in Cartesian coordinate system

If the flame is two-dimensional, we can write the mean component of the global heat-release rate as

$$\bar{q}_c = \rho_u S_l \Delta q_r \bar{A} = 2D\rho_u S_l \Delta q_r \int_a^b \sqrt{1 + \left(\frac{\partial \bar{F}}{\partial y}\right)^2}\, dy = \bar{m}\Delta q_r \ , \tag{B.4.1}$$

where D is the depth of the burner. The mean heat release rate is directly proportional to the mass flow rate and unit heat released by the chemical reaction, just like in case of an axisymmetric flame. We can write the fluctuating part of the heat-release rate up to third order as the following

$$q_c'(t) = 2D\rho_u S_l \Delta q_r \int_a^b \left[a_1 \frac{\partial F'}{\partial y} + a_2 \left(\frac{\partial F'}{\partial y}\right)^2 + a_3 \left(\frac{\partial F'}{\partial y}\right)^3 \right] dy \ , \tag{B.4.2}$$

where a_1, a_2, a_3 are constants (the same ones as in the cylindrical case) of the Taylor-series expansion. We use the fact that the general solution is of the form $F'(t, y) = F'(t - y/c)$, where $c = S_l \cos\alpha$ is the phase velocity. We can rewrite the time-derivative of the powers of the fluctuating flame position gradient as

$$\frac{\partial}{\partial t}\left(\frac{\partial F'}{\partial y}\right)^n = -c\frac{\partial}{\partial y}\left(\frac{\partial F'}{\partial y}\right)^n \ , \tag{B.4.3}$$

and therefore

$$\frac{\partial}{\partial t}\int_a^b \left(\frac{\partial F'}{\partial y}\right)^n dy = -c\left(\frac{\partial F'}{\partial y}\right)^n \Bigg|_a^b = c\left\{\left[\frac{1}{c}u'(t)\right]^n - \left[\frac{1}{c}u'\left(t - \frac{b-a}{c}\right)\right]^n\right\} \ . \tag{B.4.4}$$

Using Eq. (B.4.4) we write the nondimensional form of the heat release rate law as

$$\frac{\partial}{\partial t}\frac{q_c(t)}{\bar{q}/\chi_c} = \left[\frac{u'}{\bar{u}} - \frac{u'(t-\chi_c)}{\bar{u}}\right] + \frac{1}{2}\tan^2\alpha\left[\left(\frac{u'}{\bar{u}}\right)^2 - \left(\frac{u'(t-\chi_c)}{\bar{u}}\right)^2\right] - \\ - \frac{1}{2}\tan^2\alpha\left[\left(\frac{u'}{\bar{u}}\right)^3 - \left(\frac{u'(t-\chi_c)}{\bar{u}}\right)^3\right], \quad \text{(B.4.5)}$$

where the time-lag $\chi_c = (b-a)/S_l\cos\alpha$ is the time it takes for a perturbation to propagate along the flame front, just like in the cylindrical case.

Appendix C

Rewriting an integral equation into a differential equation

A similar method is applied in [Polyanin and Manzhirov, 2008, p.198]. An integral equation is given in the form of

$$u(t) = A_1 I_1(t) + A_2 I_2(t) \ , \tag{C.0.1}$$

where I_1 and I_2 are defined in the following way

$$\begin{aligned} I_1 &= \int_0^t e^{\lambda_1 (t-t')} q(t') dt' \ , \\ I_2 &= \int_0^t e^{\lambda_2 (t-t')} q(t') dt' \ . \end{aligned} \tag{C.0.2}$$

In order to rewrite the integral equation (C.0.1) into a differential one, we differentiate

Eq. (C.0.1) with respect to t two times

$$\frac{du}{dt} = A_1 \frac{dI_1}{dt} + A_2 \frac{dI_2}{dt} \ , \tag{C.0.3a}$$

$$\frac{d^2u}{dt^2} = A_1 \frac{d^2I_1}{dt^2} + A_2 \frac{d^2I_2}{dt^2} \ . \tag{C.0.3b}$$

We can write the first and second order time-derivatives of I_1 as

$$\frac{dI_1}{dt} = q(t) + \lambda_1 \int_0^t e^{\lambda_1 (t-t')} q(t') dt' = q + \lambda_1 I_1 \ , \tag{C.0.4a}$$

$$\frac{d^2I_1}{dt^2} = \frac{dq}{dt} + \lambda_1 \frac{dI_1}{dt} = \frac{dq}{dt} + \lambda_1 \left[q + \lambda_1 I_1 \right] = \frac{dq}{dt} + \lambda_1 q + \lambda_1^2 I_1 \ . \tag{C.0.4b}$$

We substitute with the last part of Eq. (C.0.4a) and Eq. (C.0.4b) for the R.H.S. in Eq. (C.0.3a) and (C.0.3b) to get

$$\frac{du}{dt} = A_1 (q + \lambda_1 I_1) + A_2 (q + \lambda_2 I_2) = q(A_1 + A_2) + (\lambda_1 A_1 I_1 + \lambda_2 A_2 I_2) \ , \tag{C.0.5a}$$

$$\frac{d^2u}{dt^2} = A_1 \left(\frac{dq}{dt} + \lambda_1 q + \lambda_1^2 I_1 \right) + A_2 \left(\frac{dq}{dt} + \lambda_2 q + \lambda_2^2 I_2 \right) \ . \tag{C.0.5b}$$

We substitute with $A_2 I_2 = u - A_1 I_1$ in Eq. (C.0.5a) and rewrite it

$$\frac{du}{dt} = q(A_1 + A_2) + \left[\lambda_1 A_1 I_1 + \lambda_2 (u - A_1 I_1) \right] \ , \tag{C.0.6a}$$

$$\frac{du}{dt} = q(A_1 + A_2) + \left[\lambda_1 A_1 I_1 - \lambda_2 A_1 I_1 + \lambda_2 u \right] \ , \tag{C.0.6b}$$

$$\frac{du}{dt} - \lambda_2 u - q(A_1 + A_2) = A_1 I_1 (\lambda_1 - \lambda_2) \ , \tag{C.0.6c}$$

then, again, we substitute with $A_2 I_2 = u - A_1 I_1$ in Eq. (C.0.5b) as well and write it in the following forms

$$\frac{d^2u}{dt^2} = \frac{dq}{dt}(A_1 + A_2) + q(A_1\lambda_1 + A_2\lambda_2) + (\lambda_1^2 A_1 I_1 + \lambda_2^2 A_2 I_2) \ , \tag{C.0.7a}$$

$$\frac{d^2u}{dt^2} = \frac{dq}{dt}(A_1 + A_2) + q(A_1\lambda_1 + A_2\lambda_2) + \left[\lambda_1^2 A_1 I_1 + \lambda_2^2 (u - A_1 I_1)\right] \ , \tag{C.0.7b}$$

$$\frac{d^2u}{dt^2} = \frac{dq}{dt}(A_1 + A_2) + q(A_1\lambda_1 + A_2\lambda_2) + \left[\lambda_1^2 A_1 I_1 - \lambda_2^2 A_1 I_1\right] + \lambda_2^2 u \ , \tag{C.0.7c}$$

$$\frac{d^2u}{dt^2} = \frac{dq}{dt}(A_1 + A_2) + q(A_1\lambda_1 + A_2\lambda_2) - A_1 I_1 (\lambda_1 - \lambda_2)(\lambda_1 + \lambda_2) + \lambda_2^2 u \ . \tag{C.0.7d}$$

We substitute with (C.0.6c) for $A_1 I_1 (\lambda_1 - \lambda_2)$ in Eq. (C.0.7d) to get

$$\frac{d^2u}{dt^2} - (\lambda_1 + \lambda_2)\frac{du}{dt} + \lambda_1\lambda_2 u = (A_1 + A_2)\frac{dq}{dt} - (A_1\lambda_2 + A_2\lambda_1)q \ . \tag{C.0.8}$$

Including the second mode in the transformation results in a fourth order ODE. Including n modes yields a $2n$th order ordinary differential equation.

Appendix D

Stability analysis

D.1 Scale separation

Scale separation consists of seeking a periodic solution in terms of power series of a small quantity

$$\tilde{u} = u_0(t_0, t_1, \ldots, t_n) + \epsilon u_1(t_0, t_1, \ldots, t_n) + \ldots + \epsilon^n u_n(t_0, t_1, \ldots, t_n) \ , \tag{D.1.1a}$$

$$\tilde{t} = \tilde{t}(t_0, \epsilon t_1, \ldots, \epsilon^n t_n) \ , \tag{D.1.1b}$$

$$\frac{d}{d\tilde{t}} = \frac{\partial}{\partial t_0} + \epsilon \frac{\partial}{\partial t_1} + \ldots + \epsilon^n \frac{\partial}{\partial t_n} \ . \tag{D.1.1c}$$

By applying (D.1.1a) and (D.1.1b) we can separate higher order derivatives as well. They are listed in (D.1.2).

$$
\begin{aligned}
\frac{d^2}{d\tilde{t}^2} =& \frac{\partial^2}{\partial \tilde{t}_0^2} + \epsilon^2 \frac{\partial^2}{\partial \tilde{t}_1^2} + 2\epsilon \frac{\partial^2}{\partial \tilde{t}_0 \partial \tilde{t}_1} + 2\epsilon^2 \frac{\partial^2}{\partial \tilde{t}_0 \partial \tilde{t}_2} + 2\epsilon^3 \frac{\partial^2}{\partial \tilde{t}_1 \partial \tilde{t}_2} + 2\epsilon^3 \frac{\partial^2}{\partial \tilde{t}_0 \partial \tilde{t}_3} + O(\epsilon^4) \\
\frac{d\tilde{u}}{d\tilde{t}} =& \frac{\partial \tilde{u}_0}{\partial \tilde{t}_0} + \epsilon \left[\frac{\partial \tilde{u}_0}{\partial \tilde{t}_1} + \frac{\partial \tilde{u}_1}{\partial \tilde{t}_0} \right] + \epsilon^2 \left[\frac{\partial \tilde{u}_0}{\partial \tilde{t}_2} + \frac{\partial \tilde{u}_1}{\partial \tilde{t}_1} + \frac{\partial \tilde{u}_2}{\partial \tilde{t}_0} \right] + \epsilon^3 \left[\frac{\partial \tilde{u}_0}{\partial \tilde{t}_3} + \frac{\partial \tilde{u}_1}{\partial \tilde{t}_2} + \frac{\partial \tilde{u}_2}{\partial \tilde{t}_1} + \frac{\partial \tilde{u}_3}{\partial \tilde{t}_0} \right] + O(\epsilon^4) \\
\frac{d^2\tilde{u}}{d\tilde{t}^2} =& \frac{\partial^2 \tilde{u}_0}{\partial \tilde{t}_0^2} + \epsilon \left[\frac{\partial^2 \tilde{u}_1}{\partial \tilde{t}_0^2} + 2\frac{\partial^2 \tilde{u}_0}{\partial \tilde{t}_0 \partial \tilde{t}_1} \right] + \epsilon^2 \left[\frac{\partial^2 \tilde{u}_0}{\partial \tilde{t}_1^2} + 2\frac{\partial^2 \tilde{u}_0}{\partial \tilde{t}_0 \partial \tilde{t}_2} + \frac{\partial^2 \tilde{u}_2}{\partial \tilde{t}_0^2} + 2\frac{\partial^2 \tilde{u}_1}{\partial \tilde{t}_0 \partial \tilde{t}_1} \right] + \\
& + \epsilon^3 \left[\frac{\partial^2 \tilde{u}_1}{\partial \tilde{t}_1^2} + 2\frac{\partial^2 \tilde{u}_0}{\partial \tilde{t}_1 \partial \tilde{t}_2} + 2\frac{\partial^2 \tilde{u}_0}{\partial \tilde{t}_0 \partial \tilde{t}_3} + 2\frac{\partial^2 \tilde{u}_1}{\partial \tilde{t}_0 \partial \tilde{t}_2} + 2\frac{\partial^2 \tilde{u}_2}{\partial \tilde{t}_0 \partial \tilde{t}_1} + \frac{\partial^2 \tilde{u}_3}{\partial \tilde{t}_0^2} \right] + O(\epsilon^4) \\
\frac{d^3\tilde{u}}{d\tilde{t}^3} =& \frac{\partial^3 \tilde{u}_0}{\partial \tilde{t}_0^3} + \epsilon \left[\frac{\partial^3 u_1}{\partial t_0^3} + 3\frac{\partial^3 u_0}{\partial t_0^2 \partial t_1} \right] \\
\frac{d^4\tilde{u}}{d\tilde{t}^4} =& \frac{\partial^4 \tilde{u}_0}{\partial \tilde{t}_0^4} + \epsilon \left[\frac{\partial^4 u_1}{\partial t_0^4} + 4\frac{\partial^4 u_0}{\partial t_0^3 \partial t_1} \right] + \epsilon^2 \left[\frac{\partial^4 u_2}{\partial t_0^4} + 4\frac{\partial^4 u_1}{\partial t_0^3 \partial t_1} + 4\frac{\partial^4 u_0}{\partial t_0^3 \partial t_2} + 6\frac{\partial^4 u_0}{\partial t_0^2 \partial t_1^2} \right] + \\
& + \epsilon^3 \left[\frac{\partial^4 u_3}{\partial t_0^4} + 4\frac{\partial^4 u_0}{\partial t_0 \partial t_1^3} + 12\frac{\partial^4 u_0}{\partial t_0^2 \partial t_1 \partial t_2} + 6\frac{\partial^4 u_1}{\partial t_0^2 \partial t_1^2} + 4\frac{\partial^4 u_1}{\partial t_0^3 \partial t_2} + 4\frac{\partial^4 u_2}{\partial t_0^3 \partial t_1} + 4\frac{\partial^4 u_0}{\partial t_0^3 \partial t_3} \right] + O(\epsilon^4) \\
\tilde{u}(\tilde{t} - \chi\omega_r) =& u_0(t_0 - \chi\omega_r) + \epsilon \left[u_1(t_0 - \chi\omega_r) - \chi\omega_r \frac{\partial}{\partial t_1} u_0(t_0 - \chi\omega_r) \right] + \\
& + \epsilon^2 \left[u_2(t_0 - \chi\omega) - \chi\omega \frac{\partial}{\partial t_1} u_1(t_0 - \chi\omega) - \chi\omega \frac{\partial}{\partial t_2} u_2(t_0 - \chi\omega) + \frac{1}{2}(\chi\omega)^2 \frac{\partial^2}{\partial t_1^2} u_0(t_0 - \chi\omega) \right] \\
\frac{d}{d\tilde{t}} \tilde{u}(\tilde{t} - \chi\omega_r) =& \frac{\partial}{\partial t_0} u_0(t_0 - \chi\omega_r) + \epsilon \left[\frac{\partial}{\partial t_0} u_1(t_0 - \chi\omega_r) + \frac{\partial}{\partial t_1} u_0(t_0 - \chi\omega_r) - \chi\omega_r \frac{\partial^2}{\partial t_0 \partial t_1} u_0(t_0 - \chi\omega_r) \right] \\
& + \epsilon^2 \left[\frac{\partial}{\partial t_1} u_1(t_0 - \chi\omega_r) + \frac{\partial}{\partial t_0} u_2(t_0 - \chi\omega_r) + \frac{\partial}{\partial t_2} u_0(t_0 - \chi\omega_r) - \chi\omega_r \frac{\partial^2}{\partial t_0 \partial t_1} u_1(t_0 - \chi\omega_r) \right. \\
& \left. - \chi\omega_r \frac{\partial^2}{\partial t_0 \partial t_2} u_0(t_0 - \chi\omega_r) - \chi\omega_r \frac{\partial^2}{\partial t_1^2} u_0(t_0 - \chi\omega_r) + \frac{1}{2}(\chi\omega_r)^2 \frac{\partial^3}{\partial t_0 \partial t_1^2} u_0(t_0 - \chi\omega) \right] \\
\epsilon^2 \tilde{u} \frac{d\tilde{u}}{d\tilde{t}} =& \epsilon^2 \tilde{u}_0 \frac{\partial \tilde{u}_0}{\partial \tilde{t}_0} + \epsilon^3 \left[\tilde{u}_1 \frac{\partial \tilde{u}_0}{\partial \tilde{t}_0} + \tilde{u}_0 \frac{\partial \tilde{u}_0}{\partial \tilde{t}_1} + \tilde{u}_0 \frac{\partial \tilde{u}_1}{\partial \tilde{t}_0} \right] + O(\epsilon^4) \ , \\
\epsilon^2 \tilde{u}^2 =& \epsilon^2 u_0^2 + \epsilon^3 2 u_0 u_1 + O(\epsilon^4) \ , \\
\epsilon^2 \left(\frac{d\tilde{u}}{d\tilde{t}} \right)^2 =& \epsilon^2 \left(\frac{\partial u_0}{\partial t_0} \right)^2 + \epsilon^3 \left[2\frac{\partial u_0}{\partial t_0} \frac{\partial u_0}{\partial t_1} + 2\frac{\partial u_0}{\partial t_0} \frac{\partial u_1}{\partial t_0} \right] + O(\epsilon^4) \ .
\end{aligned}
\tag{D.1.2}
$$

D.2 Instability of a burner with strong losses

If we include all of the small parameters into the linear stability analysis, we have to solve the following equation

$$\begin{aligned}\frac{d^4\tilde{u}}{d\tilde{t}^4} - 2\epsilon_\omega \frac{d^3\tilde{u}}{d\tilde{t}^3} + (1+\epsilon_\omega^2)\frac{d^2\tilde{u}}{d\tilde{t}^2} = \\ = 2\epsilon_i \frac{1}{\chi_r\omega_r}\frac{2}{1+\beta}\left\{\beta\frac{d^2\tilde{u}}{d\tilde{t}^2} - \frac{d^2}{d\tilde{t}^2}\tilde{u}(\tilde{t}-\omega_r\chi_r) + \frac{1-\beta}{\omega_r\chi_r}\left[\frac{d\tilde{u}}{d\tilde{t}} - \frac{d}{d\tilde{t}}\tilde{u}(\tilde{t}-\omega_r\chi)\right]\right\} - \\ - 2\epsilon_r \frac{1}{\chi_r\omega_r}\frac{2}{1+\beta}\left\{\beta\frac{d\tilde{u}}{d\tilde{t}} - \frac{d}{d\tilde{t}}\tilde{u}(\tilde{t}-\omega_r\chi_r) + \frac{1-\beta}{\omega_r\chi_r}\left[\tilde{u} - \tilde{u}(\tilde{t}-\omega_r\chi_r)\right]\right\} \quad , \end{aligned} \tag{D.2.1}$$

where ϵ_r, ϵ_i and ϵ_ω are given in Eqs. (6.3.6a)-(6.3.6c). We perform the similar steps which are described in Section (6.3.1), i.e. we introduce two time scales ($t_0 = \tilde{t}$, $t_1 = \epsilon_r\tilde{t}$) and transform the terms in Eq. (D.2.1). We then seek a solution in powers of ϵ_r in the form $\tilde{u} = u_0 + \epsilon_r u_1$, substitute it into Eq. (D.2.1) and collect coefficient of equal powers of ϵ_r. To the leading order (at $O(\epsilon_r^0)$) we have a harmonic oscillation, i.e.

$$\frac{\partial^2 u_0}{\partial t_0^2} + u_0 = 0 \ , \tag{D.2.2}$$

which has the solution

$$u_0 = A(t_1)\exp(-it_0) + C.C. \ . \tag{D.2.3}$$

At the order of $O(\epsilon_r^1)$ we get

$$\epsilon_r \frac{\partial^4 u_1}{\partial t_0^4} + 4\epsilon_r \frac{\partial^4 u_0}{\partial t_0^3 \partial t_1} - 2\epsilon_\omega \frac{\partial^3 u_0}{\partial t_0^3} + \epsilon_r \frac{\partial^2 u_1}{\partial t_0^2} + 2\epsilon_r \frac{\partial^2 u_0}{\partial t_0 \partial t_1} =$$
$$= -2\epsilon_r \frac{1}{\chi_r \omega_r} \frac{2}{1+\beta} \left[\beta \frac{\partial u_0}{\partial t_0} - \frac{\partial u_0(t_0 - \chi_r \omega_r)}{\partial t_0} \right] - 2\epsilon_r \frac{1}{\chi_r \omega_r} \frac{2}{1+\beta} \frac{1-\beta}{\chi_r \omega_r} \Big[u_0 - u_0(t_0 - \chi_r \omega_r) \Big]$$
$$+2\epsilon_i \frac{1}{\chi_r \omega_r} \frac{2}{1+\beta} \left[\beta \frac{\partial^2 u_0}{\partial t_0^2} - \frac{\partial^2 u_0(t_0 - \chi_r \omega_r)}{\partial t_0^2} \right] - 2\epsilon_r \frac{1}{\chi_r \omega_r} \frac{2}{1+\beta} \frac{1-\beta}{\chi_r \omega_r} \Big[\frac{\partial u_0}{\partial t_0} - \frac{\partial u_0(t_0 - \chi_r \omega_r)}{\partial t_0} \Big] . \tag{D.2.4}$$

We rearrange Eq. (D.2.4) and eliminate the secular terms to obtain the following equation for $A(t_1)$

$$\frac{\partial A}{\partial t_1} = A \left[\frac{\epsilon_\omega}{\epsilon_r} + (\varphi_i - i\varphi_r) + \frac{\epsilon_i}{\epsilon_r} (\varphi_r + i\varphi_i) \right] , \tag{D.2.5}$$

where φ_i and φ_r are given in Eqs. (6.3.11a)-(6.3.11b). Eq. (D.2.5) is of first order and linear in A. The solution is

$$A(t_1) = c_0 \exp \left\{ t_1 \left[\frac{\epsilon_\omega}{\epsilon_r} + (\varphi_i - i\varphi_r) + \frac{\epsilon_i}{\epsilon_r} (\varphi_r + i\varphi_i) \right] \right\} , \tag{D.2.6}$$

where c_0 is a constant and with Eq. (D.2.3) we obtain

$$u_0 = a_0 \exp \left[t_0 \left(\epsilon_\omega + \epsilon_r \varphi_i + \epsilon_i \varphi_r \right) \right] \sin \left[\zeta_0 + t_0 \left(1 + \epsilon_r \varphi_r - \epsilon_i \varphi_i \right) \right] , \tag{D.2.7}$$

where a_0 and ζ_0 are the initial conditions. The terms $\epsilon_i \varphi_r$ and $\epsilon_i \varphi_i$ represents small corrections in the gain and the phase respectively.

Appendix E

Properties of the LIMOUSINE burner

E.1 Measured properties of the LIMOUSINE burner

quantity	notation	value [dimension]
adiabatic flame temperature	$\bar{T}_{ad}$	2200 [K]
maximum measured temperature	$\bar{T}(x_q)$	1320 [K]
reflection at the inlet	R_0	0.80+i0.22
reflection at the outlet	R_1	-0.954-i0.137
length of the inlet region	l_1	0.324 [m]
length of the flame region	$l_2 - l_1$	0.070 [m]
length of burner	L	1.424 [m]
temperature at the inlet	T_0	340 [K]
temperature at $x = l_1$	T_1	400 [K]
temperature at $x = l_2$	T_2	1320 [K]
temperature at the outlet	T_3	1120 [K]
specific gas constant	$\mathcal{R}$	286.9 [J/kgK]
heat capacity ratio	γ	1.35
operating mean pressure	$\bar{p}$	1 [atm]
cross sectional area of inlet	$\mathscr{A}_0$	0.0045 $[m^2]$
cross sectional area of outlet	$\mathscr{A}_1$	0.0090 $[m^2]$

Table E.1: Measured properties of the LIMOUSINE burner

E.2 Calculated properties of the LIMOUSINE burner

quantity	notation	value [dimension]	
		first mode	second mode
passive damping rate	ω_i	−32.3 $[1/s]$	−72.98 $[1/s]$
passive eigenfrequency	ω_r	760.3 $[1/s]$	1757.0 $[1/s]$
real part of $\partial\hat{g}/\partial x$	$Re[\partial\hat{g}/\partial x]$	−152.6 $[1/s]$	83.5 $[1/s]$
imaginary part of $\partial\hat{g}/\partial x$	$Im[\partial\hat{g}/\partial x]$	−6.2 $[1/s]$	15.32 $[1/s]$
relative damping	ϵ_ω	−0.04	−0.04
real part of $\partial\hat{g}/\partial x/\omega_r$	ϵ_r	−0.2	0.05
imaginary part of $\partial\hat{g}/\partial x/\omega_r$	ϵ_i	−0.01	0.01
heat-loss coefficient	η_T	0.60	
flame holder radii ratio	β	1	
hydraulic flame holder radii ratio	β_h	0.56	
combustion enthalpy of methane	$(\Delta q_r/c_p T_{ad})_{st}$	0.78	

Table E.2: Calculated properties of the LIMOUSINE burner